Mechanical Devices for Harvesting Human Kinetic Energy

XIE, Longhan

A Thesis Submitted in Partial Fulfillment

of the Requirements for the Degree of

Doctor of Philosophy

In

Automation & Computer-Aided Engineering

The Chinese University of Hong Kong

May, 2010

Thesis Assessment Committee

Professor Wang, Yu Michael (Chair)

Professor Hui, Kin-chuen (Committee Member)

Professor Chen, Yonghua (External Examiner)

Professor Du, Ruxu (Thesis Supervisor)

Abstract

This thesis discusses the feasibility of mechanical power generators driven by human motion, with the focus on their architecture design and performance analysis. The main objective is to develop effective power generators for harvesting the energy from human motion, and use it to power portable electronic devices.

In modern life, human have become dependent on portable electronics, such as cell phones, MP3 and handheld computers, most of which are powered by batteries. Although the performance of batteries is being continuously improved, the limited energy storage and service life constrain the lasting use of these mobile electronics. Therefore it is desirable to find alternative or supplementary methods to solve this problem from its root cause. It is known that human body contains rich chemical energy, part of which is converted to mechanical energy up to 200W when in motion, so it is ideal to harvest a small fraction of the human kinetic energy to power mobile electronic devices.

In this thesis, first, the previous work done by other researchers on energy harvesting from human motion, especially from unintentional human motion, such as arm swing and leg moving, is reviewed. Then the fundamental principles to mechanically harvest motion energy are discussed, including the mechanical oscillating mechanisms and electromagnetic transduction. Derived from the general harvesting model, four different devices are designed and analyzed.

The first one is the automatic winding mechanism of mechanical movement. It consists of an oscillating weight, a ratchet mechanism, a gear set and a mainspring. The mechanism can be modeled as a double pendulum when worn on a user's wrist. Its kinematical performance is analyzed with experimental validation.

To directly convert the human arm motion to electricity, the second novel energy harvester is designed, analyzed and simulated. It mainly consists of an eccentric rotor made of permanent magnet, and a set of coils as a stator. The eccentric rotor, as a simple pendulum, acts as the kinetic energy harvester which absorbs the motion from human body in motion. With the permanent magnets on the rotor, the moving rotor produces a changing magnetic field, from which the stator induces electricity. In this design, a torsion spring is also added onto the rotor so that the harvester works even when the motion is on horizontal plane.

Shoe is important for human, one of which functions is to serve as shock-absorber to protect foot from the large impact force. As the foot strikes the ground, the shoe is subject to not only large force but also large displacement in the heel. The third new device is designed to insert in the shoe heel to harvest the kinetic energy from foot strike, and at the same time to function as a shock absorber for foot. Considering the stability and efficiency, a spring-slider-crank mechanism is used in this harvester to covert the up-down foot strike motion into unidirectional rotation to drive an AC generator. The spring and slider compose an oscillating system to absorb the foot strike motion, and crank and slider make up the conversion mechanism to transfer the bi-directional translation into unidirectional rotation. A set of gear is used to speed up the rotation. The kinematical performance of the harvester is also analyzed.

When foot strikes the ground, a large acceleration is produced. The fourth new energy harvester uses dual-oscillating mode. It contains two oscillating mechanisms: one is spring-mass oscillator to absorb the vibration from footstep motion, and the other is cantilever beam using the tip mass to amplify the vibration. Analysis shows that the dual-oscillating mechanism can be more effectively harvest the foot step motion. The energy conversion sub-mechanism is based on the electromagnetic induction, where the coils fixed at the tip end of the cantilever beam serves as the slider, and the fixed permanent magnets and yoke produce the changing magnetic field. Mathematical analysis and simulation are included.

摘 要

本文讨论了机械式微型发电机在携带式电子产品中的潜在应用，本文的主要研究目的是开发几款微型发电机，这些发电机可以通过捕获人体动能而为便携式电子产品供电。

在现代生活中，人们越来越依赖电子产品，例如手机，MP3，掌中计算机等。目前这些便携式电子产品大都是由电池供电。尽管电池的性能在不断提高，但有限的储能及使用寿命限制了携带式电子产品的使用时间。因此，有必要寻找替换方法来解决便携式电子产品能源短缺的问题，或者至少是寻找一种可以不断补充电能储能的途径。人体富含化学能，其中一部分转换为机械能以支持日常活动，人体活动是这些机械能可达 200W。因此，捕获一小部分机械能并将其转换为电能以供给电子设备工作是十分理想的。

本文首先调研了前人已经做过的关于人体能量捕获的相关研究，着重分析了如何捕获非意识人体动能的方法（例如行走与摆手）。在此基础上，给出了以机械方法捕获人体动能的基本理论，包括机械振荡系统和电磁转换模型。从这些基本模型出发，本文提出了 4 种不同的能量捕获装置，以收集并转换人体动能。

第一种是机械手表的自动上条装置，其工作原理是一个双摆，通过双摆的运动捕获手臂的动能。自动上条装置主要包括振荡质量块、棘轮机构、齿轮系和主弹簧。本文对其运动性能进行了详细的数学分析和实验验证。该项工作是首次对机械手表自动上条装置进行详细理论研究。

为了直接将人体摆手的机械运动直接转换为电能，本文的第二个设计是一款新型的能量捕获装置。该装置主要包含了一个以永磁磁铁制成的偏心转子、及绕在电钢上的线圈所组成的定子。 偏心转子，类似一个单摆，充当了动能捕获器，它直接捕获人体的摆手运动。所捕获的运动使偏心转子上的永磁磁铁在周围空间产生变化的磁场，定子上的线圈在这个变化磁场中产生感应电流。该装置还在转子及转子轴上增加了一个扭簧，从而使该转子可以在任何平面内工作，因此增大了装置捕获能量的效能。

鞋子对人体十分重要；其主要功能之一是作为减震器以吸收脚部着地时所带来的冲击。脚部着地时鞋跟具有很大的冲击加速度，也有一定的位移。因此，本文根据人脚步特点设计了一个新型的脚部动能捕获装置，放置在鞋跟内；它

在捕获脚步动能的同时还可以缓和冲击力对脚跟的影响。考虑到稳定性和效率，本装置采用了弹簧－滑块－曲杆结构，将脚步冲击的上下运动转换成单向的转动，并将转动通过加速齿轮传递给微型交流发电机。其中的弹簧－滑块结构组成了振荡系统吸收了脚步的冲击运动。捕获的上下振荡滑动则通过曲杆－滑块结构调整为单向的圆周运动。加速齿轮系放大了曲杆传递出来的圆周运动。本文对该系统机构进行了详细的数学分析。

人体运动时，脚部着地的加速度很大。本文第四个设计是一个基于双振荡模式的新型装置以方便捕获这一加速度。该加速度能量捕获器包括的两级振荡机构：第一级是质量弹簧系统用于吸收来自脚部冲击所产生的加速度，第二级是固定在第一级的质量块上的悬臂梁及其末端的质量块用于放大第一级的振荡。分析表明这一双模式振荡系统可以更加有效的收集脚部的加速度。从机械能转换为电能是基于电磁感应原理，主要是依靠固定的永磁磁铁所产生的磁场使缠绕在悬臂梁末端质量块上的线圈产生感应电流。本文还包括详细的数学分析。

Acknowledgements

If I have been able to see farther, it was only because I stood on the shoulders of giants.

——Isaac Newton

Figuratively speaking, this doctoral thesis has been possible because I was able to stand on the 'shoulders' of many people:

First and foremost, this thesis would not be possible without the kindness and generosity of my advisor, Professor Du Ruxu. He was very patient with me and gave me the opportunity to carry out research and write a Ph.D thesis in the exciting and promising field of energy harvesting. His encouragement, support and advice have been immensely valuable, both in personal and professional terms.

Special thanks go to my thesis committee members, Professor Chen Yonghua, Professor Hui Kin-chuen, and Professor Wang Yu Michael. Each devoted significant time and effort on my thesis, and their suggestions and comments led to substantial improvement in the final thesis.

Institute of Precision Engineering of the Chinese University of Hong Kong deserves my gratitude for providing me with the open-minded research atmosphere. I would like to extend my gratitude to Dr. Tom Kong, Dr. Fu Yu, Dr. Ching Ho, Dr. Mao Jian, Mr. Zhang Peng, Mr. Luo Yuanxin, Mr. Wu Zhihui, Miss Su Shuang, Mr. Ko Puihang Billy, Mr. Chen Xianshuai, Mr. Lei Man Cheong Michael, Dr. Guo Yuhua, Mr. Wang Yingnan, and the rest of members in the Institute of Precision Engineering of CUHK for their help and precious friendship. I would list them all and all that they have done for me, but that document would be longer than this thesis.

I owe lots of thanks to my parents, parents-in-law and my family, who supported and encouraged me in all situations. In the past three years, without them I would not have stepped into this stage, which would be an important milestone during my whole life. Finally, I would like to extend my special thanks to my wife, Lin Wei, for her understanding, support and unconditional love.

Table of Contents

Abstract i

Acknowledgements v

List of the Figures viii

Chapter 1 Introduction 1

1.1 Motivation 1

1.2 Objectives 4

1.3 The Organization of the Thesis 5

Chapter 2 Literature Review on Harvesting Human Kinetic Energy 7

2.1 Electromagnetic Transduction 7

2.2 Piezoelectric Transduction 15

2.3 Electrostatic Transduction 20

2.4 Comparison and Discussion 23

Chapter 3 The Principle for Harvesting Energetic Motion 26

3.1 The Procedure to Design Energy Harvester 26

3.2 Mechanical Oscillating Mechanism 28

3.3 Electromagnetic Transduction 35

Chapter 4 The Automatic Winding Mechanism 39

4.1 Introduction 39

4.2 The Model of the Automatic Winding Device 40

4.3 The Kinematical Model 43

4.4 Simulation and Experiment Results 50

4.5 Summary 55

Chapter 5 The Magnetic Pendulum Mechanism 57

5.1 The Design of the Harvester 57

5.2 Electromagnetic Analysis 61

5.3 Kinematical Analysis 65

5.4 Coupled Analysis 68

5.5 Discussion and Summary 74

Chapter 6 The Crank-Slider Mechanism 76

6.1 Introduction 76

6.2 Description of the Harvester 78

6.3 Analysis of the Crank-slider Mechanism 83
6.4 Analysis and Optimization of the Slider-spring Mechanism 86
6.5 Transmission Analysis and Power Output 87
6.6 Discussion and Summary 91
Chapter 7 The Dual-Oscillating Mechanism 93
7.1 The Harvester Structure 93
7.2 Electromagnetic Analysis 96
7.3 Kinematical Analysis 103
7.4 Coupled Analysis and Power Output 107
7.5 Optimization and Discussion 114
7.6 Summary 120
Chapter 8 Conclusions 121
8.1 Summary of the Achievements 121
8.2 Future Work 123
Bibliography 124

List of the Figures

Fig.1-1: Possible power recovery from body-centered sources 4
Fig.2-1: The Seiko automatic generating system 8
Fig.2-2: The inertial linear-based generators placed inside the shoe sole 9
Fig.2-3: The suspended-load backpack 10
Fig.2-4: Schematic of miniature imbricated-pole permanent-magnet generator 11
Fig.2-5: General concept for linear PM motion harvester 12
Fig. 2-6: The micro cantilever generator 13
Fig.2-7: Stator and translator of used generator architecture 13
Fig.2-9: The knee-mounted biomechanical energy harvester 14
Fig.2-10: The 3D schematic of the axial flux generator 15
Fig.2-11: The piezoelectric stack actuated by hydraulic amplifiers 16
Fig.2-12: A piezoelectric PVDF stack under bending 17
Fig.2-13: The impact-based piezoelectric generators 18
Fig.2-14: Embedded piezoelectric generators inside a knee implant 19
Fig.2-15: Embedded piezoelectric generators in line with backpack straps 19
Fig.2-16: The working principle of electrostatic transduction 20
Fig.2-17: Fundamental structure of a honeycomb-type variable capacitor 21
Fig.2-18: Electrostatic generators with variable-gap parallel-plate capacitor 22
Fig.2-19: Electret generator with overlapped area capacitor 23
Fig.3-1: The procedure to design and analyze the energy harvester 27
Fig.3-2: A mass-spring oscillating system mounted on a vibration base 28
Fig.3-3: the cantilever beam with concentrated mass at the end 33
Fig.3-4: the beam on two simple supports 33
Fig.3-5: Eccentric rotational mass system and the notation for analysis 34
Fig.3-6: The schematic diagram for electromagnetic transduction 35
Fig. 3-7: FEA model and solving results 36
Fig.3-8: Measure and export of the simulation result 37
Fig.3-9: A magnet structure and its MEC model 37
Fig. 4-1: The working of an automatic winding device 40
Fig. 4-2: The CAD model of the automatic winding device, front view 41
Fig. 4-3: The CAD model of the automatic winding device, back view 41

Fig. 4-4: Illustration of the reversing mechanism 42
Fig. 4-5: Schematic diagram of winding system when arm is swinging 44
Fig. 4-6: The force diagram of the system 45
Fig. 4-7: The gear train of the automatic winding device 47
Fig. 4-8: Reaction force of the mainspring as a function of the winding angle 48
Fig. 4-9: The angular displacement of the upper and lower pendulum 50
Fig. 4-10: The angular velocity of the upper and the lower pendulum 51
Fig. 4-11: The angular acceleration of the upper and lower pendulum 51
Fig. 4-12: the winding curves with different swing amplitudes 52
Fig. 4-13: the winding curves with different arm swing periods 52
Fig. 4-14: Total input energy in terms of time 53
Fig. 4-15: The system efficiency as a function of the swinging period 55
Fig. 4-16: The setup for experimental testing 56
Fig.5-1: The overview of the energy harvester for arm motion 58
Fig.5-2: Mechanism for manual harvesting 59
Fig.5-3: The clutching mechanism in release 59
Fig.5-4: The clutching mechanism in engagement 60
Fig.5-5: The gear train for the manual harvesting 60
Fig.5-6: The rotor-stator mechanism in the harvester 61
Fig.5-7: The cross-section view of the rotor and stator, and the flux path 61
Fig.5-8: The 2D model for electromagnetic analysis with Ansys 62
Fig.5-9: Magnetic flux density in the rotor and stator shown in 2D flux lines 62
Fig.5-10: Flux distribution shown in vector 63
Fig.5-11: Magnetic equivalent circuit for the half of rotor and stator 63
Fig.5-12: Lumped parameter model of the harvester 66
Fig.5-13: The working model of the harvesting device 69
Fig.5-14: Kinematical performance for a sine wave as external excitation 70
Fig.5-15: Kinematical performance for a step function as external excitation 70
Fig.5-16 power output performance versus the sector angle of each magnet 71
Fig.5-17: Power output versus different arm swing frequencies 73
Fig.5-18: Power output versus different arm swing amplitudes 74
Fig.6-1: Shoe with air cushion for buffering heel strike 77
Fig.6-2: The Z-Coil® footwear with a spring coil attached to the shoe heel 77
Fig.6-3: The general view of the harvester 78

Fig.6-4: The crank slider mechanism 79
Fig.6-5: The close view of the crank slider mechanism 79
Fig.6-6: The fixed component of the harvester 80
Fig.6-7: The gear train 80
Fig.6-8: The schematic diagram of the harvester 81
Fig.6-9: Flow chart of the harvester 82
Fig.6-10: Offset crank-slider mechanism 83
Fig.6-11: Extreme positions in offset crank slider linkage 84
Fig.6-12: Solution for deadlock 85
Fig.6-13: Trajectories of the slider crank mechanism 85
Fig.6-14: The gear train for each generator 88
Fig.6-15: Step duration during normal walking 89
Fig.6-16: The velocity and position of the slider 89
Fig.6-17: The status when springs are fully pressed 91
Fig.7-1: The overview of the dual-oscillating harvester 94
Fig.7-2: The structure for producing magnetic field 94
Fig.7-3: The structure of the oscillating mechanism 95
Fig.7-4: The schematic diagram of the dual-oscillating harvester 96
Fig.7-5: Schematic diagram of magnetic structure and the flux paths 97
Fig.7-6: FEA model and its mesh in Ansys 97
Fig.7-7: The magnetic flux density plotted in vector 98
Fig.7-8: 2D Flux distribution of the magnetic field 98
Fig.7-9: The x-component of magnetic flux density (perpendicular to coils) 99
Fig.7-10: Distribution of flux density at the gap center 99
Fig.7-11: The peak value of flux density along the center line of pole pitch 100
Fig.7-12: The distribution of flux density along Z direction 100
Fig.7-13: The distribution curve of electrical damping coefficient 102
Fig.7-14: The schematic model of the oscillating mechanism 104
Fig.7-15: Acceleration performance during foot swinging 108
Fig.7-16: the velocity response from step impulse 109
Fig.7-17: Velocity response from external acceleration in sine wave 110
Fig.7-18: Velocity response from external acceleration in square function 110
Fig.7-19: Velocity response from square function and sine wave 111
Fig.7-20: Velocity response from external excitation in close circuit 112

Fig.7-21: The transient power output in terms of time 113
Fig.7-22: The average power output in terms of the spring ratio 115
Fig.7-23: The average power output in terms of the spring ratio, where the electrical damping coefficient is constant for each curve 116
Fig.7-24: The average power output in terms of electrical damping coefficient, where the spring ratio is constant for each curve 116
Fig.7-25: The maximum displacement of coil in Z direction in terms of electrical damping coefficient, where spring ratio is constant for each curve 117
Fig.7-26: The maximum displacement of coil in Z direction in terms of mass ratio, where the spring ratio is constant for each curve 118
Fig.7-27: The average power output in terms of mass ratio, where the spring ratio is constant for each curve 118
Fig.7-28: The average power output in terms of electrical damping coefficient, where the spring ratio is 0.4 and mass ratio is 0.5 119

Chapter 1

Introduction

1.1 Motivation

Over the years, humans have become increasingly dependent on technology, particularly electronic devices. During the past decade, electronic devices have become more mobile, enabling people to use mobile phones and global positioning systems as they move around cities or in the wilderness. People are seeking to make electronic devices smaller and longer lasting, which makes the power problem more and more critical.

The current approach for powering mobile electronics is to use batteries. Batteries can be classified into two categories: primary batteries and secondary batteries. Primary batteries, or disposable batteries, irreversibly (within limits of practicality) transform chemical energy to electrical energy. When the supply of chemical reactants is exhausted, energy cannot be restored to the battery by electrical means. These batteries are intended to be used once and discarded. Secondary batteries can be recharged, that is, they can have their chemical reactions reversed by receiving electrical energy, restoring to their original state. Among various rechargeable batteries, lithium-ion (Li-ion) batteries are the most popular type, whose advantages include high energy density and long cycle life. A typical Li-ion battery has around 160 Wh/kg gravimetric energy density and 1,200 cycle life. However, there are drawbacks with rechargeable batteries. First of all, they need to recharge frequently, which requires accessing to a power grid and a suitable charger. Secondly, even though it has a long cycle life, rechargeable battery needs to be replaced after reaching the limit, which is environmentally hazard. Nowadays, billions of disposed batteries have become a major concern to our tender environment.

Considering the increasing concerns on energy and environment, it has become clear that we need to find alternative methods to solve the power problem of portable electronics.

One solution is the fuel cell. It has been widely investigated as an alternative power source [1] due to their high energy density and clean to the environment. A fuel cell is an electrochemical cell. The electricity is generated through the reaction, triggered in the presence of an electrolyte, between the fuel (on the anode side) and an oxidant (on the cathode side). The reactants flow into the cell, and the reaction products, the electricity, flow out, while the electrolyte remains within. Fuel cells can operate virtually continuously as long as the necessary flows are maintained. Many combinations of fuels and oxidants are possible. For example, hydrogen fuel cell uses hydrogen as its fuel and oxygen (usually from air) as its oxidant. However, there are several shortcomings for fuel cell. In addition to the cost, safety is the major concern when used as power source in portable electronics, particularly with respect to handling and transporting the fuel, which is seen as hazardous materials by United Nations. Therefore, fuel cell is considered unsuitable to power mobile electronics.

Energy harvesting from environment is another alternative for mobile electronics. Energy from environment includes vibration [2-5], solar light [6, 7], pressure [8, 9], motion [10, 11], and etc. However, they are typically of low energy density; and the conversion devices are usually stationed somewhere and hence difficult for portable electronics.

Portable electronics, such as mobile phone, are usually taken by human, so human energy is also ideal source of power. The human body is a tremendous resource of energy. Just one gram of fat can be converted to 9,000 calories or 37.7 kJ. An average person of 68 kg with 15% body fat stores energy approximately equivalent to 384 MJ [12]. During daily life, human body consumes chemical energy to support various functions, such as breathing, motion, and etc. It is estimated that everyday human activities consume power at a rate of 81-1630 W, though only 20% of that are in use [12]. In other words, such energy is wasted into environment, such as body heat, and negative kinetic motion. Thus, even if a very small fraction of this energy could be extracted, a portable device would have a large and renewable resource to draw on.

Since the energy is taken from human body, there are several advantages. Firstly, it produces no pollution. Secondly, it has no need for recharging or replenishment. Last but not least, it has no cycle limitation, which makes the power source last forever.

On the difficult side, human energy has lower density, and some are available only in some condition, for example, human kinetic energy is available only in motion. So the energy harvester should be designed with great care. But anyway, the energy harvesting from human body is an alternative or supplement to conventional power source for portable electronics.

There are several kinds of possible body energy to scavenge, such as body heat, breathing, motion, and etc. Figure 1-1 shows the possible power recovery from various body sources, where the value is the maximum recovery power reported in literatures, and the total power for each action is included in parentheses. From the figure, it is seen that except the arm motion and footfall, the available power for other kind of human activities is rather limited. However, there are much room for the harvesting energy from the human arm motion and footfall. Actually, some researchers have explored to extract energy from body heat [13, 14], breathing [15], typing [16], arm motion [12], and walking [8-9]. Few of the designs are convenient, especially in the unintentional mode. Therefore, further research should be made to design new devices for conveniently powering electronic devices without adding considerable burden to human body.

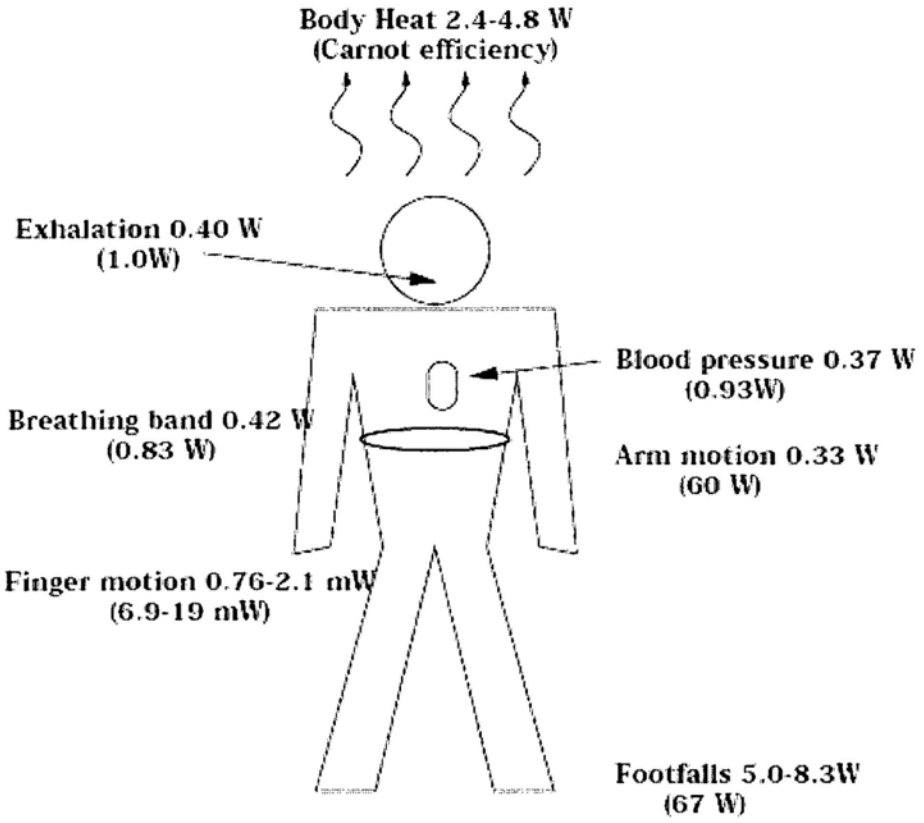

Fig.1-1: Possible power recovery from various body sources. The value is the maximum recovery power reported by literatures and the total power for each action is included in parentheses [12]

1.2 Objectives

There are two main objectives in this thesis:

(1) Explore the basic principles for harvesting the kinetic energy from human body motion;

(2) Design devices for harvesting human arm motion and foot motion as power source for portable electronics.

By analyzing the characteristics of human motion, this thesis proposes the basic harvesting principles through mechanical oscillating and electromagnetic transduction. These basic principles can be used not only to harvest human kinetic energy, but also to apply for harvesting similar kinetic energy, such as the kinetic energy from some mechanical devices.

Four types of harvesters are designed and analyzed. Two of them are designed to harvest human arm motion: one is to convert the kinetic energy from human arm motion into the potential energy of spring, which has been long applied in the automatic winding of mechanical watch movement. The other is to convert kinetic energy into electricity, which can be used to power various portable electronics. Another two are designed to harvest human foot motion. During foot strike there is significant impact force and displacement. One design is based on mechanical transmission directly to convert motion into electricity via spring-slider-crank mechanism. Since there is large acceleration in foot strike, the other device is based on vibration to harvest acceleration and convert to electricity. For each design, detailed mathematical analysis is given.

1.3 The Organization of the Thesis

The rest of this thesis is organized as follows:

Chapter 2 reviews the work done by other researchers on the human energy harvesting. In particularly, this chapter will pay attention to the methods of energy harvesting classified based on electromagnetic transduction, piezoelectric transduction and electrostatic transduction. Discussions on the existing harvesting methods are given.

Chapter 3 gives the basic methods to harvest kinetic energy. Firstly a general procedure to design an energy harvester is proposed. Then the general harvesting principle is given, including mechanical oscillating mechanism and electromagnetic transduction model, which helps to direct the design of harvesting devices.

Chapter 4 introduces the energy conversion from kinetic energy of human arm motion into spring potential energy. The automatic winding mechanism in mechanical watch movement is analyzed and experimentally validated.

Chapter 5 introduces the energy conversion from human arm motion into electricity. A novel harvester is designed and analyzed. It is a pendulum that uses mass-spring

principle and electromagnetic induction to convert mechanical energy to electricity.

Chapter 6 introduces the energy harvesting from human footstep motion into electricity, based on direct mechanical transmission. A harvester, as an integrate component to insert into shoe heel, is designed and analyzed. It employs slider-crank-spring mechanism to capture footstep strike motion, and transmit to gear train and then AC micro generator to produce electricity.

Chapter 7 introduces the energy harvesting from the acceleration of human footstep strike into electricity. It is a dual-oscillating mechanism including a mass-spring mechanism and a mass-cantilever mechanism. The harvester is also designed to insert into shoe heel, but it has no transmission components, which makes the harvester more reliable and stronger.

Chapter 8 contains conclusions summarize the achievements. A list of future work is also given.

Chapter 2

Literature Review

The process of extracting energy from the surrounding environment is termed as energy harvesting, or energy scavenging. Originated from the windmill and water wheel, energy harvesting is widely considered as a low-maintenance solution for a wide variety of applications, such as alternative for battery, power for embedded systems, wireless sensor networks and low-power electronics. In recent years, several energy harvesting approaches have been proposed using electromagnetic, piezoelectric, and electrostatic schemes. In this thesis, research is focused on harvesting human kinetic energy, which mainly performs as vibration and movements. In this chapter, literature review is conducted to facilitate readers to understand harvesting human kinetic energy.

2.1 Electromagnetic Transduction

Electromagnetic induction, first discovered by Faraday in 1831, is the generation of electric current in a conductor located within a magnetic field. The conductor typically takes the form of a coil and the electricity is generated by either the relative movement of the magnet and coil, or because of changes in the magnetic field. In the former case, the amount of electricity generated depends upon the strength of the magnetic field, the velocity of the relative motion and the number of turns of the coil. The basic foundations summarized in this section are sufficient to provide an understanding of the electromagnetic phenomena and the methods available to exploit it for energy harvesting purposes.

Williams and Yates derived the equations of motion for a nonspecific generator that consisted of a seismic mass on a spring and a damper [21]. The power output was derived from the energy that could be dissipated through the damper by converting mechanical to electrical energy. Based on the derived equations, the power output of such a generator is proportional to the cube of the vibration frequency and that the

deflection of the seismic mass should be as large as possible. The proposed harvesting system utilized an electromagnetic harvesting scheme. For a very small (5 mm x 5 mm x 1 mm) generator, they predicted 1 μW at an excitation frequency of 70 Hz and 0.1 mW at 330 Hz.

Automatic winding mechanism of mechanical watch movement has invented for more than one hundred years. Some researchers have studied the feasibility to use the automatic winding mechanism to transducer kinetic energy into electricity to power an implanted medical device. One example is presented by Goto [22]. The study showed the feasibility of using the Seiko wristwatch AGS mechanism, as shown in Fig.2-1, which includes the oscillating mass, the gear train, the generator, the half-wave rectification circuit and the capacitor, to power a circuit to pace a dog's heart. The generator was placed on the right ventricular wall of the dog's heart and produced 80 mJ of energy after rectification and storage in the capacitor over a 30 minutes period for a heart rate of 200 beats per minute. Gorge tested Seiko's wristwatch mechanism tapped to the chest of a person working in an office environment [23]. Over a period of 8 hours, the power output varied between 0.2 and 3.1 μW, with an average value of 0.5 μW. They considered the power output to be 10 to 100 times less than what would be needed for recharging a typical pacemaker battery. They also tested a different generator with fewer mechanical parts, but the power output was found to be no greater than from Seiko's system.

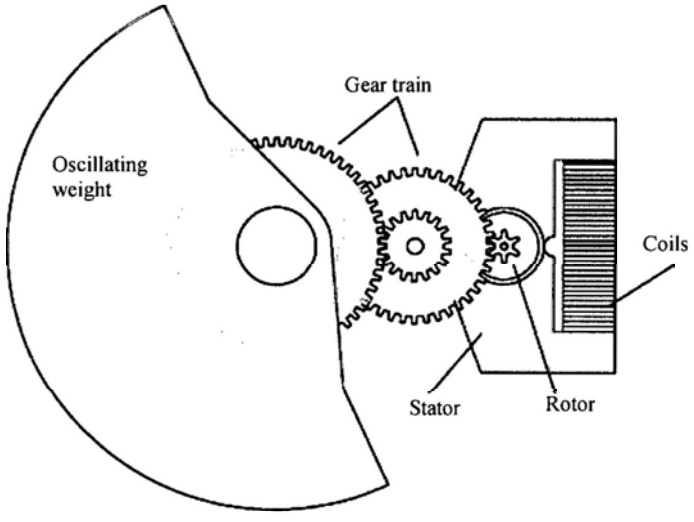

Fig.2-1: The Seiko automatic generating system

El-hami proposed a vibration-based electromechanical power generator to extract kinetic energy from vibrating environment [24]. The design utilizes an electromagnetic transducer and its operating principle is based on the relative movement of a magnet pole with respect to a coil. The approach is suitable for embedded remote microsystem structures with no physical links to the outside world. Power generation of more than 1mW within a volume of 240mm^3 at a vibration frequency of 320 Hz has been obtained.

Duffy and Carroll described a sliding magnet generator placed inside the shoe sole for harvesting energy during human walking [25]. This wire-wound arrangement is composed of two opposing magnets bonded together and a three-segment coil (around 13 mm in diameter, 45 mm in length). This generator was able to produce up to 8.5 mW of power when tested at 5 Hz. It also presented a smaller set of three generators using opposing magnets, one fixed and the other movable with a coil in between, to be placed in the shoe insole. This set delivered up to 230 μW of power at 5 Hz. A later project of Carroll and Duffy improved the design and evaluated a rectification circuit [26], as shown in Fig.2-2. A half-wave and a full-wave rectification circuit were compared with a doubler and quadrupler voltage multiplier; the doubler was found to provide a higher voltage and power output. A six-coil generator with sliding magnets was evaluated at a frequency of 2 Hz, and for this, output voltages of 4 V were recorded. The voltage doubler was found to offer the best performance giving an output power close to 1 mW.

Fig.2-2: The inertial linear-based generators placed inside the shoe sole [26]

Rome had taken a different approach for generating energy from walking. He developed a suspended-load backpack, as shown in Fig.2-3, which scavenges the energy from the up-and-down movement of the carried load when walking [10]. Power output for this device is higher than from inertial generators, reaching up to 7.4 W, but at the expense of bearing heavy loads (38 kg). This was presented as a solution for individuals already carrying such weights with the added advantage that the metabolic work is reduced and the load peak force can be decreased up to 12% when compared to transporting a fixed payload. It is recognized that a person travels an average vertical distance of 5 cm while walking, and if a heavy backpack is used the cargo undergoes the same vertical translation. Thus, this vertical load displacement can be employed for energy scavenging. The author also discusses that this approach generates energy more efficiently than anticipated and reduces the metabolic cost for the human body, even saving battery weight in favor of carrying extra food rations for more power generation.

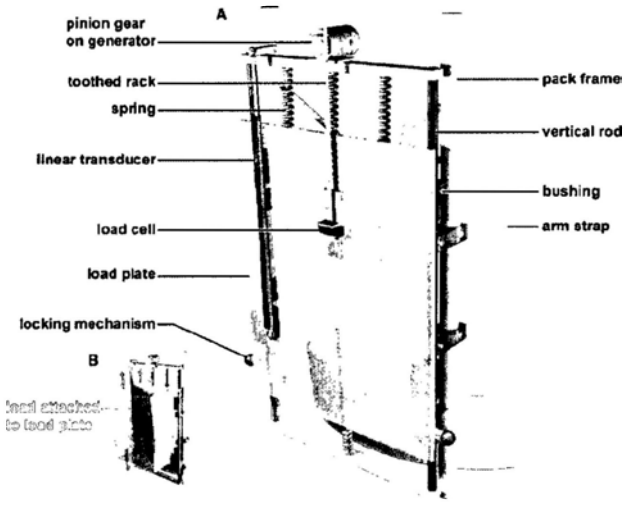

Fig.2-3:The suspended-load backpack, the pack frame is fixed to the body, but the load, mounted on the load plate, is suspended by springs from the frame.

Sasaki presented two energy harvester designs for human-based activities: a rotational and a linear device [27]. The rotational design resembles the one found on the self-winding wristwatches with an integrated miniature generator. Once given the right conditions to produce rotations, this self-excitation can continue in synchronization with the applied input motion generating up to ten times more energy than when only a swinging motion was applied. Although the rotational

generator under swinging motion at 1 Hz was able to produce 15 μW, the self-excited rotational generator was capable of producing 170 μW at 2 Hz. The second design presented was a linear resonant harvester with a natural resonant frequency of 6 Hz and an overall volume of 500 cm^3. It consisted of a permanent magnet suspended by springs surrounded by a 400-turn coil. The reported power output was 90 mW when subjected to the vibration amplitude of 5.5 mm at its natural resonant frequency of 6 Hz.

Wang et al have demonstrated a miniature eight-pole permanent magnet generator with an imbricated-pole stator made with a single wire-wound coil and a four-pair-pole rotor [28], as shown in Fig.2-4. Their aim was to offer an improved generator design (with an energy density increase from about 7.5 mW/cm^3 to 50 mW/cm^3) to be used in self-winding wristwatch-like mechanisms where the kinetic energy of the wearer can drive a high-speed miniature generator. A prototype generating 15 mW/cm^3 was reported. The power output and energy density of this generator are significantly higher than those of the typical two-pole generator from Seiko wristwatches (kinetic brand). The power output generated was 15 mW for a harvester volume of slightly more than 1 cm^3 after being rectified by a Schottky-diode bridge. The generator is rated to operate at 6000 rpm (100 Hz), similar to the operation of the mentioned commercial wristwatch mechanism after the 100-fold increase in speed from its gear train.

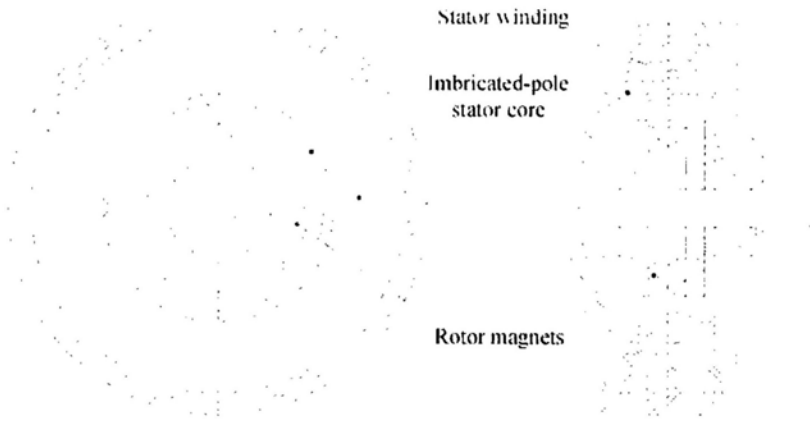

Fig.2-4: Schematic of miniature imbricated-pole permanent-magnet generator [28]

Niu evaluated three human motions (arm swinging, foot movement and trunk displacement) for potential locations of energy scavengers on the human body [29]. A linear electromagnetic generator was placed at the three locations and open-circuit voltage and rectified power measured for battery charging were recorded, as shown in Fig.2-5. A peak voltage of 7 V and an average power output of 10 mW after rectification were reported for a scavenger placed on a swinging arm. For a device placed in a backpack, a peak voltage of about 20 V and a power of 50–80 mW into a battery were mentioned. The generator while worn on a shoe gave an open-circuit output peak voltage close to 27 V and an average power output of 80 mW.

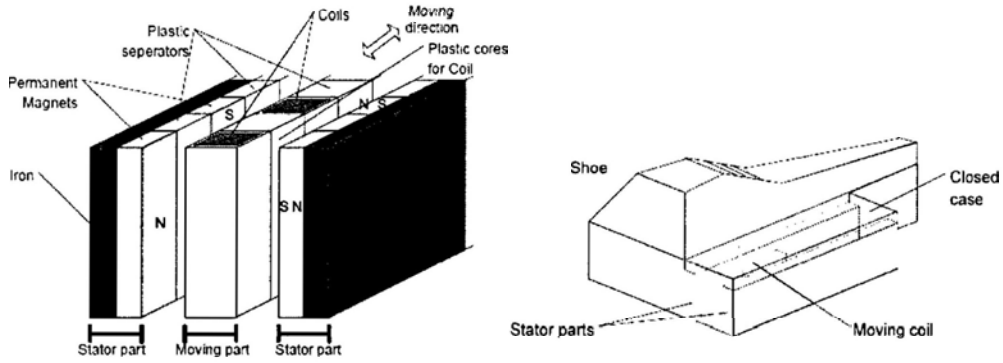

Fig.2-5: General concept for linear PM motion harvester (left) and the foot motion sliding generator topology (right) [29]

Beedy presented a small (component volume 0.1 cm^3, practical volume 0.15 cm^3) electromagnetic generator utilizing discrete components and optimized for a low ambient vibration level based upon real application data [30], as shown in Fig.2-6. The generator uses four magnets arranged on an etched cantilever with a wound coil located within the moving magnetic field. The harvester produces 46 μW in a resistive load of 4 kΩ from just 0.59 m/s^2 acceleration levels at its resonant frequency of 52 Hz.

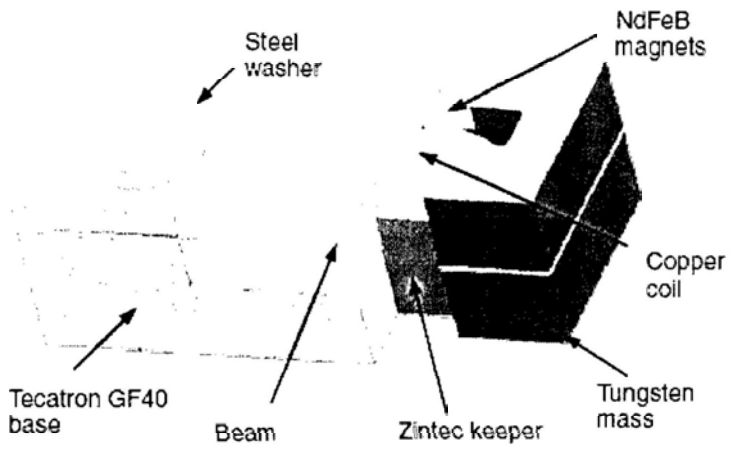

Fig. 2-6: The micro cantilever generator [30]

Von Buren had presented an electromagnetic generator design and its optimization for energy harvesting while walking [31], as shown in Fig.2-7. The device consisted of an air-cored tubular structure (a flexure bearing, and several magnets and coils), as shown in Fig.2-7. The cylindrical arrangement is composed of several stacked magnets with multiple stator coils surrounding them. Optimized scavengers, carrying between 6–9 magnets and 6–10 coils, were analyzed with a generator volume of 0.25 cm^3. The power output varied according to the location of the generator on the human body, but on average 2–25 μW was presented. A 0.5 cm^3 prototype consisting of six magnets and five coils, and 15 mm in length with a diameter of 6 mm, was built to test and validate the results. The prototype when mounted below a person's knee while walking was able to generate a peak power up to 1 mW, and produced 35μW of power on average with an electrical efficiency of 66% to a 10 Ω load.

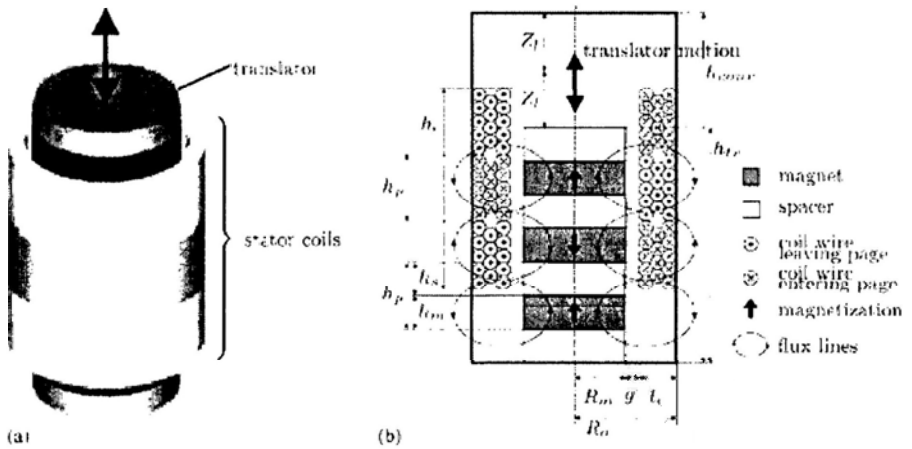

Fig.2-7: Stator and translator of used generator architecture [31]

Donelan Proposed a knee-mounted biomechanical energy harvester to harvest energy during human walking was introduced [11]. A custom knee brace was modified to accommodate a gear train and a small permanent magnet generator with a wire-wound coil, as shown in Fig.2-8. The generator, rather than continuously extracting power while walking, was designed to harness the energy from leg deceleration similar to the regenerative breaking process from hybrid cars. When a person is walking, the gait process is composed of two stages: swing and stance. It is from the swing phase, when the leg is being brought from behind the body and moved forward, that the body spends energy decelerating the leg. When using generative breaking with this device at the knee joint at the right times, the electrical power peaked close to 20W, producing an average 4.8 ± 0.8W of power. The metabolic cost reported for the generative breaking was less than 1 W of metabolic power to produce 1 W of electrical power. In contrast, over 2 W of body work is required to generate 1 W of electrical power for a generator working continuously. However, the weight of each such setup is about 1.5kg, which is obviously not very convenient to use.

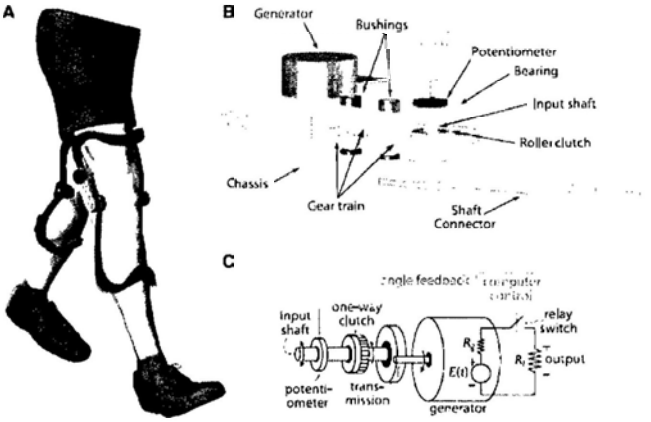

Fig.2-9: The knee-mounted biomechanical energy harvester [11]

Romero (2009) proposed a rotational energy scavenger for human-based activities [32]. The structure of the generator, as shown in Fig.2-10, consists of three main components: an eccentric weight connected to a multipole permanent magnet (PM) ring rotor, a gear-shaped planar coil on the stator and a jewel bearing arrangement. It produces energy by induction when the eccentric weight rotates as a result of an external movement. A preliminary meso-scale prototype (1.5 cm^3, 2.2 g mass)

composed of 20 discrete pole pairs NdFeB PM (5.1mm X 1.1mm X 1.1 mm) inserted in a 25 mm slotted PMMA disc with an eccentric brass mass was constructed and evaluated. A maximum power output of 3.5 μW at 2.8 Hz on a laboratory shaker, and 3.9 μW when placed on the ankle while walking was reported. It was estimated that there will be a tenfold increase for prototypes employing a higher number of printed circuit coil layers.

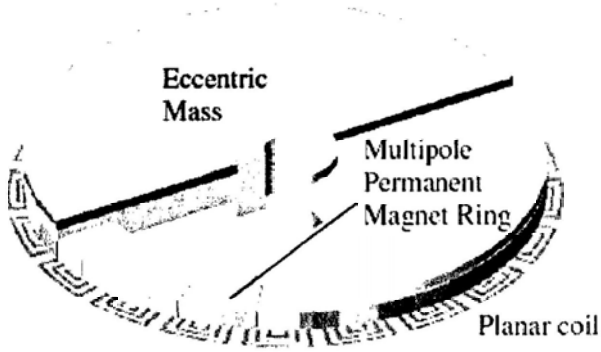

Fig.2-10: The 3D schematic of the axial flux generator [32]

2.2 Piezoelectric Transduction

Piezoelectric materials convert mechanical energy from pressure, vibrations or force into electricity. They are capable of generating electrical charge when a mechanical load is applied on them. This property of piezoelectric materials is considered by the researchers to develop various piezoelectric harvesters in order to power different applications. Due to their inherent ability to detect vibrations, piezoelectric materials have become a viable energy scavenging source. Currently a wide variety of piezoelectric materials are available and the appropriate choice for sensing, actuating, or harvesting energy depends on their characteristics. Some are naturally occurring materials such as quartz. Polycrystalline ceramic is a common piezoelectric material. Lead Zirconate Titanate (PZT) is being considered since it shows a high efficiency of mechanical to electrical energy conversion [33]. With their anisotropic characteristics, the properties of the piezoelectric material differ depending upon the direction of forces and orientation of the polarization and electrodes [34]. Using piezoelectric materials to harvest energy requires a mode of storing the energy generated. This

means they can either implement a circuit used to store the energy harvested or a circuit developed to utilize the energy harvested in producing excess energy [35].

Antaki had reported energy generators using piezoelectric transduction in shoes for powering artificial organs [36]. The generator used two hydraulic cylinders in the insole to activate PZT piezoelectric stacks while walking, as shown in Fig.2-11. Hydraulic pulse amplifiers placed beneath the toes and heel region were employed to convert the low-frequency footfall pulsations into higher frequency pulses. A set of experiments with a 1/17 scale prototype were done to validate this approach. Results under walking conditions produced 150-675 mW, and simulated jogging tests showed 675-2100 mW, for an average power of 5.7 ± 2.2 mW/kg while walking, and 23.6 ± 11.6 mW/kg while jogging. It was estimated that a maximum of 6.2 W could be harvested from a 75 kg individual.

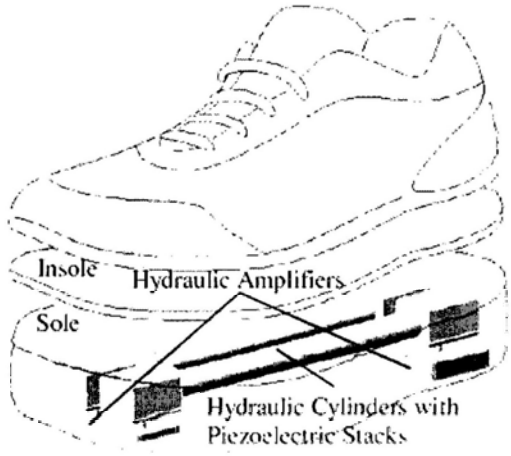

Fig.2-11: The piezoelectric stack actuated by hydraulic amplifiers

Perhaps the most common type of human powered energy generation involves implanting piezoelectric material into shoes. Shoe inserts are attractive not only because of their ability to convert everyday human activity into useful energy, but because of their ease of implementation. Kymissis introduced the concept of parasitic power generation to capture the energy of human body when walking, which is normally wasted or dissipated into the environment [37]. The author presented and compared two piezoelectric designs, as shown in Fig.2-12. The first one consisted of a stack of Polyvinylidinefluoride (PVDF) sheets with a shape similar to a standard

shoe sole for harnessing the bending of the sole. When the PVDF stack is bent, the outside PVDF sheets are stretched into longitudinal extension while the inner sheets are compressed generating a voltage of ± 60 V and an average power output of 1.1 mW. The second generator was designed to harness the pressure exerted by the heel strike. This was made with a Unimorph strip of spring steel bonded to a piezoelectric material sheet (lead zirconate titanate, PZT). When the heel presses and bends the strip of steel, the PZT is under extension, and when the pressure is released, the unimorph springs back. The voltage output peaks up to 150 V and average power outputs of 1.8 mW were reported for this design. In addition to investigating PVDF film in bending mode, Shenck also researched harvesting the energy lost during heel strike using prestressed PZT unimorphs [38]. The research focused on implementing effective power harvesters into shoes while maintaining the design and comfort of the shoe. When testing the so-called PVDF 'stave,' it was implanted into the front of an athletic shoe because of the shoe's toe flexibility. The average power delivered by the stave to a 250 kΩ load at a 0.9 Hz walking pace was 1.3 mW. The PZT unimorphs working off heel strike energy, on the other hand, were implemented into a US Navy work boot because of the boots' rigid heel cup. The so-called PZT dimorph, consisting of two initially curved unimorphs in a clam shell configuration, produced 8.4 mW of power into a 500 kΩ load. Mateu also modeled and tested piezoelectric films inserted into a shoe for harvesting foot strike energy [39, 40].

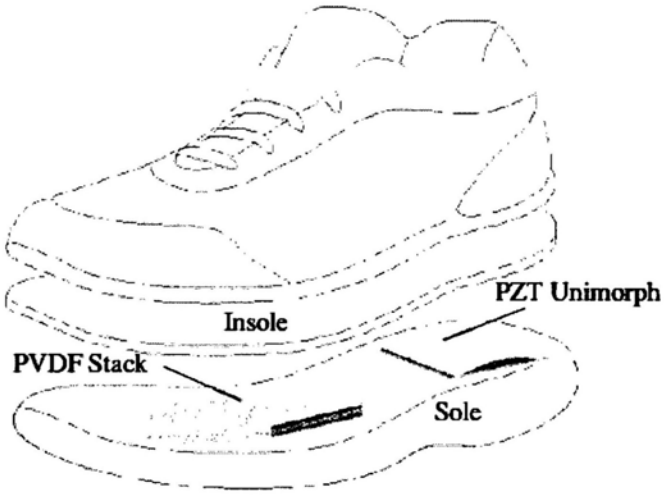

Fig.2-12: A piezoelectric PVDF stack under bending and a PZT unimorph under pressure in a shoe sole

Generators using the impact force of a moving mass hitting a piezoelectric structure have also been developed. Renaud had devised a linear impact-based generator aimed at harvesting energy from human-limb motion [41, 42]. The generator is composed of a free sliding mass (750 mg) inside a frame (12mm×10 mm) with piezoelectric cantilever beams at its ends for a maximum of 10 mm displacement, as shown in Fig.2-13. Every time the mass hits the cantilever beams, they resonate and energy is generated. It has an estimated power output of 40 μW. Further work by Renaud devised a prototype capable of producing 47 μW when rotated every second (25 cm^3 and 60 g), and 600 μW was obtained for a 10 Hz frequency with a 10 cm linear displacement amplitude [43]. Cavallier also presented an impact-based energy harvester using tin balls and piezoelectric cantilever beams inside a 14 mm circular casing that was 2mm high [44]. The package contained eight PZT cantilever beams and four 40 mg tin balls. Testing was done with only one element at 6 Hz producing 62 nW of power. An estimated power output of 0.5 μW would be expected when all the elements on the device are used to generated energy.

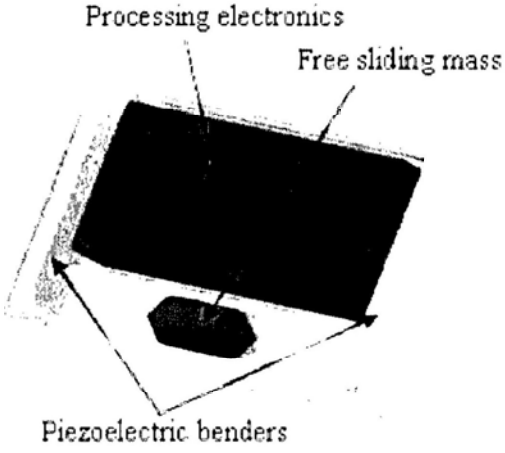

Fig.2-13: The impact-based piezoelectric generators

Platt designed a piezoelectric generator to be placed in the interior of a knee implant for powering orthopedic devices [45, 46], as shown in Fig.2-14. It takes advantage of the fact that the knee can be exposed to forces up to three times higher than the body weight. For this approach, three piezoelectric stacks (1 cm × 1 cm × 2 cm) were placed inside a prototype model for laboratory testing. When applying 900 N of force over Topical Review R51 one piezoelectric stack up to 1.6 mW of raw power was produced, meaning that the three stacks would provide up to 4.8 mW. The entire

prototype was able to produce 850 μW of regulated continuous power with an overall electrical efficiency of 19% and a continuous electromechanical efficiency of 20%.

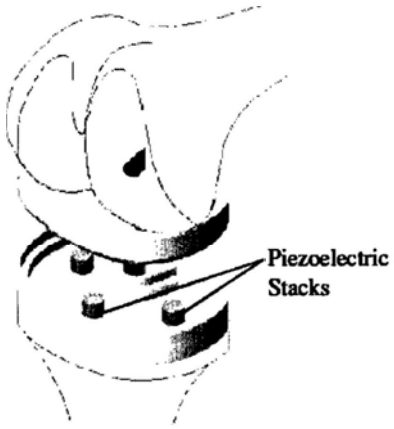

Fig.2-14: Embedded piezoelectric generators inside a knee implant

Feenstra had targeted backpack straps as locations for piezoelectric generators. For this, a piezoelectric stack is placed in series with the backpack straps [47], as shown in Fig.2-15. The tension force that the piezoelectric stack receives from the cyclic loading is mechanically amplified and converted into a compressive load. The average power output measured when walking on a treadmill with a 40 lb load was reported as 176 μW. The maximum power output for the device is expected to be 400 μW.

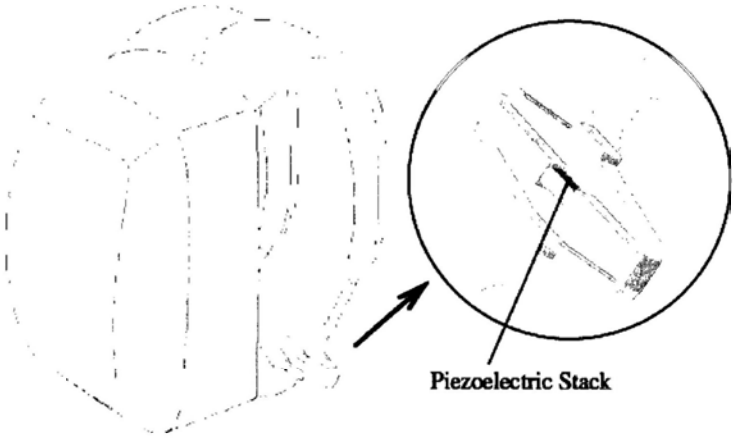

Fig.2-15: Embedded piezoelectric generators in line with backpack straps

2.3 Electrostatic Transduction

Energy harvesting by electrostatic transduction is based on the changing capacitance of vibration-dependent varactor (variable capacitor). Vibrations separate the plates of an initially charged varactor, and mechanical energy is converted into electrical energy. Electrostatic generators are mechanical devices that produce electricity by using manual power [48]. The harvested energy is provided with work done against the electrostatic force between the plates of the capacitor used, as shown in Fig.2-16. If Q, d, l, w, and ϵ are charge on the capacitor, the distance between plates, the length of the plate, the width of the plate, and the dielectric constant respectively in a simple rectangular parallel plate capacitor, then the voltage V across the capacitor is given by the following equation.

$$V = \frac{Q}{C} = \frac{Qd}{\varepsilon lw} \tag{2-1}$$

If the charge Q is held constant, the voltage can be increased by reducing the capacitance C, which can be accomplished either by increasing d, or reducing l or w. Therefore, with the dimensions of capacitor changing, electricity will be produced. Roundy [49] explained the classification of the electrostatic generators into three types which are: in-plane overlap, in-plane gap closing and out-of-plane gap closing [52]. The significant advantage of using the electrostatic converters is their ability to integrate with microelectronics and they do not need any smart material. One of the disadvantages of using electrostatic converters is that they need an additional voltage source to initially charge the capacitor.

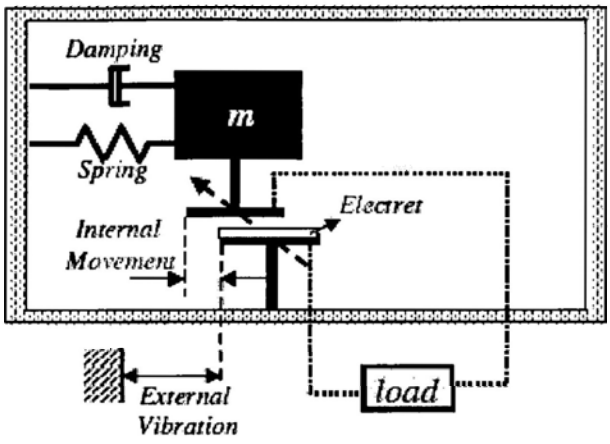

Fig.2-16: The working principle of electrostatic transduction [50]

Tashiro developed a variable-capacitance-type electrostatic generator, employing a honeycomb structure, to harvest the ventricular wall motion [51], as shown in Fig.2-17. The left ventricular wall motion of a dog's heart was measured to test a small prototype designed to resonate at 6 Hz. The prototype consisted of strips of corrugated aluminum evaporated on a polyester film (50 mm × 30 mm × 30 μm) stacked to 50 layers with 20 cells per layer with a 780 g mass on top of the stack. A test setup was constructed with an accelerometer placed on a dog's heart driving the generator with the same motion as the heart. The energy produced was used to pace the same dog's heart at 180 beats per min (bpm) for more than 2 h. An average power output of 36 μW was recorded for a power consumption of 18 μW for the stimulation pulse.

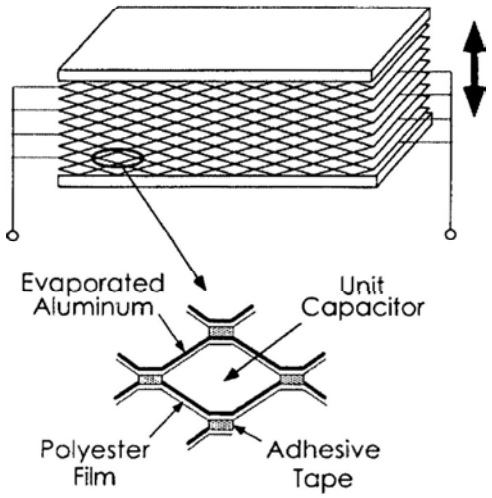

Fig.2-17: Fundamental structure of a honeycomb-type variable capacitor

Mitcheson reported an electrostatic non-resonant prototype using a variable-gap parallel-plate capacitor under a constant charge mode [52, 53]. It was pre-charged to 30 V generating an output voltage of 250 V for an energy generation of 0.3 μJ per cycle. This device design follows the coulomb-force parametric-generator (CFPG) architecture which was described as well suited for large amplitudes and low frequencies. This coulomb-force generator uses the contact force to damp the movement of the parallel plate capacitor. Energy is generated when the inertial force is greater than the damping force. An active capacitor plate area of 200 mm^2 with a proof mass composed of three stacked silicon plates (10 mm × 11 mm × 0.4 mm) with a maximum displacement of about 450 μm was fabricated. A capacitance variation from 15 pF to 127 pF produced a final discharge voltage of 250 V with 11 pF of parasitic capacitance. Miao further developed this non-resonant capacitive energy harvester for biomedical applications [54], as shown in Fig.2-18. This variable capacitor generated energy when the plates were separated due to inertial forces on the proof mass attached to the only moving plate. Energy levels up to 120 nJ were reported per cycle with output voltages up to 220 V. It was theorized that an optimized device operating at 30 Hz can generate about 80 μW or 2.6 μJ per cycle when using silicon as the proof mass material. It was also mentioned that using gold as the proof mass material could produce a tenfold increase in the power output.

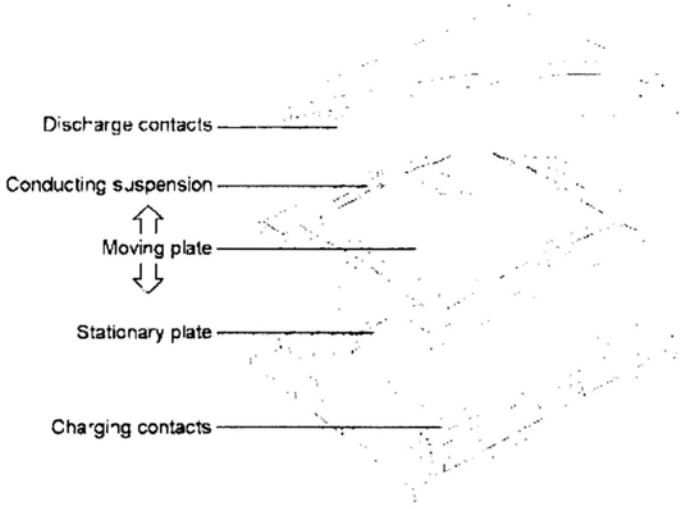

Fig.2-18: Electrostatic generators with variable-gap parallel-plate capacitor [54]

Arakawa presented an electret-based overlapped area capacitor using amorphous perfluoropolymer (CYTOP) as the dielectric [55]. A surface charge density of 0.68

mC/m^2 was obtained producing 6 μW of power with a 1 mm sinusoidal input oscillation at 10 Hz. Tsutsumino further developed this design [56], as shown in Fig.2-19. The electret material was charged through corona discharging for a charge density as large as 1.37 mC/m^2 with an average surface voltage close to 1000 V. The maximum power output was 38 μW tested at 20 Hz with a 2 mm amplitude vibration, and about a 150 V sinusoidal peak-to-peak waveform was measured.

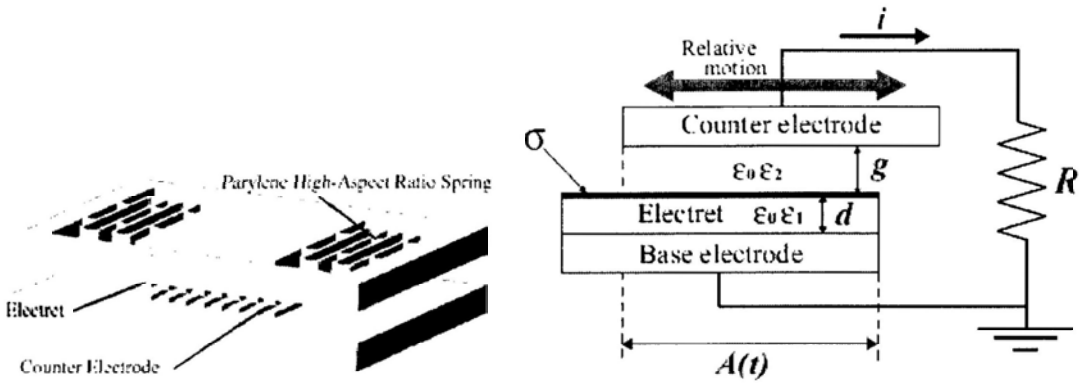

Fig.2-19: Electret generator with overlapped area capacitor

2.4 Comparison and Discussion

From the above discussion, there is little doubt that the field of mechanical energy harvesting from human body continues to expand apace. There are three main approaches that can be used to implement a generator powered by human vibration or movement: electromagnetic transduction, piezoelectric transduction, and electrostatic transduction. Each of the technologies has their own advantages and disadvantages.

The electromagnetic transduction offers a well-established technique of electrical power generation and the effect has been used for many years in a variety of electrical generators. There is a wide variety of spring/mass configurations that can be used with various types of material that are well suited and proven in cyclically stressed applications. Comparatively high output current levels are achievable at the expense of low voltages (typically less than 1 V). High-performance bulk magnets and multi-turn, macro-scale coils are readily available. Wafer-scale systems, however,

are quite difficult to achieve owing to the relatively poor properties of planar magnets, the limitations on the number of turns achievable with planar coils and the restricted amplitude of vibration (hence magnet/coil velocity). Inevitably, there are also problems associated with the assembly and alignment of sub-millimeter scale electromagnetic systems.

The piezoelectric transduction offers the simplest approach, where structural vibrations are directly converted into a voltage output by using an electroded piezoelectric material. There is no requirement for having complex geometries and numerous additional components. Piezoelectric generators are the simplest type of generator to fabricate and can be used in force and impact coupled harvesting applications, but not suitable to used in low-frequency movement. There is a wide range of piezoelectric materials available for different application environments. One major advantage is that this transduction principle is particularly well suited to microengineering, since several processes exist for depositing piezoelectric films (thin and thick). The piezoelectric method is capable of producing relatively high output voltages but only at low electrical currents. The piezoelectric materials are required to be strained directly and therefore their mechanical properties will limit overall performance and lifetime. Also the transduction efficiency is ultimately limited by piezoelectric properties of materials employed. The output impedance of piezoelectric generators is typically very high (>100 kΩ).

The electrostatic transduction is easily realizable as a MEMS and much processing know-how exists on the realization of in-plane and out-of-plane capacitors. Energy density of the generator can be increased by decreasing the capacitor spacing, facilitating miniaturization. The energy density, however, is also decreased by reducing the capacitor surface area. High transduction damping, at low frequencies, is achievable by incorporating small capacitor gaps and high voltages. Unfortunately, electrostatic generators require an initial polarizing voltage or charge. This is not an issue in applications that use the generator to charge a battery, as this can be used to provide the necessary initial excitation level. Electrostatic generators can utilize electrets to provide the initial charge and these are capable of storing charge for many years. The output impedance of the devices is often very high and this makes them less suitable as a power supply. The output voltage produced by the devices is

relatively high (>100 V) and often results in a limited current-supplying capability; this can lead to the requirement for custom circuit implementation processes for the realization of challenging circuit designs. Parasitic capacitances within the structure can sometimes lead to reduced generator efficiency and there is risk of capacitor electrodes shorting or of stiction in wafer-scale implementations.

Piezoelectric and electrostatic transduction mechanisms benefit from microscale fabrication techniques due to the fact that there is no need for complex geometries, and their manufacturing processes are well established. Fabrication of electromagnetic scavengers takes advantage of high-performance bulk magnets and wire-wound coils. However, the micro manufacturing of electromagnetic devices is limited by the performance of thin- and thick-film magnets, and by the fabrication of planar coils with characteristics comparable to structures on the macro-scale. Electromagnetic energy generation is usually associated with low voltages and moderate electrical currents for generators at small scales. Piezoelectric and electrostatic energy generators are the opposite of electromagnetic ones, and they have relatively high voltages and low currents. Therefore, current output is sacrificed for piezoelectric and electrostatic generation at the microscale while voltage is reduced for electromagnetic generators.

Since electrostatic transduction needs separate voltage source for charge the two conductors, it is inconvenient for human use and the additional device to provide the extra voltage will add unnecessary afford to human. Since the piezoelectric transduction mainly converts the mechanical deformation to electricity, it needs high acceleration. Therefore for extracting kinetic energy of human movement, which performs in small acceleration, it will be inefficient to use piezoelectric conversion to harness the human arm motion or footstep motion. For generator in meso scale by electromagnetic transduction, the well-established technology to manufacture the generator can make the manufacturing cost lower. And electromagnetic transduction, via some kind of mass-spring system, can effectively extract human motion both in movement (low frequency and low acceleration) and strike (low frequency and high acceleration). Therefore the electromagnetic transduction is chose to design the harvesters to harness human arm motion and footstep strike.

Chapter 3

The Principle for Harvesting Energetic Motion

Energy harvesting is defined as the conversion of energy already presented in the surrounding environment into usable electrical energy. In this chapter, the mechanical oscillating mechanisms to capture energetic motion and electromagnetic transduction are discussed in detail.

3.1 The Procedure to Design Energy Harvester

There are three main steps to transform mechanical energy into electricity: (1) capture the mechanical energy; (2) convert the captured mechanical energy into electricity by some transducer; (3) rectify the time-variable AC electricity into usable DC electricity. Usually mechanical oscillating mechanism is used to capture human energetic motion, which includes cantilever beam with tip mass, spring-mass, eccentric rotational mass, and their combined system. Since human energetic motion mainly performs in large displacement and small acceleration such as arm motion, or in small displacement and large acceleration such as footstep strike, an optimal motion-captured mechanism should be exploited effectively to convert the human energy. As discussed in the chapter 2, three kinds of transducers: electromagnetic, piezoelectric and electrostatic, can be employed to transducer mechanical energy into electricity. These transducers are not the same for different kinds of mechanical energy, so transduction mechanism should match the performance of energetic motion.

Figure 3-1 summarizes the procedure to harvest mechanical energy. To build an energy harvester, it is first to analyze the performance of the mechanical energy, then to select the most suitable oscillating mechanism to capture energetic motion and transducer. The selection of oscillating mechanism and transducer should be constrained by application place and requirements. The electromagnetic sub-system is connected with mechanical sub-system through the electrical damping force, which is usually expressed as the product of velocity and electrical damping

coefficient, *i.e.* $C_e \cdot \dot{x}$. The electrical damping coefficient exhibits the system ability of converting mechanical energy into electricity. The expression of electrical damping coefficient will be obtained in the electromagnetic analysis, which is necessary before the kinematical performance is conducted. The power output can be obtained by calculating the work done by the electrical damping force in a unit time. Therefore, the power output performance can be analyzed by coupling the electromagnetic and kinematical analysis. From the power output performance, optimization can be carried out to achieve the design goal.

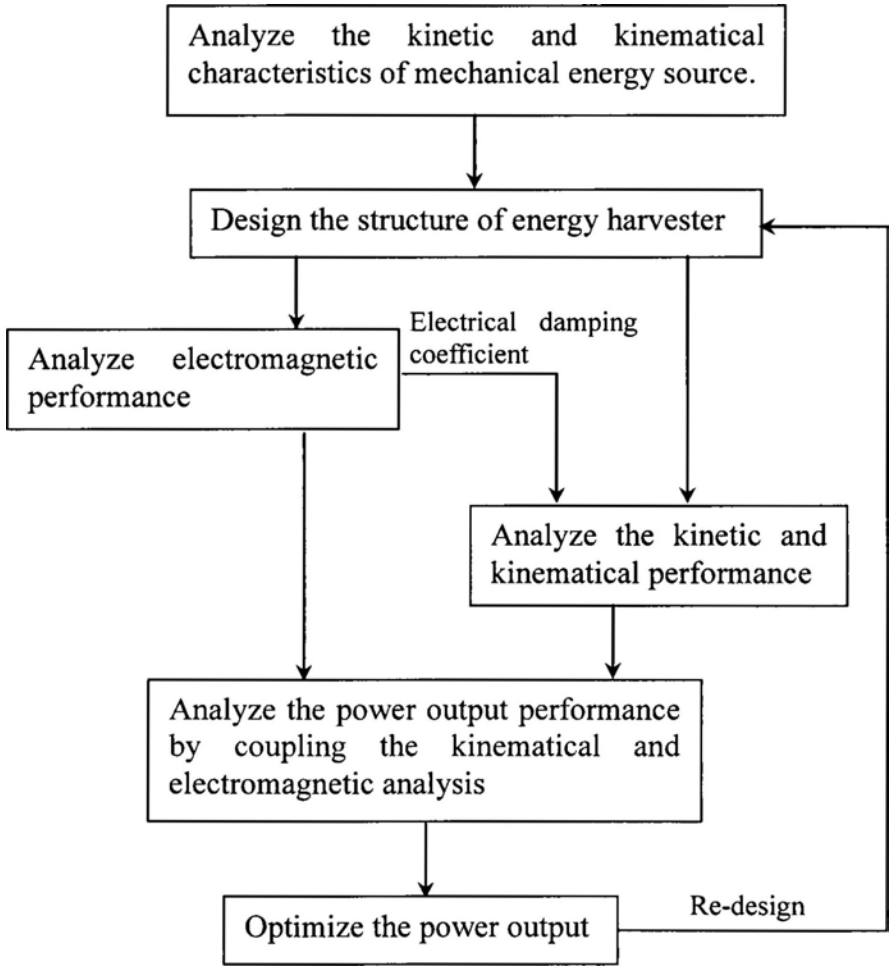

Fig.3-1: The procedure to design and analyze the energy harvester

3.2 Mechanical Oscillating Mechanism

Considering the single degree-of-freedom mechanical oscillating system, mainly including mass-spring system, cantilever beam with tip mass system, and eccentric rotational mass system, three fundamental passive elements should be defined: mass, stiffness and damping. Figure 3-2 shows the simplest mechanical oscillating system, which are composed of mass, spring and damping.

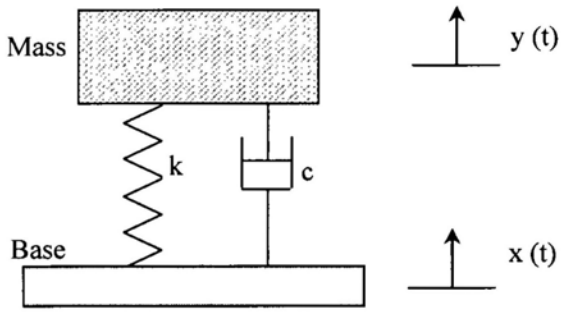

Fig.3-2: A mass-spring oscillating system mounted on a vibration base

Mass, or proof mass, is usually a rigid body in the mechanical oscillating system, whose acceleration is proportional to the resultant **F** of all the forces acting on this body according to the Newton's Law. Here m is the total mass of the body, and **x** is the displacement on the body.

$$\mathbf{F} = m\frac{d^2\mathbf{x}}{dt^2} \tag{3-1}$$

In the case of rotational movement, the displacement $\boldsymbol{\theta}$ has the dimension of rad/s^2, so the constant of proportionality is the moment of inertia of the body noted as I_θ. Therefore the inertia moment $\boldsymbol{\Gamma}$ is expressed as:

$$\boldsymbol{\Gamma} = I_\theta \frac{d^2\boldsymbol{\theta}}{dt^2} \tag{3-2}$$

The stiffness, k, is the resistance of an elastic body to deformation by an applied force, which is a measure of the resistance offered by an elastic body to deformation

(bending, stretching or compression). In the case of linear movement, the stiffness k is the proportionality of the variation of force $\mathbf{F}_k$ applied on the body and deflection produced by force such as the deflection $\Delta\mathbf{x}$ of a beam or the change in length of spring, which is expressed as following. Here the minus sign indicates that the force is opposed to the displacement, which is called restoring force.

$$\mathbf{F}_k = -k\Delta\mathbf{x} \tag{3-3}$$

In the case of rotation around an axis, since the deflection is the change of angular displacement $\Delta\boldsymbol{\theta}$ measured in radian, the restoring force should be replaced by the restoring moment $\boldsymbol{\Gamma}_k$ measured in Newton meter, and their relationship should comply with the following expression. Here the spring constant k_θ should be measured in Newton meter per radian.

$$\boldsymbol{\Gamma}_k = k_\theta\Delta\boldsymbol{\theta} \tag{3-4}$$

Certain systems comprising several elastic elements can be reduced to the simple case of only one spring by calculating its equivalent stiffness. For example, the equivalent stiffness of two springs in parallel is equal to the sum of their stiffnesses, *i.e.* $k_{eq} = k_1 + k_2$. And the inverse of the stiffness of two springs in series is equal to the sum of the inverse of their stiffness, *i.e.* $\frac{1}{k_{eq}} = \frac{1}{k_1} + \frac{1}{k_2}$.

In physics and engineering, damping can be mathematically modeled as a force synchronous with the velocity of the object but opposite in direction to it. If such force is also proportional to the velocity, as for a simple mechanical viscous damper, the force $\mathbf{F}_d$ is related to the velocity $\frac{d\mathbf{x}}{dt}$, expressed as following, where c is the viscous damping coefficient, given in units of Newton-seconds per meter.

$$\mathbf{F}_d = -c\frac{d\mathbf{x}}{dt} \tag{3-5}$$

Similar to the stiffness, the damping in the case of rotation can be expressed as the following equation, where c_θ is the viscous damping constant in rotation and $\mathbf{\Gamma}_d$ is the damping torque. For those systems comprising several damping elements can use an equivalent damping constant c_{eq} to express the system damping factor by the same method as the stiffness, that is, $c_{eq} = c_1 + c_2$ for the parallel case, and $\frac{1}{c_{eq}} = \frac{1}{c_1} + \frac{1}{c_2}$ for the series case.

$$\mathbf{\Gamma}_d = -c_\theta \frac{d\boldsymbol{\theta}}{dt} \tag{3-6}$$

Since the energy harvester is applied to harness the environment vibration, there should be a vibration base to provide energetic motion. As shown in Fig.3-2, the mass-spring oscillating system is mounted on a vibration base, and the base is subject to environment excitation, $x(t)$, which will stimulate the mass-spring system to oscillate and capture the energetic motion from the environment. Usually the environment motion can be expressed as displacement, velocity or acceleration, which will contribute to different kinematical expression.

Suppose the base, in the Fig.3-2 receives an excitation defined by a known acceleration $\ddot{x}(t)$. The excitation is propagated towards the proof mass through the spring and damping, and the proof mass undergoes a response movement $y(t)$. Here, assume the proof mass undergoes a resultant force $\mathbf{F}(t)$, including the gravity force *mg*. Therefore, according to the Newton' Law, the equation for the movement can be expressed as following.

$$m\frac{d^2\mathbf{y}}{dt^2} = -k(\mathbf{y}-\mathbf{x}) - c(\frac{d\mathbf{y}}{dt} - \frac{d\mathbf{x}}{dt}) + \mathbf{F} \tag{3-7}$$

The relative displacement of the mass relative to the base is equal to

$$z(t) = y(t) - x(t) \tag{3-8}$$

Then the Eq.(3-17) can be rewritten as:

$$m\frac{d^2\mathbf{z}}{dt^2} = -k\mathbf{z} - c\frac{d\mathbf{z}}{dt} - m\frac{d^2\mathbf{x}}{dt^2} + \mathbf{F} \tag{3-9}$$

$$\frac{d^2\mathbf{z}}{dt^2} + \frac{c}{m}\frac{d\mathbf{z}}{dt} + \frac{k}{m}\mathbf{z} = -\frac{d^2\mathbf{x}}{dt^2} + \frac{\mathbf{F}}{m} \tag{3-10}$$

If we set

$$\xi = \frac{c}{2m\omega_0} \tag{3-11}$$

$$\omega_0^2 = \frac{k}{m} \tag{3-12}$$

Then Eq.(3-10) becomes

$$\frac{d^2\mathbf{z}}{dt^2} + 2\xi\omega_0\frac{d\mathbf{z}}{dt} + \omega_0^2\mathbf{z} = -\frac{d^2\mathbf{x}}{dt^2} + \frac{\mathbf{F}}{m} \tag{3-13}$$

Here, ω_0 is the natural frequency, or angular frequency, of the system measured in radians per second; ξ is the damping factor or damping ratio, which is

$$\xi = \frac{c}{2\sqrt{km}} \tag{3-14}$$

Therefore, if the acceleration of the base is given and the resultant force of external force is known, then from the Eq.(3-13) the relative response of proof mass can be obtained.

If the excitation is known in displacement $x(t)$ of the base, then the Eq.(3-7) is rewritten as:

$$\frac{d^2\mathbf{y}}{dt^2} + 2\xi\omega_0\frac{d\mathbf{y}}{dt} + \omega_0^2\mathbf{y} = 2\xi\omega_0\frac{d\mathbf{x}}{dt} + \omega_0^2\mathbf{x} + \frac{\mathbf{F}}{m} \tag{3-15}$$

Therefore, the absolute response of the proof mass can be resolved from the above equation.

If the excitation is known in velocity $\dot{x}(t)$ of the base, then by differentiating the Eq.(3-15), one obtains:

$$\frac{d^2\dot{\mathbf{y}}}{dt^2} + 2\xi\omega_0 \frac{d\dot{\mathbf{y}}}{dt} + \omega_0^2 \dot{\mathbf{y}} = 2\xi\omega_0 \frac{d\dot{\mathbf{x}}}{dt} + \omega_0^2 \dot{\mathbf{x}} + \frac{\dot{\mathbf{F}}}{m} \tag{3-16}$$

So from the above equation, the response in absolute velocity of the proof mass can be resolved.

From the Eqs.(3-13), (3-15), and (3-16), there is a common form as following,

$$\frac{d^2\mathbf{u}}{dt^2} + 2\xi\omega_0 \frac{d\mathbf{u}}{dt} + \omega_0^2 \mathbf{u} = \boldsymbol{\psi}(t) \tag{3-17}$$

Here, $\mathbf{u}$ is the response of the proof mass from the known external excitation in some kind of forms, and $\boldsymbol{\psi}(t)$ is the total excitation including the external force and base excitations. When the excitation can be expressed in a suitable analytical form, the above second order differential equation can be explicitly solved for $\mathbf{u}(t)$ by universal mathematical methods such as Laplace transform. However, in most cases, there exists an analytical expression for the excitation, so some numerical method should be used to obtain the response, such as Runge-Kutta method. Before solving the second order differential equation, the relative damping coefficient ξ should be determined, whose value can affect the response performance of the proof mass.

Another mechanical oscillating system of a cantilever beam with tip mass can be also applied to harvest environment vibration. As shown in Fig.3-3, there is a cantilever beam with concentrated mass at the end. Such oscillating system can be equivalent to lumped spring mass system of a vibrating rigid body, whose characteristic parameters can be described by damping constant c_{eq} and stiffness constant k_{eq}. For the one end mounted cantilever with a tip mass at the end, the stiffness is given by $k_{eq} = \frac{3EI}{L^3}$, where E is the modulus of elasticity, I is the moment of inertia, and L is the length of beam. The moment of inertia for a rectangular cross-sectional can be obtained by

$I = \frac{bh^3}{12}$, where b and h are the width and thickness of the beam in transverse direction, respectively. For the cantilever beam with external excitation on the base, the governing equation of motion can also rewritten as following, similar to that of spring-mass oscillating. Through transformation, Equation (3-18) be rewritten into that of Eq.(3-17).

$$m\frac{d^2\mathbf{y}}{dt^2} = -k_{eq}(\mathbf{y}-\mathbf{x}) - c_{eq}(\frac{d\mathbf{y}}{dt} - \frac{d\mathbf{x}}{dt}) + \mathbf{F} \tag{3-18}$$

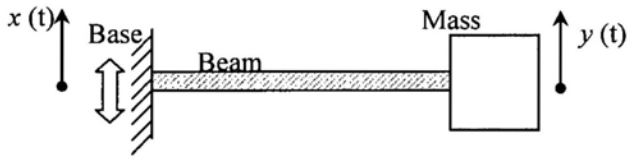

Fig.3-3: the cantilever beam with concentrated mass at the end

For the beam on two simple supports, with a concentrated mass at the middle, it can also be equivalent as a mass spring oscillating system, which has the same governing equation of motion as Eq.(3-18). The stiffness of such double support beam should be calculated by $k_{eq} = \frac{48EI}{L^3}$.

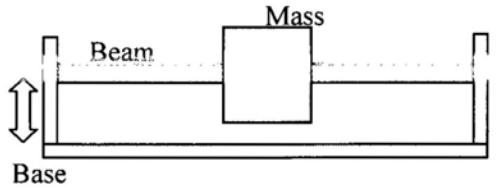

Fig.3-4: the beam on two simple supports, with a concentrated mass at the middle

An eccentric rotational mass placed in the plumb plane forms an oscillating system with the gravity force. As shown in Fig.3-5, the eccentric rotational mass is contained in a vibration base and rotates around the base center. Since it is a rotation system, work is only done on the tangential direction. Therefore, considering the forces on the tangential direction, there are the damping force and the projection of the gravity force. Here the gravity force acts as the restoring force, likely the spring in the mass

spring oscillating system. Suppose the base excitation is $\alpha(t)$, and the response of the rotational mass is $\beta(t)$, and the damping coefficient is notated as c_θ measured in Newton-meter per radian. Then the governing equation of motion can be expressed as following.

$$mr\frac{d^2\beta}{dt^2} = -c_\theta(\dot{\beta}-\dot{\alpha}) - mg\sin\beta \tag{3-19}$$

Here, r is the distance from the axis to the center of mass. If the angular displacement of mass response is small, $\sin\beta$ is approximated to β, and then the above equation can be rewritten as following.

$$\frac{d^2(\beta-\alpha)}{dt^2} + \frac{c_\theta}{mr}\frac{d(\beta-\alpha)}{dt} + \frac{g}{r}(\beta-\alpha) = -\frac{d^2\alpha}{dt^2} - \frac{g}{r}\alpha \tag{3-20}$$

Let $2\xi\omega_0 = \frac{c_\theta}{mr}$, $\omega_0^2 = \frac{g}{r}$, $\psi(t) = -\frac{d^2\alpha}{dt^2} - \frac{g}{r}\alpha$ and $\gamma = \beta - \alpha$, then the above equation is rewritten as following, which is the same as the form of Eq.(3-17).

$$\frac{d^2\gamma}{dt^2} + 2\xi\omega_0\frac{d\gamma}{dt} + \omega_0^2\gamma = \psi(t) \tag{3-20}$$

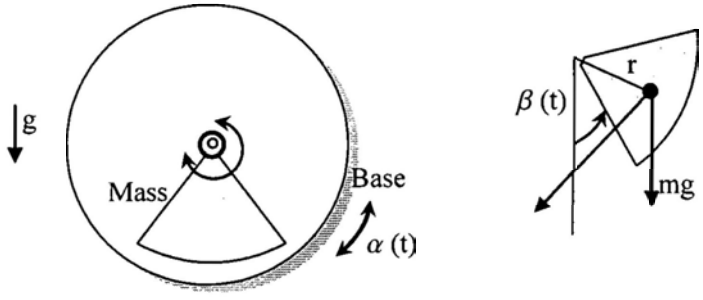

Fig.3-5: Eccentric rotational mass system and the notation for analysis

From the above discussion, mechanical oscillating systems have almost the same form of governing equation of motion. These three kinds of oscillating systems can combine to improve the harness efficiency or achieve other design goal.

3.3 Electromagnetic Transduction

Energy harvesting from electromagnetic transduction is based on the induced voltage on a coil by a change of the magnetic flux through that coil. Figure 3-6 provides a general schematic for the basic operating principle of the electromagnetic transducer. Voltage *v(t)* is induced by a change in the magnetic environment. This change is manifested in a variety of techniques such as magnetic field strength fluctuation, drawing coils in and out of magnetic field, and rotating the coils relative to the magnetic field. The amount of power generated depends on the strength of the magnetic field, the number of turns of the coil and the rate of change of the magnetic flux density through the coil due to the external input movement source.

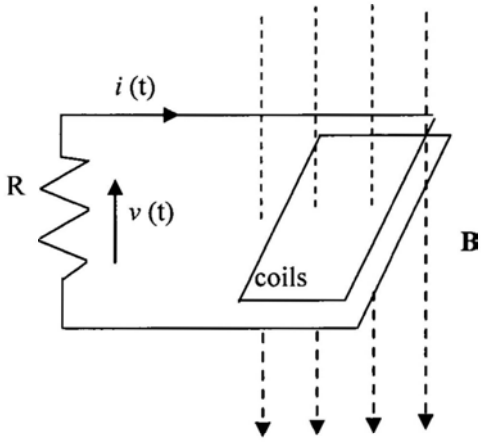

Fig.3-6: The schematic diagram for electromagnetic transduction

According to the Faraday's law, the induced voltage is given in the Eq. (3-21) for any case, where, ε is the induced electromotive force, and Φ_B is the magnetic flux density. For the case of moving coils in a uniform magnetic field, the induced voltage can be calculated by Eq. (3-22), N is the number of turns in the coil, B is the strength of the magnetic field, l is the length of one coil, and y is the distance the coil moves through the magnetic field.

$$\varepsilon = -\frac{d\Phi_B}{dt} \tag{3-21}$$

$$V_{oc} = NBl\frac{dy}{dt} \tag{3-22}$$

In the application of energy harvester, the analytical expression or value of the magnetic flux density may be different to know. However, in order estimate the power output performance or to conduct the optimization procedure, the magnetic flux density should be obtained. Therefore, alternative methods should be used. Analysis with FEA software, such as Ansys®, should a good method to analyze the magnetic field. Analyzing magnetic field by Ansys, a FEA model should be built and import into Ansys firstly, and then apply material properties and other information to the FEA model. After meshing the FEA model, it can be solved to view the analysis results and to measure and export necessary information. Figure 3-7 shows the FEA model and analysis results conducted in Anays. And Figure 3-8 shows the measurement and export of the simulation result.

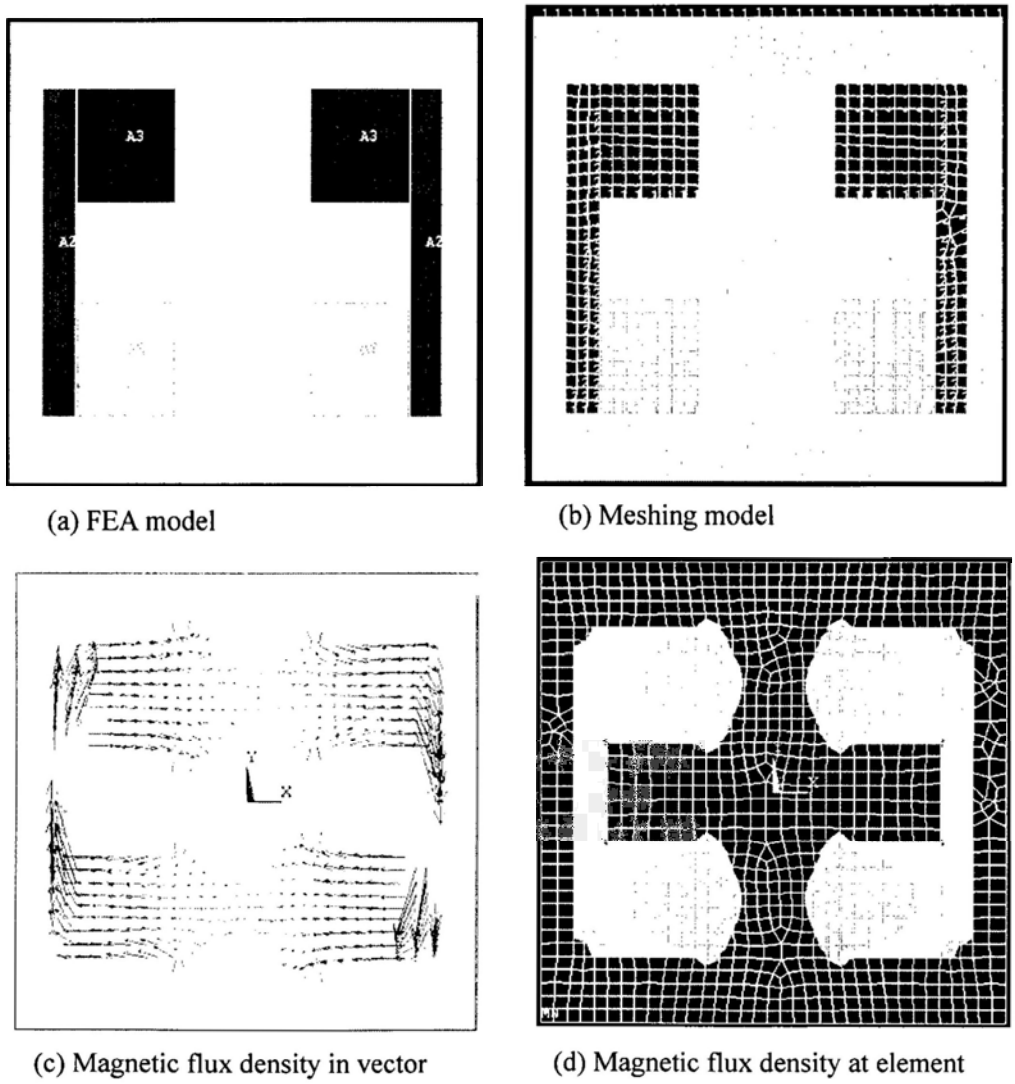

(a) FEA model

(b) Meshing model

(c) Magnetic flux density in vector

(d) Magnetic flux density at element

Fig. 3-7: FEA model and solving results

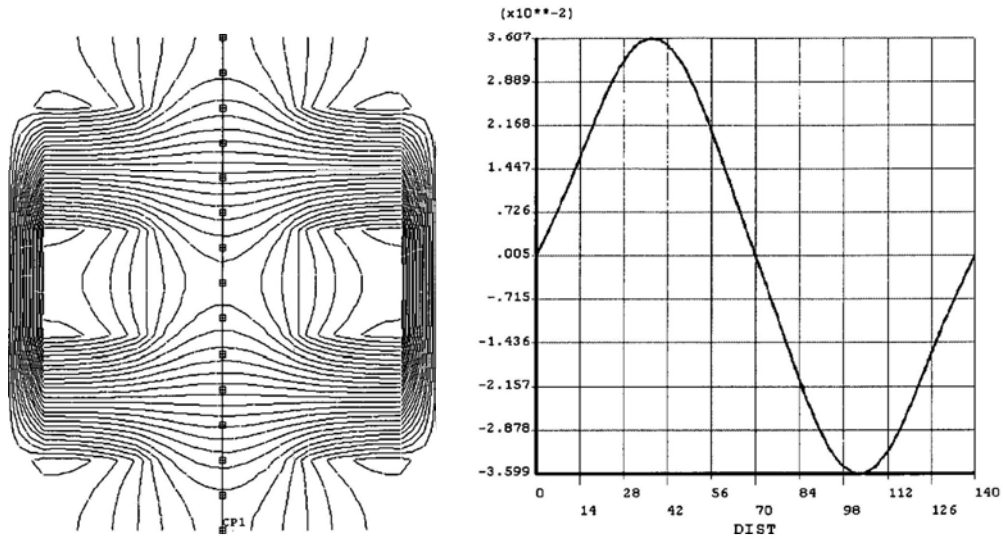

Fig.3-8: Measure and export of the simulation result

There is another method, magnetic equivalent circuit (MEC), to analyze the magnetic field. The basic idea of MEC method is to model the magnetic source, such permanent magnets, as the voltage in the electrical circuit, and model the flux path reluctance as the resistance. Thus the flux through the path can be solved as current in the electrical circuit. A magnetic structure and its MEC model are shown in Fig.3-9.

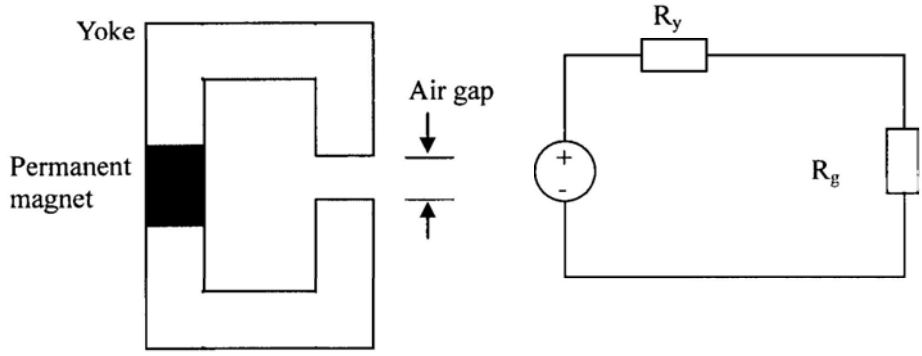

Fig.3-9: A magnet structure and its MEC model

In the MEC model, the permanent magnet is modeled as a voltage V_{pm}, i.e. magnetomotive force:

$$V_{pm} = \frac{B_r W_m}{\mu_m} \tag{3-23}$$

Where, B_r is the permanent magnet residual flux density, W_m is the width of the magnet, and μ_m is the permanent permeability. The reluctance of the flux path in the magnetic structure is computed by:

$$R_y = \frac{W_y}{\mu_y LD} \tag{3-24}$$

Where, W_y, L, and D are the width, total length and depth of the yoke, respectively, and μ_k is the yoke material permeability. Similarly, the reluctance of the flux path in the air gap is computed by:

$$R_g = \frac{W_g}{\mu_g L_g D} \tag{3-24}$$

Where, L_g is the air path length and μ_g is the air permeability. Therefore, the total flux through the path can be computed by:

$$\Phi = \frac{V_{pm}}{R_y + R_g} \tag{3-25}$$

Chapter 4

The Automatic Winding Mechanism for Energy Harvesting from Arm Motion

Invented more than two hundred years ago, the automatic winding device of mechanical watch movement is one of the most successful energy harvesting devices. It harvests the kinematical energy from body movements and drives the mechanical watch movement. According to the literatures, however, few have studied its kinematics in details. In this chapter, with following the ETA's design, the kinematical model of automatic winding device is firstly analyzed and simulated. The model is a pendulum model with a set of gears that converts the bidirectional motion to unidirectional motion. The simulation shows that the efficiency of the device is about 46.3%. Experiment validations are also conducted, which confirms the simulation results. With some modifications, it can be used to drive various mobile electronic devices.

4.1 Introduction

The automatic winding device of mechanical watch movement is one of the most successful energy harvesting devices. The first self-winding watches were invented in 1770 in Switzerland [58].The energy produced by the movements of wearer's arm are captured using an asymmetric oscillating weight (the rotor) and transmitted through a reduction gear train to wind up the mainspring, as shown in Figure 4-1. The external movement, i.e., the movement of the arm, is the energy source. With the arm swinging, the oscillating weight rotates to drive the train wheels, and finally winds the main spring in the barrel storing the potential energy in the mainspring. As illustrated in Fig. 4-1, this system can be regarded as a double pendulum, where the swinging arm is the upper pendulum pivoted at the shoulder (point *O*), and the oscillating weight is the lower pendulum pivoted at the oscillating bearing.

Throughout the years, several kinds of automatic winding devices have been invented [59, 60]. However, few have studied their kinematical performance in

details. This paper focuses on a particular kind of automatic winding device and develops a kinematical model to study its performance.

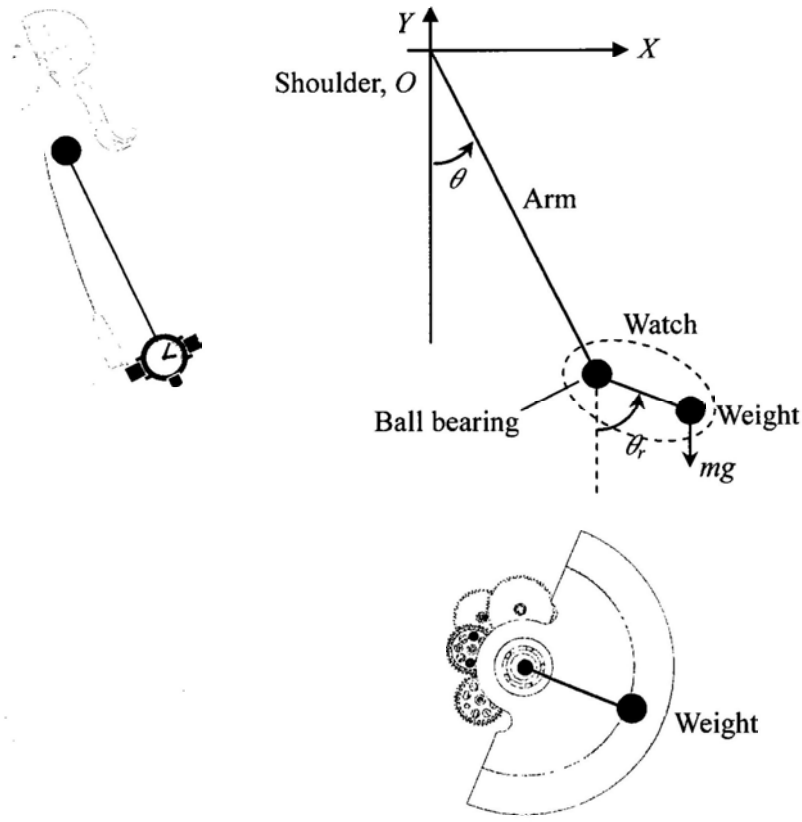

Fig. 4-1: The working of an automatic winding device

4.2 The Model of the Automatic Winding Device

We studied a kind of automatic winding device developed by ETA Inc. [61]. It mainly comprises an asymmetric oscillating weight mounted on a bearing acting as the rotor, and a gear train to transmit the motion to the mainspring; both of them are mounted onto a framework to keep their relative positions. Figures 4-2 and 4-3 show the CAD model of the automatic winding device in front and back. This device can harvest the energy from the movements in both directions (clockwise and counterclockwise), because of its ingenious gear train design as shown in Fig. 4-4. It includes two special pawl-wheels that transfer the bidirectional movement to unidirectional movement. A stop mechanism is also included to prevent the wounded

mainspring from turning back. When the mainspring is completely wound, this friction-based mechanism keeps it from being over-wounded.

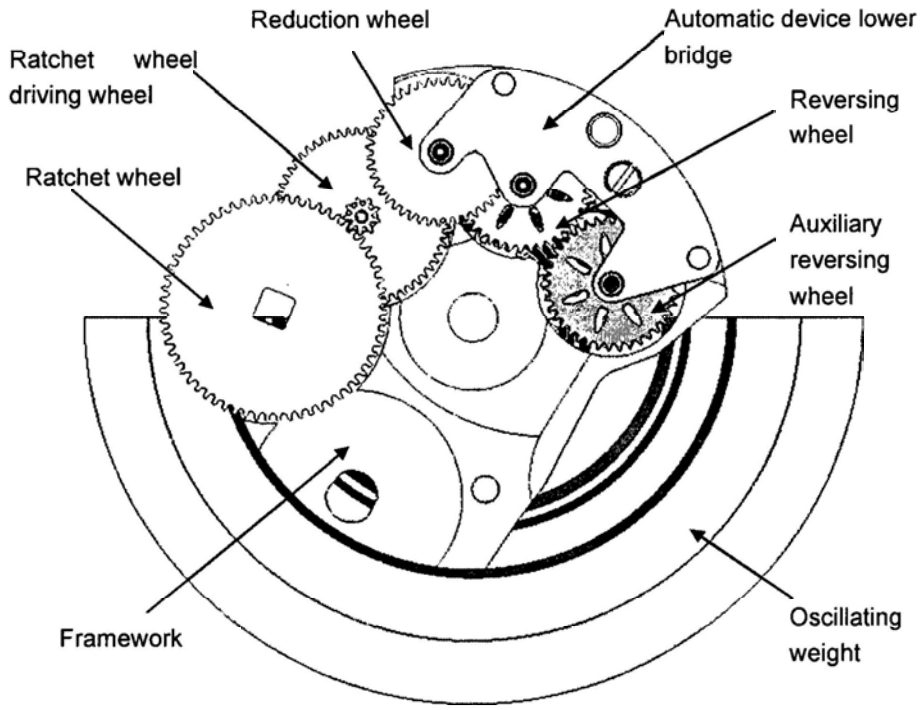

Fig. 4-2: The CAD model of the automatic winding device, front view

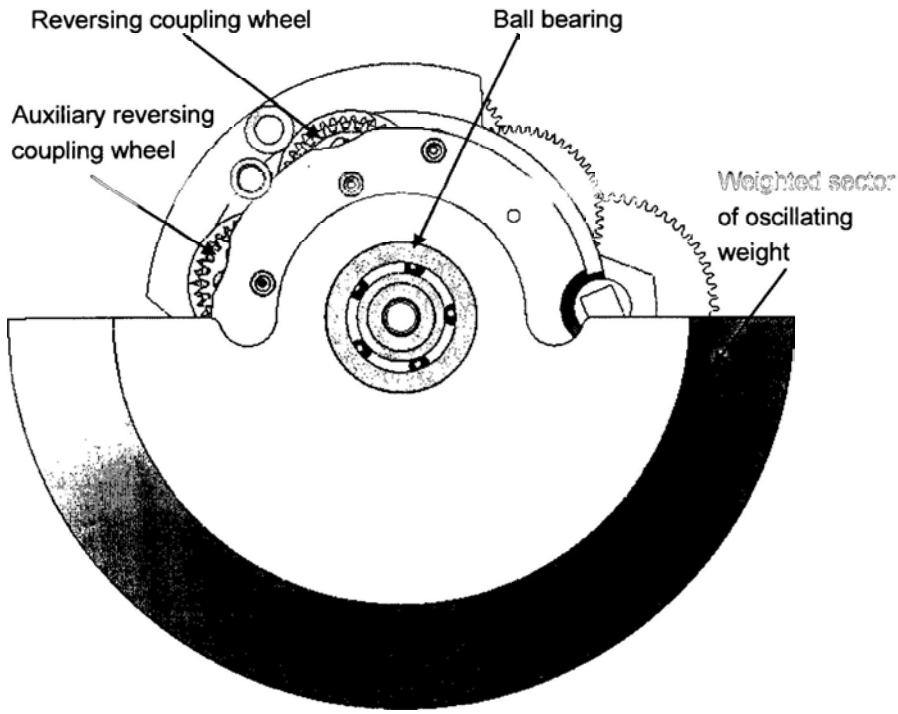

Fig. 4-3: The CAD model of the automatic winding device, back view

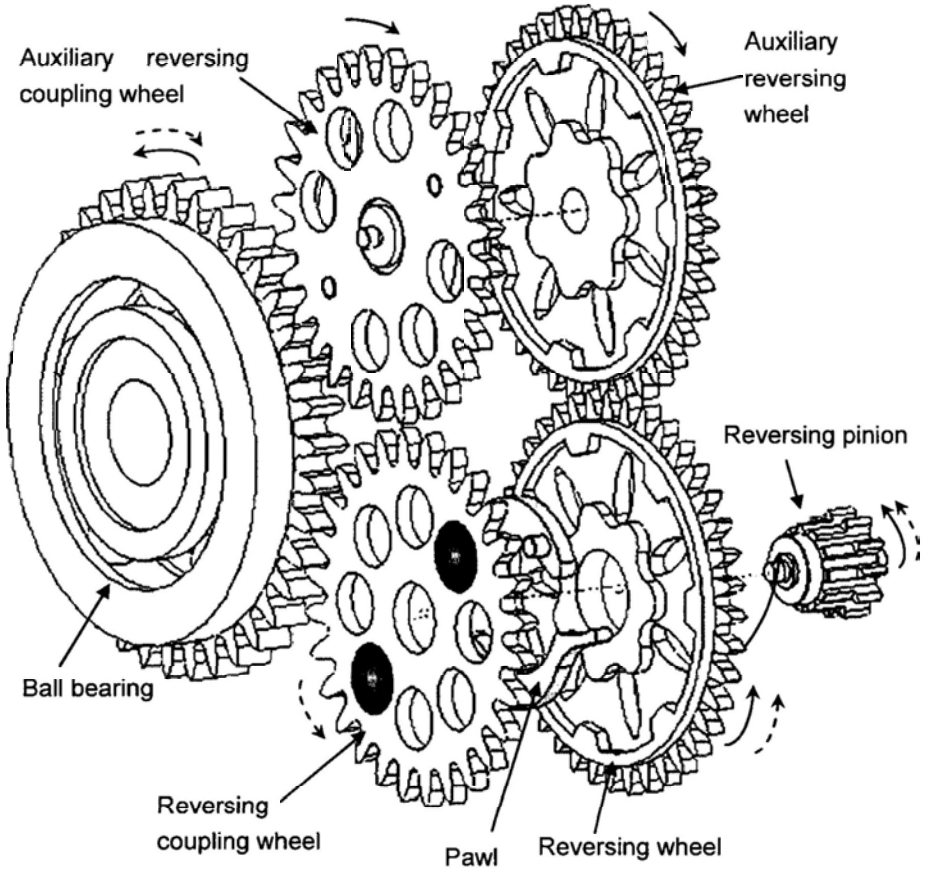

Fig. 4-4: Illustration of the reversing mechanism

Specifically, as soon as the wearer's arm moves the oscillating weight swings around its pivot at the center of the watch due to its moment of inertia. The oscillating weight contains two parts: the support part must be flexible to absorb the received shocks, while the weighted part is responsible to produce a high moment. The rotations are transmitted to the gears connected to the ball bearing. The ball bearing guarantees minimum friction and the gear transmits the motion to the two coupling wheels. The two coupling wheels are a part of the reversing mechanism. The reversing mechanism is designed to convert the swing (the bidirectional swinging) to the unidirectional rotation. As shown in Fig. 4-4, the reversing mechanism consists of an auxiliary reversing wheel, an auxiliary reversing coupling wheel, a reversing coupling wheel, a reversing wheel, and four pawls. Both the auxiliary and the reversing coupling wheels with their pawls must transmit the moment when the oscillating weight is turning in one direction (counterclockwise for the auxiliary coupling wheel and clockwise for the reversing coupling wheel) and uncouple the mechanism when the oscillating weight is turning in the other direction.

When the oscillating weight turns counterclockwise (see the solid arrow), the auxiliary reversing coupling wheel turns clockwise and drives the auxiliary reversing wheel turning clockwise through the pawls. The auxiliary reversing wheel then drives the reversing wheel and the reversing pinion turning counterclockwise. On the other hand, the reversing coupling wheel also turns; though, its multi-cam profile makes the pawls slide over. As a result, the reversing wheel will not be moved. In other words, the reversing coupling wheel is effectively decoupled from the reversing wheel at this moment. Similarly, when the oscillating weight turns clockwise (see the dashed arrow), the auxiliary reversing coupling wheel turns counterclockwise, but its multi-cam profile makes the pawls slide over. As a result, the auxiliary reversing coupling wheel and the auxiliary reversing wheel are decoupled. On the other hand, the reversing coupling wheel turns counterclockwise and drives the reversing wheel and the reversing pinion turns counterclockwise through the pawls. Note that in both cases, the reversing pinion.

In order for the automatic winding device to function well, a reduction gear train is used to increase the force for winding the mainspring. Starting from the reversing pinion, the reduction gear train includes a reduction wheel, a ratchet driving wheel and a ratchet wheel (refer to Figure 4-7). As a rule in the watch making industry, the reduction ratio of the ratchet and the oscillating weight is between 1:110 and 1:180 [13]. The ratchet wheel transmits the movement and the force to wind the mainspring in the barrel. If the ratchet wheel turns by a certain angle the mainspring turns the same angle as well.

4.3 The Kinematical Model

From a physical point of view, the automatic winding device can be modeled by a double pendulum in the *XOY* plane. As shown in Fig. 4-5, the swinging arm can be considered as the upper pendulum pivoted at the shoulder, and the rotor (the oscillating weight) can be considered as the lower pendulum pivoted at the ball bearing. The angle θ is the angle of upper pendulum and θ_r is the angle of the rotor.

For convenience, following symbols are introduced:

M – the mass of upper pendulum;

m – the mass of rotor;

L – the length of the upper pendulum;

r – the distance from the center of rotor to the center of mass of the rotor;

(x_1, y_1) – the coordinate of the end of arm, which is also the pivot of rotor;

(x_2, y_2) – the coordinate of the center of mass of the rotor;

θ – the swinging angle of the arm (0 is vertical downward, and positive in counter-clock direction)

θ_r – the swinging angle of rotor (0 is vertical downward, and positive in counter-clock direction)

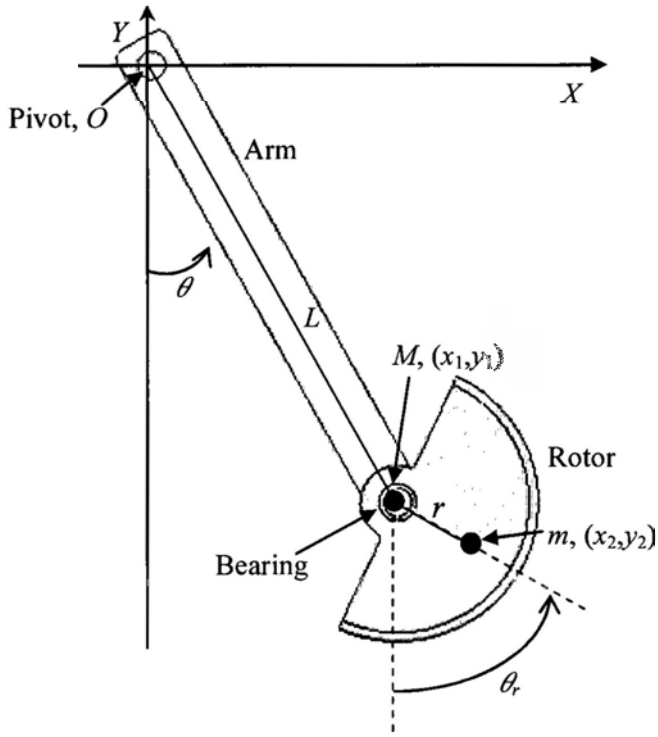

Fig. 4-5: Schematic diagram of winding system when arm is swinging

In the model, the upper pendulum rod is regarded as massless and rigid with a point mass M at the end, and the rotor is also considered as point mass. By trigonometry, the following four expressions can be deduced to express the positions x_1, y_1, x_2, y_2 in terms of the angles θ and θ_r.

$$\begin{cases} x_1 = L\sin\theta \\ y_1 = -L\cos\theta \\ x_2 = x_1 + r\sin\theta_r \\ y_2 = y_1 - r\cos\theta_r \end{cases} \tag{4-1}$$

Subsequently, it follows:

$$\begin{cases} \dot{x}_1 = L\dot{\theta}\cos\theta \\ \dot{y}_1 = L\dot{\theta}\sin\theta \\ \dot{x}_2 = \dot{x}_1 + \dot{\theta}_r r\cos\theta_r \\ \dot{y}_2 = \dot{y}_1 + \dot{\theta}_r r\sin\theta_r \end{cases} \tag{4-2}$$

$$\begin{cases} \ddot{x}_1 = -L\dot{\theta}^2\sin\theta + L\ddot{\theta}\cos\theta \\ \ddot{y}_1 = L\dot{\theta}^2\cos\theta + L\ddot{\theta}\sin\theta \\ \ddot{x}_2 = \ddot{x}_1 - \dot{\theta}_r^2 r\sin\theta_r + \ddot{\theta}_r r\cos\theta_r \\ \ddot{y}_2 = \ddot{y}_1 + \dot{\theta}_r^2 r\cos\theta_r + \ddot{\theta}_r r\sin\theta_r \end{cases} \tag{4-3}$$

The force diagram of the system is shown in Fig. 4-6. The forces acted on the upper pendulum include the tension from the upper rod T_1, the tension from the lower rod T_2, and the gravity force Mg. The forces acted on the lower pendulum include the tension from the lower rod T_2, and the gravity force mg. According to Newton's law, following equations can be deduced. Note that both the friction of the upper pendulum and the friction of the lower pendulum are very small and thus, have been neglected.

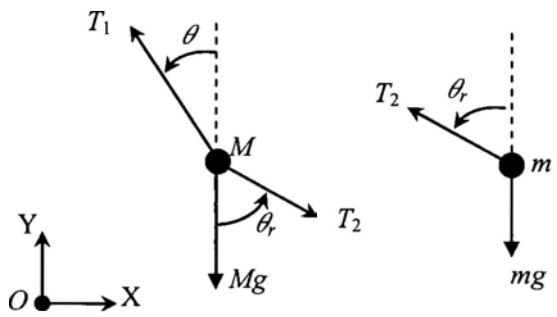

Fig. 4-6: The force diagram of the system

$$M\ddot{x}_1 = -T_1 \sin\theta + T_2 \sin\theta_r \tag{4-4}$$

$$M\ddot{y}_1 = T_1 \cos\theta - T_2 \sin\theta_r - Mg \tag{4-5}$$

$$m\ddot{x}_2 = -T_2 \sin\theta_r \tag{4-6}$$

$$m\ddot{y}_2 = T_2 \cos\theta_r - Mg \tag{4-7}$$

When there is no external input, from Eq. (4-1) ~ (4-7), the angular acceleration of the upper and lower pendulum can be derived:

$$\begin{cases} \ddot{\theta} = \dfrac{-g(2M+m)\sin\theta - mg\sin(\theta-2\theta_r) - 2\sin(\theta-\theta_r)m(\dot{\theta}_r^2 r + \dot{\theta}^2 L\cos(\theta-\theta_r))}{L(2M+m-m\cos(2\theta-2\theta_r))} \\ \ddot{\theta}_r = \dfrac{2\sin(\theta-\theta_r)(\dot{\theta}^2 L(M+m) + g(M+m)\cos\theta + \dot{\theta}_r^2 rm\cos(\theta-\theta_r))}{r(2M+m-m\cos(2\theta-2\theta_r))} \end{cases} \tag{4-8}$$

This double pendulum system may undergo chaotic motion, and exhibits a motion pattern that is dependent on the initial condition of θ and θ_r. Though, if the initial conditions satisfies the following inequality [62],

$$3\cos\theta + \cos\theta_r \geq 2 \tag{4-9}$$

Then it is energetically impossible for either pendulum to flip, that is, the system must be stable. In our study, the initial values of θ and θ_r satisfy Eq. (4-9). Moreover, Eq. (4-8) can be solved by numerical methods, such as the Runge-Kutta method.

In practice, the upper pendulum (the swinging arm) acts as the energy input, while the lower pendulum, the rotor, is the output. In other words, θ is the input, while θ_r is the output. Assume the input θ is a sinusoidal function, that is $\theta = a\sin(\omega t)$, then the output function θ_r can be solved from the following equation:

$$\begin{cases} \theta = a\sin(\omega t) \\ \ddot{\theta}_r = \dfrac{2\sin(\theta-\theta_r)(\dot{\theta}^2 L(M+m) + g(M+m)\cos\theta + \dot{\theta}_r^2 rm\cos(\theta-\theta_r))}{r(2M+m-m\cos(2\theta-2\theta_r))} \end{cases} \tag{4-10}$$

In this case, only θ_r is unknown, and it can be solved by ODE method.

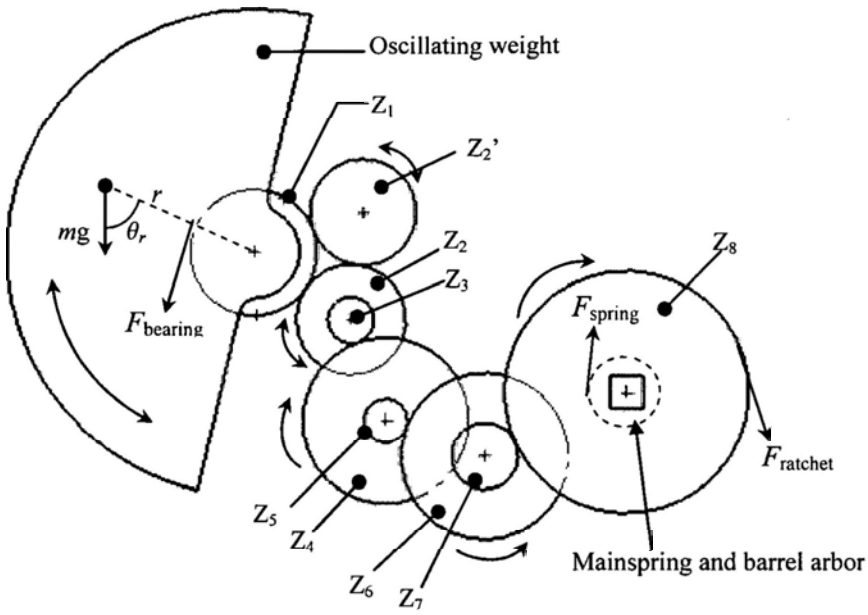

Fig. 4-7: The gear train of the automatic winding device

Shown as the Fig.4-7, the reduction gear train consists of four gear sets. The motion is generated by the oscillating weight which is fixed with the gear bearing (Z_1). The gear Z_1 drives the reversing mechanism (Z_2) and auxiliary reversing mechanism (Z_2'). As stated in section 4.2, these two mechanisms have almost the same structures which can convert the bi-directional motion of oscillating weight into unidirectional motion. The pinion (Z_3), fixed in the reversing mechanism, drives the reduction wheel (Z_4) which rotates with the reduction pinion (Z_5). The motion from Z_5 is transferred to gear Z_6 which fixed with another pinion (Z_7). Finally Z_7 drives the ratchet wheel (Z8), which is connected with other components to store the movement in the mainspring.

It is assumed that the energy loss between gears are same, then the ratio of the torque acted on the first axis (the bearing) and the torque acted on the last axis (the ratchet) can then be expressed as follows:

$$\frac{M_{bearing}}{M_{ratchet}} = \frac{F_{bearing} r_{bearing}}{F_{ratchet} r_{ratchet}} = \frac{Z_1 \cdot Z_3 \cdot Z_5 \cdot Z_7}{Z_2 \cdot Z_4 \cdot Z_6 \cdot Z_8} \cdot \eta^4 \tag{4-11}$$

Where, Z_i is the number of teeth of Gear i, r_i is the radius of gear in its base circle, i = 1, 2, …, 8, and η is the energy efficiency of one pair of gears. Based on the experiments in [58], one pair of gears alone loses about 10% of the energy. Thus, the overall efficiency of the gears between the oscillating gear and the ratchet wheel will be $\eta_{total} = \eta^4 \approx 0.9^4 = 0.656$. Therefore the actual torque acted on the ratchet wheel can be expressed as follows:

$$M_{ratchet} = M_{bearing} \cdot \frac{Z_1 \cdot Z_3 \cdot Z_5 \cdot Z_7}{Z_2 \cdot Z_4 \cdot Z_6 \cdot Z_8} \cdot \eta^4 \tag{4-12}$$

The mainspring is served as the energy accumulator. During the winding process, the force to wind up the mainspring received from the oscillating weight is not completely used for winding because it has to counter the reaction force of the already wound spring. This reaction force increases as the mainspring is more wounded. Figure 4-8 shows the reaction force of the mainspring, which was collected experimentally using a specially designed instrument, called the Variocouple [63]. In this figure, the vertical axis is reaction force in mN, and horizontal axis is the winding angle of the mainspring. The two curves are the winding curve (upper) and the unwinding curve (lower).

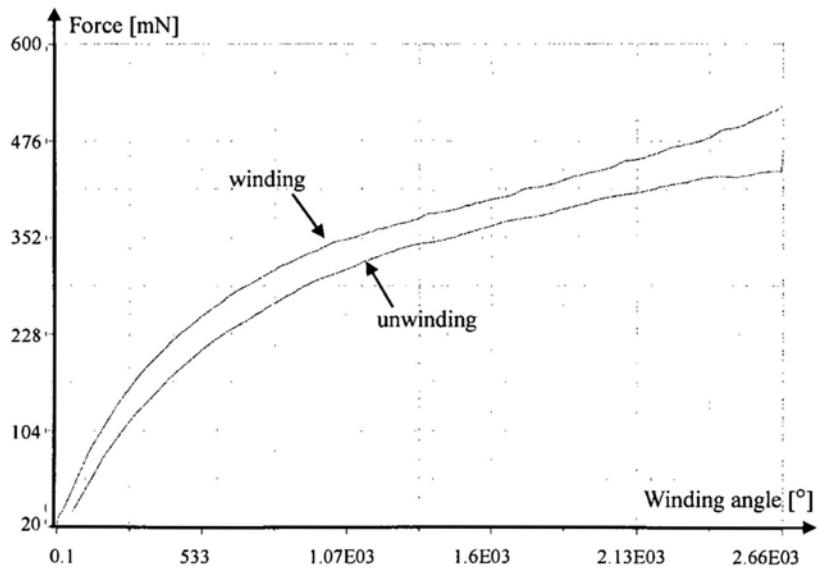

Fig. 4-8: Reaction force of the mainspring as a function of the winding angle

In order to winding the mainspring, the torque acted on the ratchet wheel must be greater than the reaction torque of the mainspring and hence, the following inequality must be held:

$$M_{spring} < M_{ratchet} \tag{4-13}$$

In practice, and the radius M_{spring} can be calculated by multiplying the measured data of the reaction force, F_r, and the radius of the barrel arbor, r_{arbor}. Moreover, from Fig. 4-6, the following expression can be obtained:

$$mgr\sin\theta_r = M_{bearing} = F_{bearing} \cdot r_{bearing} \tag{4-14}$$

Combine Eq. (4-12) ~ (4-14),

$$M_{spring} = F_r \cdot r_{arbor} < mgr\sin\theta_r \cdot \frac{Z_1 \cdot Z_3 \cdot Z_5 \cdot Z_7}{Z_2 \cdot Z_4 \cdot Z_6 \cdot Z_8} \cdot \eta^4 \tag{4-15}$$

Or

$$\sin\theta_r > \frac{F_r \cdot r_{arbor}}{mgr \cdot \eta^4} \cdot \frac{Z_2 \cdot Z_4 \cdot Z_6 \cdot Z_8}{Z_1 \cdot Z_3 \cdot Z_5 \cdot Z_7} \tag{4-16}$$

From the equation above, it is seen that a minimum $\theta_{r,\min}$ is required to wind the mainspring. From Fig. 4-7, $\theta_{r,\min}$ should be within $(-\pi/2, \pi/2)$, therefore, the minimum angle of the oscillating weight to drive the mainspring can be calculated by:

$$\theta_{r,\min} = \arcsin\left(\frac{F_r \cdot r_{arbor}}{mgr \cdot \eta^4} \cdot \frac{Z_2 \cdot Z_4 \cdot Z_6 \cdot Z_8}{Z_1 \cdot Z_3 \cdot Z_5 \cdot Z_7}\right) \tag{4-17}$$

Finally, the effective angle to accumulate onto the mainspring can be obtained by multiplying the ratio of the gear train with the difference between θ_r and θ, $\theta_{r,\min}$:

$$\Delta_{eff}\theta = \max\{(\theta_r - \theta - \theta_{r.\min}), 0\}\frac{Z_1 \cdot Z_3 \cdot Z_5 \cdot Z_7}{Z_2 \cdot Z_4 \cdot Z_6 \cdot Z_8} \cdot \eta^4 \quad (4\text{-}18)$$

4.4 Simulation and Experiment Results

In order to test the aforementioned model, numerical simulations are conducted. The system parameters for simulation are shown in Tab.4-1.To simulate the swinging of the arm, the movement of the upper pendulum is defined as sinusoidal curve, in which the maximum swinging angle is 27° (0.471 rad.), and the angular velocity is 1.21 rad./sec (the period is 5.19 sec). The simulation program is written using Matlab®. Solving Eq. (4-10) with the initial conditions $\theta_r(0) = 0, \dot{\theta}_r(0) = 0$, which satisfies the condition in Eq. (4-9), the angular displacements, angular velocities and angular accelerations of the upper pendulum and the lower pendulum can be obtained, as shown as Fig. 4-9 , 4-10 and 4-11 respectively.

Tab.4-1: System parameters

The mass of swing arm	1.8kg
Arm length	0.5m
Oscillating weight	3g
Effective radius of oscillating weight	15mm
Teeth of Gear 1	38
Teeth of Gear 2 and 2'	39
Teeth of Gear 3	11
Teeth of Gear 4	47
Teeth of Gear 5	9
Teeth of Gear 6	61
Teeth of Gear 7	9
Teeth of Gear 8	63
Transmission efficiency for each gear set	90%

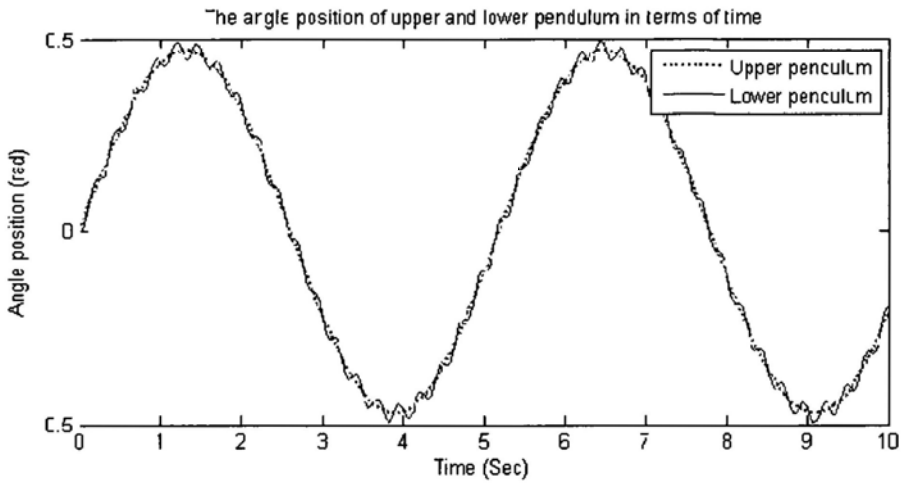

Fig. 4-9: The angular displacement of the upper pendulum and the lower pendulum

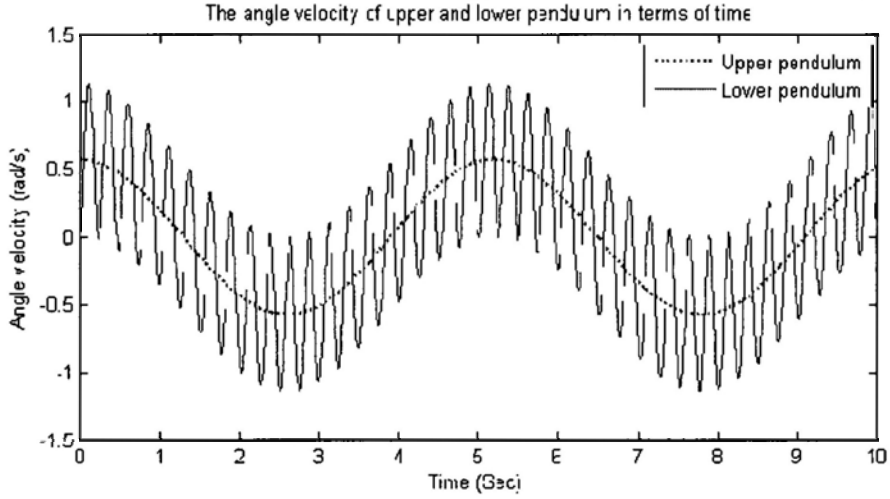

Fig. 4-10: The angular velocity of the upper pendulum and the lower pendulum

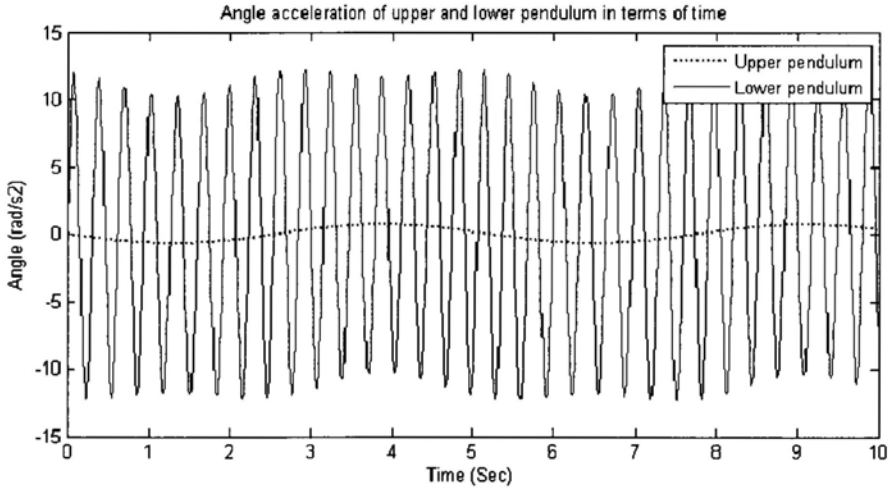

Fig. 4-11: The angular acceleration of the upper pendulum and the lower pendulum

According to the measured data about from Variocouple [63] (refer to Fig. 4-8), the mainspring of a mechanical movement (ETA2824) is completely wound at the angle of 14.77π, or 46.4 rad. The simulation results indicated that the time to fully wind the mainspring is 61360 s, or about 17.12 h. It should be pointed out that the watch can work without being fully wound. In fact, after a few swings, the watch will start to work. A fully wound watch will work for approximately 42 hours.

Figure 4-12 shows the winding performance in terms of time with different amplitude. It is seen that the higher the amplitude (the higher the arm swings), the shorter time is needed to fully wind the mainspring. If the amplitude is small, the influence of the reaction force is significant, and the winding curve is nonlinear. Moreover, if the amplitude is big, the influence of the reaction force can be neglected, and the winding curve is approximately linear. Figure 4-13 shows the winding performance in terms of time with different swing speed. It is seen that the shorter the period (the faster the arm swings), the shorter the time needed to fully wind the mainspring.

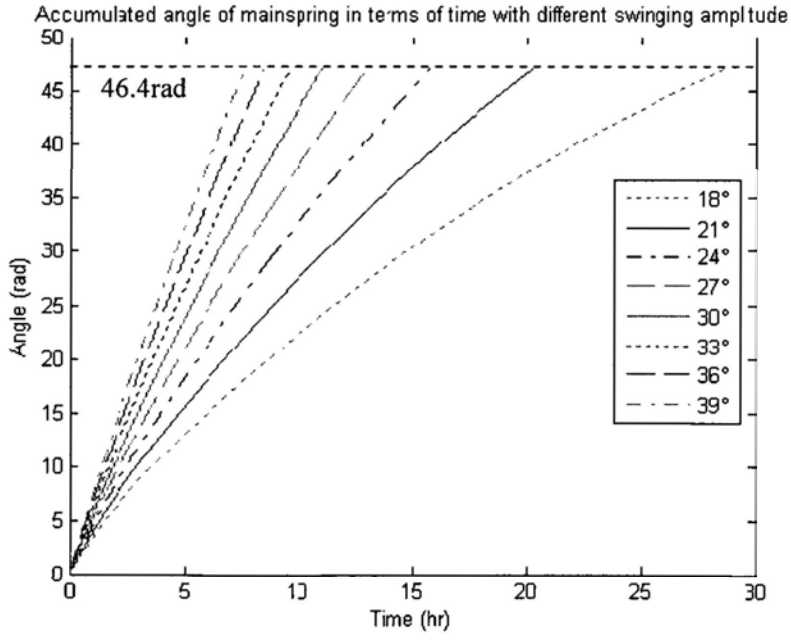

Fig. 4-12: the winding curves with different swing amplitudes, the period is 5.19s

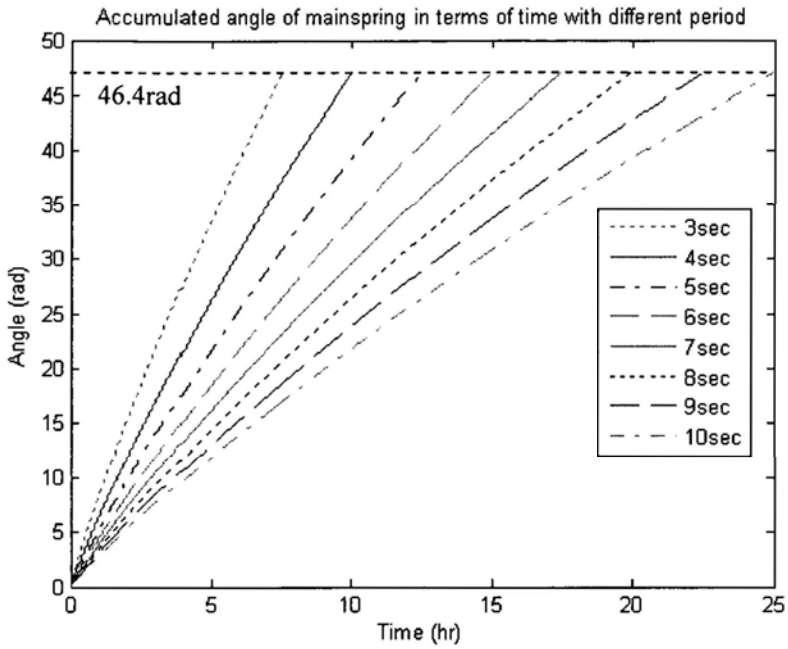

Fig. 4-13: the winding curves with different arm swing periods, the amplitude is 27°

Let the relative angular displacement $\gamma = \theta_r - \theta$. Then the total input of the system can be calculated by the following equation:

$$E = \int_0^T J_r \ddot{\gamma}\dot{\gamma} dt \tag{4-19}$$

where, J_r is the moment of the rotor, and T is total winding time. The total input energy in terms of time is shown in Fig. 4-14. If the upper pendulum swings as $\theta = 0.471\sin(1.21t)$ (rad.), then the theoretic energy input is 1.204 J.

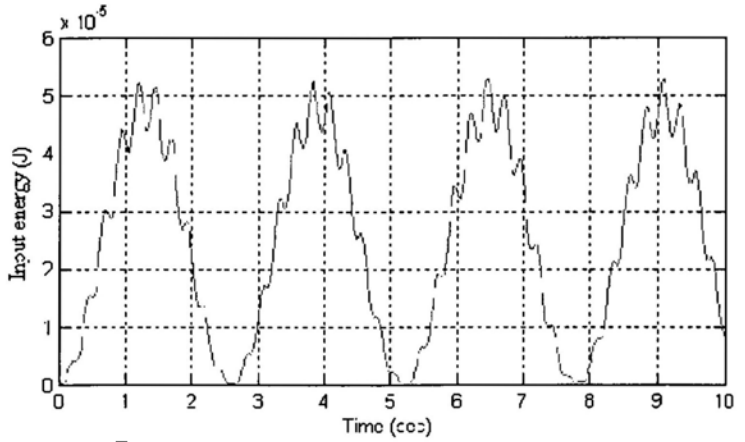

Fig. 4-14: Total input energy in terms of time

The theoretic energy stored in the main spring, on the other hand, can be calculated by the following expression [58]:

$$E_{store} = \frac{e \cdot h \cdot l}{6} \cdot \frac{\sigma_{\max}^2}{E_0} \tag{4-20}$$

where, E_{store} is the maximum energy stored in mainspring, $\sigma_{\max}$ the acceptable maximum stress of the mainspring, E_0 the modulus of elasticity, e the thickness of the main spring, h the height of the mainspring, l the length of the mainspring.

For the testing mainspring (ETA2824), e = 0.134 mm, h = 1.23 mm, l = 400 mm, $\sigma_{\max}$ = 3340 MPa, and E_0 = 2.3×10^5 MPa, the total energy stored in mainspring is E_{stored} = 557.2 mJ. Therefore the energy efficiency of the automatic winding system is:

$$\eta_{transfer} = \frac{E_{store}}{E_{input}} \times 100\% = \frac{0.5572}{1.204} \times 100\% \approx 46.3\% \tag{4-21}$$

The loss of efficiency is due mainly to the friction of the gears (refer to Section 4.3) and the reversing pawls (refer to Section 4.2), and to the reaction force of the mainspring.

Different swinging amplitude and period are used would have different efficiency. As shown in Fig. 4-15, the high swinging period can produce high efficiency. However, it will saturate at the period of 6 sec. However, different swing amplitude has little effect on the efficiency.

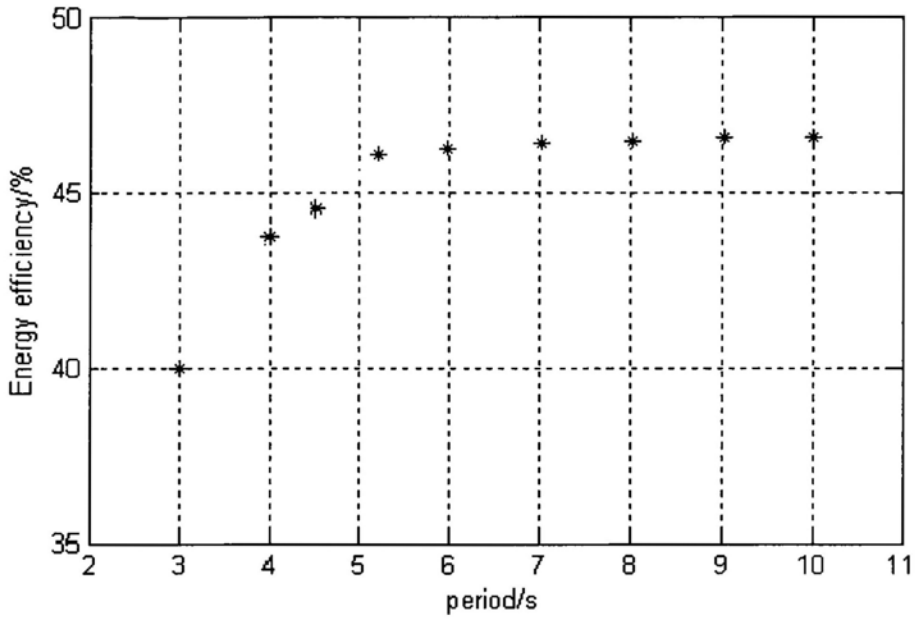

Fig. 4-15: The system efficiency as a function of the swinging period (under constant swinging amplitude)

The simulation results are validated experimentally. We built a simple fixture as shown in Fig. 4-16. The watch is fixed on a holder, which is mounted on an aluminum bar of the length of the arm (distance between motor and the watch is 0.5 m. The bar is propelled by a servomotor that has a motion control capability following different patterns of arm swing. To observe the winding of the main spring, the ratchet wheel was marked and a web camera was fixed on the bar facing the ratchet wheel to monitor its motion. During the experiment, the arm swing is set to 27°. It is found that the total winding time is 19 hours. Comparing to the simulation result of 17.12 hr, the difference is caused by several reasons. Firstly, the simulated arm swing is not very stable. In fact, the swing angle varies between 24.5° and 30.7°. Second, in the simulation model, the frictions between the gears is not considered, which may prolong the winding time.

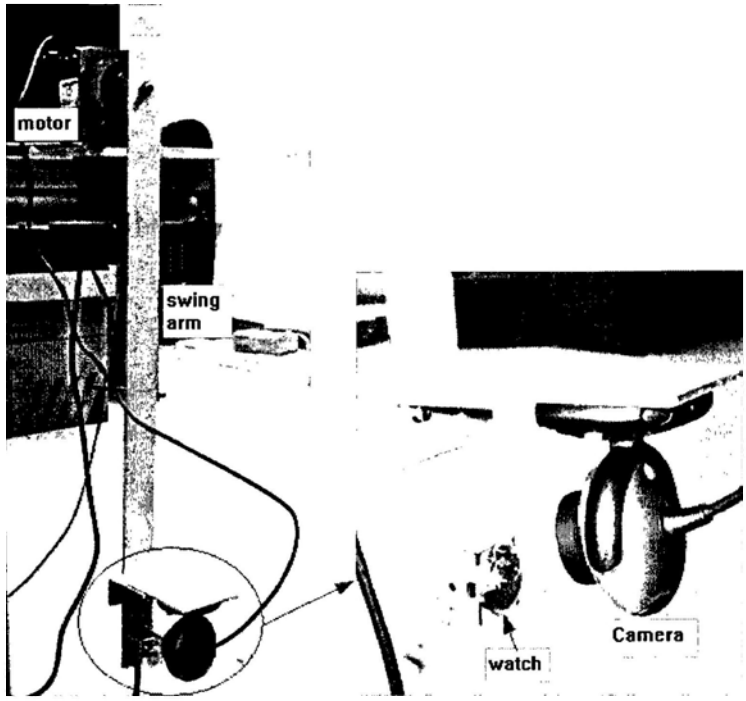

Fig. 4-16: The setup for experimental testing

4.5 Summary

Based on the discussions above, following conclusions can be drawn:

(1). The automatic winding mechanism of a mechanical watch movement can be considered as a double pendulum system, the upper pendulum is the arm and the lower pendulum is the oscillating weight (the rotor). It also includes a gear train that converts bidirectional motion to the unidirectional motion, and a reduction gear train that winds the mainspring.

(2). When the arm swinging as a sinusoidal function, the motion of the rotor is nearly a sinusoidal function with different frequency. The bigger the amplitude and/or the faster the arm swing, the faster the mainspring being wound.

(3). In a typical condition, the mainspring is fully wound in 17.2 hours. Comparing to the experimental result of 19 hours, the model is rather accurate.

(4). The efficiency of the system is about 46.3%. The lost of energy is mainly attributed to the friction in various gears and the reaction force of the mainspring. Moreover, increasing the swinging speed can improve the efficiency. Though, the change of swinging amplitude has little effect.

Chapter 5

The Magnetic Pendulum Mechanism for Energy Harvesting from Arm Motion

There is rich kinetic energy in human body when in motion, especially in wrist where swing magnitude is largest. This chapter presents an energy harvester, based on magnetic pendulum mechanism, to unintentionally extract the human kinetic energy from arm swing and directly to convert it to electricity, which can serve as power source for portable electronics. The harvester mainly consists of an eccentric rotor made of permanent magnet, electric steel and coils as stator. The eccentric rotor, as a simple pendulum, acts as the kinetic energy harvester which can absorb the motion from human body during walking. With the permanent magnets on the rotor, the moving rotor can produce changing magnetic field, where electric coils can induce electricity. A torsion spring is also added onto the rotor such that the harvester works even when placed on horizontal plane where the gravitational acceleration fails. The electromagnetic and kinematical model is built to analyze the performance. Numerical analysis and system optimization are also conducted. Simulation shows that the harvester with 40mm in diameter and 50 g in weight, worn on the wrist, can produce dozens of miliwatts electricity during normal walking.

5.1 The Design of the Harvester

Inspired from the mechanical watch movement which employs a pendulum mechanism to capture and convert human kinetic energy to mainspring's potential energy to drive the watch, the energy harvester also uses a pendulum to harness kinetic energy from human motion. Figure 5-1 shows the energy harvesting mechanism, which mainly includes an eccentric mass made of permanent magnet as the rotor, and wire coils fixed with the shell as stator. The harvester is like a mechanical watch, which can be fixed on the wrist. When arm swinging, the rotor works as a pendulum to convert the kinetic energy of human movement and produces changing magnetic field to induce current in the coils. Without any gear in this

mechanism, it is more efficient because of less friction loss. In order to effectively harvest the accelerations in both directions a torsion spring is used. The torsion spring creates an initial torque, drawing the rotor to an equilibrium position away from the vertical direction. With the spring, even vertical motion will start up the motion of the rotor. The harvester also has a manually driven mechanism for urgent use, by which user can turn the handle to generate electricity. The harvester has a power outlet, through which various mobile electronic devices can be charged.

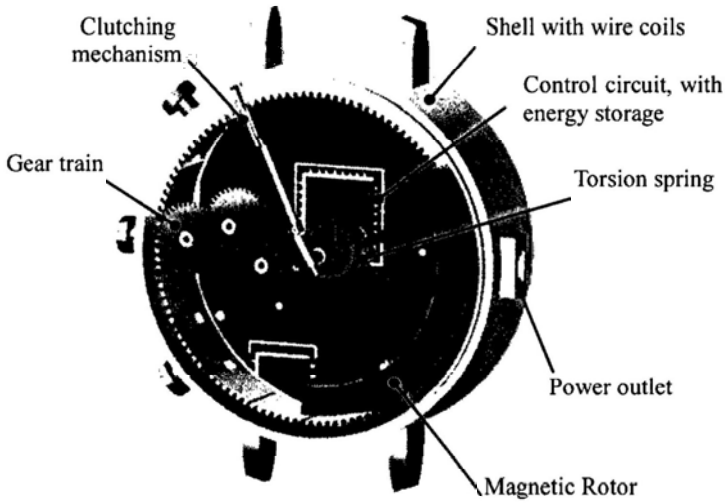

Fig.5-1: The overview of the energy harvester for arm motion

In order to accommodate the emergency usage, the harvester also has the manual cranking function. As shown as in Fig.5-2, it is made of a clutching mechanism and a gear train. The clutching gear set acts as a switch between the automatic and manual operation. The lower clutching gear and the upper clutching gear are usually separated, allowing the harvester to work in the automatic harvesting mode. When the upper clutching gear is pressed down the clutching mechanism is activated connecting the upper clutching gear to the lower clutching gear; at the mean time, the torsion spring and the rotor are disabled. User can then turn the handle to drive the 4 stage gear train to transfer the motion to the rotor. As a result, the electricity is generated, as that of automatic operation.

The harvester mainly includes three sub-mechanisms: clutching mechanism, gear train and rotor-coil mechanism. Shown as Fig. 5-3 and 5-4, the clutching mechanism is used to switch between automatic harvesting and manual harvesting. When

automatic harvesting, the handle is pulled down and pressed into the Harvester cover, which causes the 'rod 4' to release force on the upper clutching gear, therefore the upper clutching gear separates from the lower clutching gear, as shown in Fig. 5-3. When user wants to manually drive the harvester, the handle is pulled out and can stand upright, which makes the rod 4 load force on the upper clutching gear and engage the lower clutching gear, as shown in Fig. 5-4. A gear train is used to transfer the motion from handle and accelerate the angular velocity, as shown in Fig.5-5.

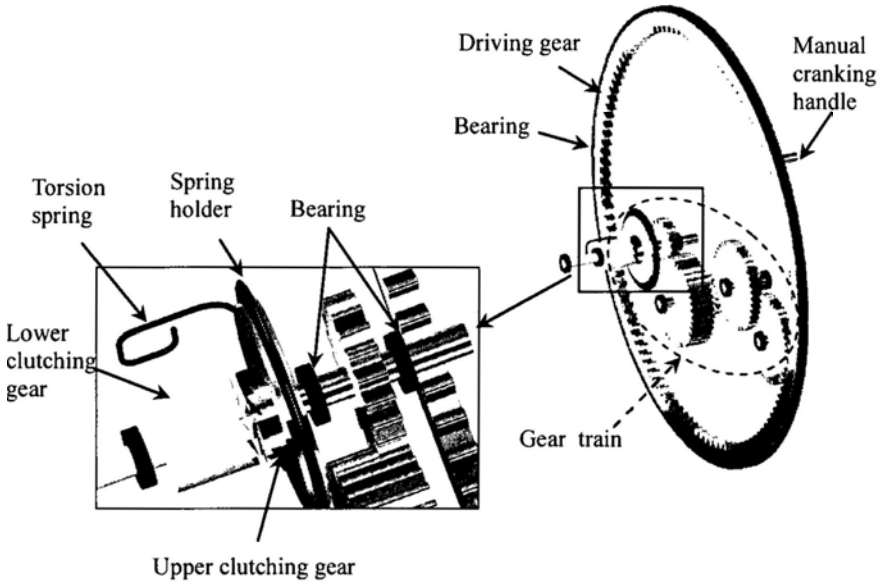

Fig. 5-2: Mechanism for manual harvesting

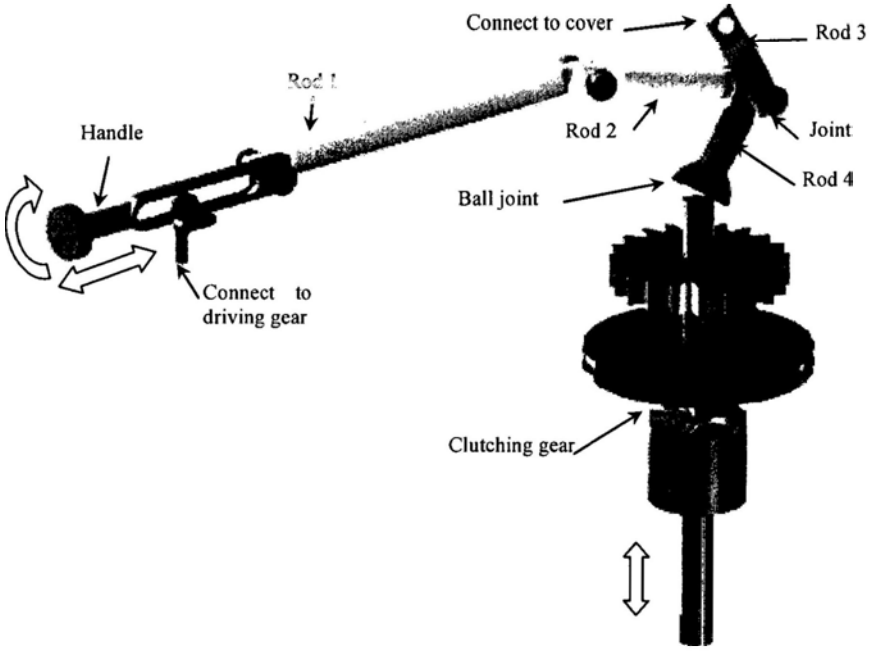

Fig.5-3: The clutching mechanism in release

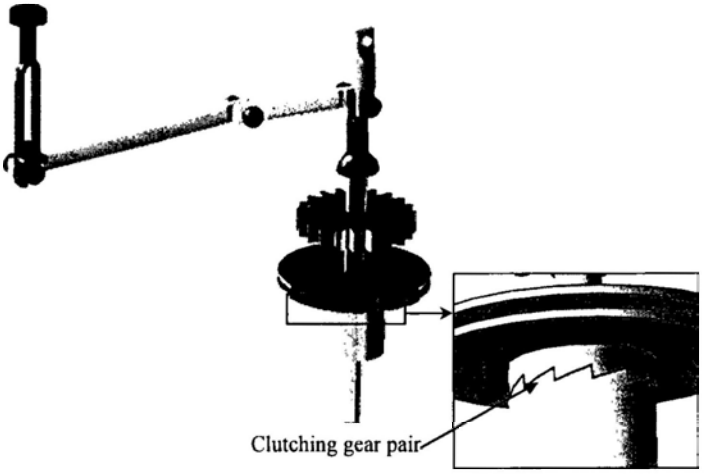

Fig.5-4: The clutching mechanism in engagement

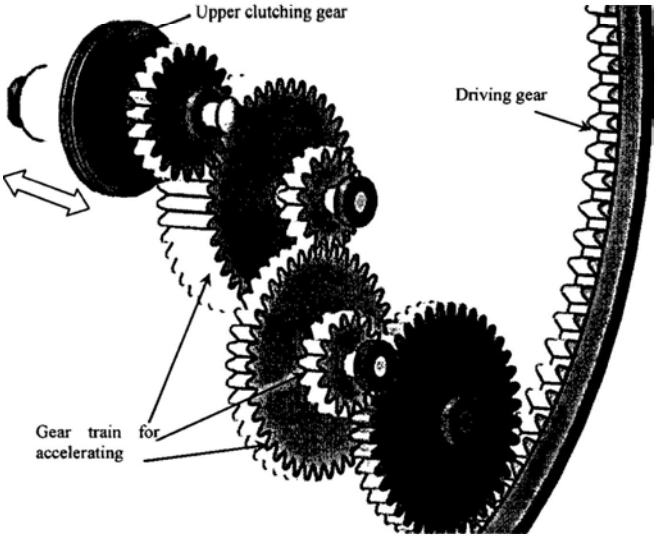

Fig.5-5: The gear train for the manual harvesting

The kinetic energy harvesting and conversion mechanism includes three key components: magnetic rotor, torsion spring, and stator. Figure 5-6 shows the detail structure of these components. The rotor comprises of three permanent magnets, arranged alternating magnetization direction, and separated by two plastic separators. Magnets and separators are all fixed to an armature made of electrical steel, which is attached to the bracket made of aluminum and can rotate around the shaft. The stator, made of electrical steel, has 18 poles, around which copper coils are wound. The torsion spring is attached to the rotor, one end of which is fixed on the bracket of the rotor, the other fixed on the shaft.

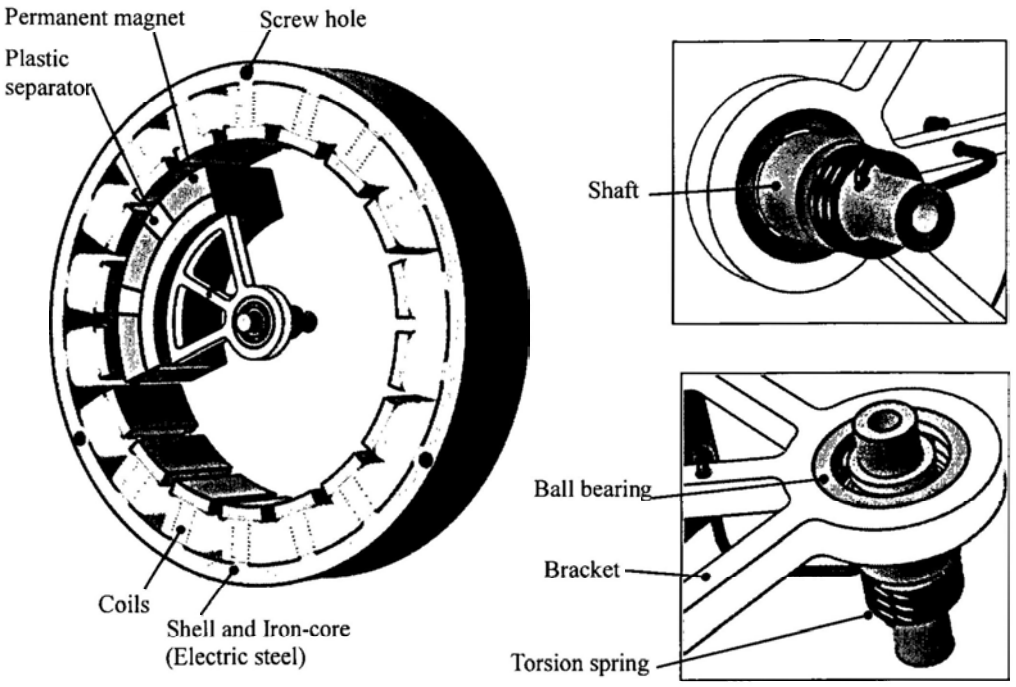

Fig.5-6: The rotor-stator mechanism in the harvester

5.2 Electromagnetic Analysis

On the electromagnetic analysis, the magnetic equivalent circuit (MEC) method is introduced to calculate the flux density through the air gap. Before building the MEC model, the magnetic field in the air gap is analyzed using Ansys®, by extracting half of the cross section of the harvester and based on the topology showed in Fig. 5-7.

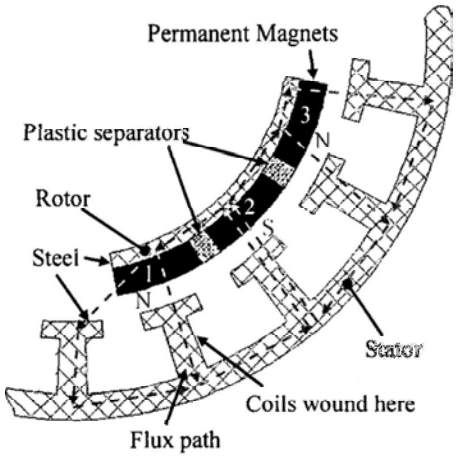

Fig.5-7: The cross-section view of the rotor and stator, and the flux path

For simplification, a 2D model is extracted from the physical 3D model, as shown in Fig.5-8, for electromagnetic analysis with Ansys®. The 2D model includes all the permanent magnets and their steel armature, half part of the steel stator, and air around the harvester. After analysis, the 2D flux lines, shown in Fig.5-9, are mainly concentrated in six poles and formed two flux paths which are in accordance with the topology in Fig.5-7. Figure 5-10 shows the flux path in vector, which obviously shows there are two magnetic paths.

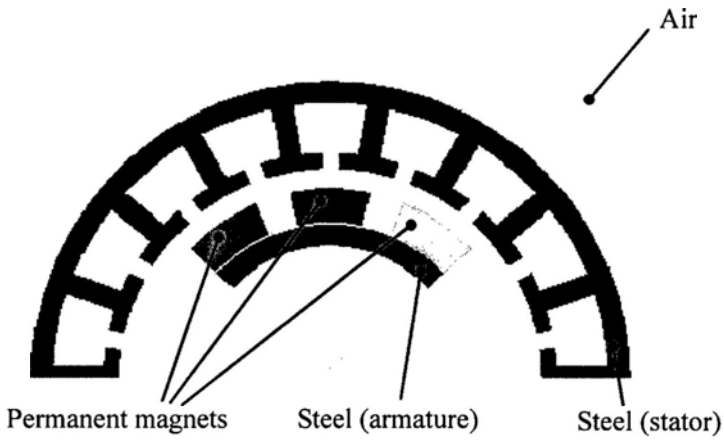

Fig.5-8: The 2D model for electromagnetic analysis with Ansys®

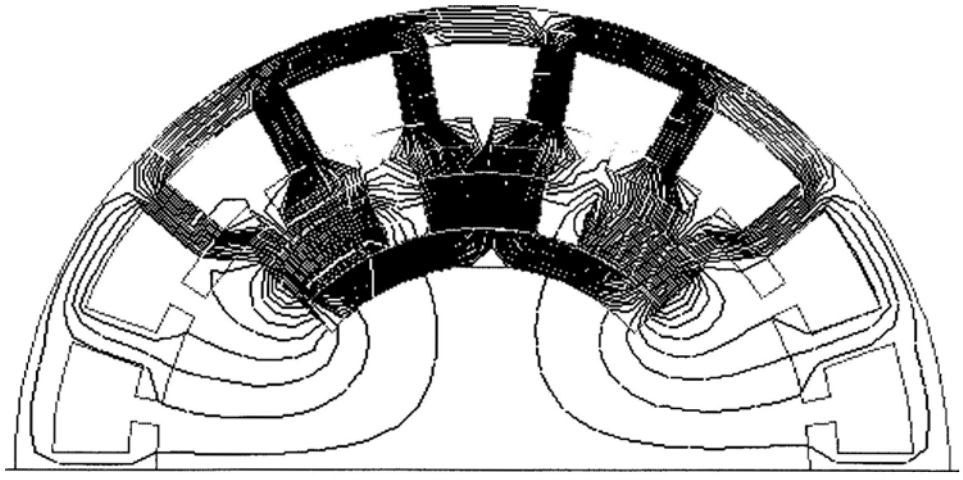

Fig.5-9: Magnetic flux density in the rotor and stator shown in 2D flux lines

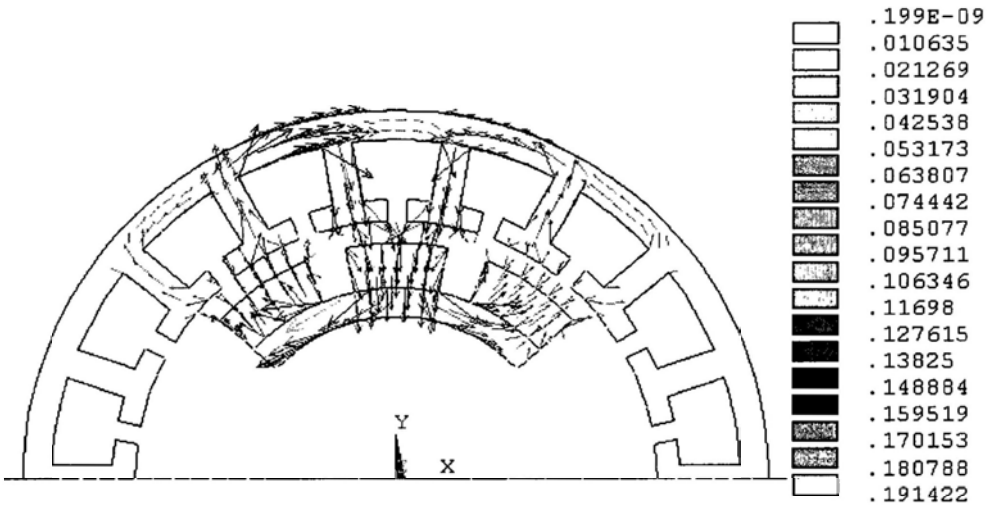

Fig.5-10: Flux distribution shown in vector

The MEC method to analyze magnetic source is to model the permanent magnets as voltage source, flux path reluctance as resistance, and flux through the path as current in the electrical circuit. Since the rotor is symmetric, just the right half of the rotor (half of the central magnet and the right magnet) and three related poles are considered in the MEC model, as shown in Fig. 5-11. In this model, due to the large permeability of electrical steel, the reluctance of armature and stator are very small, compared with the air gap reluctance and the magnet reluctance. Thus the reluctance of electrical steel is neglected.

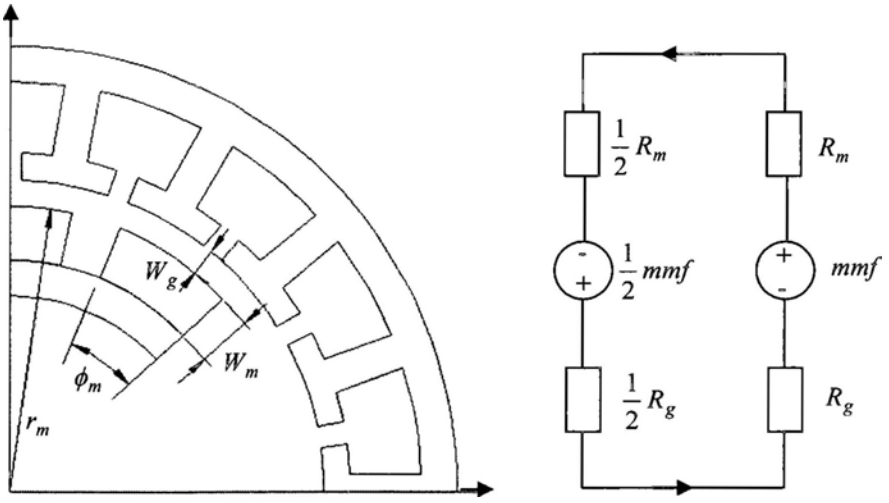

Fig.5-11: Magnetic equivalent circuit for the half of rotor and stator

In the MEC model, mmf is the magnetomotive force, R_m is the reluctance of magnet, and R_g is the reluctance of air gap, which can be calculated by the following equations:

$$mmf = \frac{B_r W_m}{\mu_m} \tag{5-1}$$

$$R_m = \frac{W_m}{\mu_m D(r_m - \frac{W_m}{2})\phi_m} \tag{5-2}$$

$$R_g = \frac{W_g}{\mu_0 r_m \phi_m D} \tag{5-3}$$

Where, B_r is the residual flux density of permanent magnet; W_m is the width of the cross section of permanent magnet; μ_m is the permeability of permanent magnet; D is the height of the permanent magnet; r_m is the lager radius of permanent magnet; ϕ_m is the angle of the magnet sector; and μ_0 is the air permeability. Thus, the total flux in the MEC model can be computed as following:

$$\Phi = \frac{mmf}{R_m + R_g} \tag{5-4}$$

From the topology and the MEC model, the flux through three magnets is:

$$\Phi_1 = \frac{1}{2}\Phi_2 = \Phi_3 = \Phi \tag{5-5}$$

Based on the topology shown in Fig.5-7, if the sector angle of the plastic separator is ϕ_s and the sector angle of each pole of the stator is ϕ_p, then the number of poles which has effective magnetic flux can be expressed as:

$$n_e = \left\lceil \frac{2\phi_s + 3\phi_m}{\phi_p} \right\rceil + 1 \tag{5-6}$$

Where the $\lceil\ \rceil$ is the ceiling function to the next largest integer. From simulation by Ansys® shown in Fig. 5-9, the flux through each pole is proportional to overlapping area between the pole and the magnet, and assumed that the rotor rotates with the angular velocity $\dot{\theta}$ relative to the stator, so the magnetic flux changing rate through each pole can be calculated as following:

$$\left|\frac{d\Phi_{pn}}{dt}\right| = \frac{\Phi_x}{\phi_m} \cdot \dot{\theta} \tag{5-7}$$

Where, Φ_x is the magnetic flux through one of magnets. Therefore the total changing rate of magnet flux can be expressed as:

$$\sum\left|\frac{d\Phi_{pn}}{dt}\right| = \frac{4n_e\Phi}{3\phi_m} \cdot \dot{\theta} \tag{5-8}$$

$$u_{ind} = N \cdot \sum\left|\frac{d\Phi_{pn}}{dt}\right| = \frac{4n_e N\Phi}{3\phi_m} \cdot \dot{\theta} \tag{5-9}$$

Finally, the total induced voltage of the harvesting device can be computed as the following equation, assuming that the coil number on each pole is N and the voltage induced by each pole coil is rectified to the same direction. From Eq.(5-9), the induction voltage is only proportional to the relative angular velocity of the rotor for a harvester

5.3 Kinematical Analysis

Figure 5-12 shows the lumped parameter model of the harvester for analyzing the kinetic performance, where the left part is the mechanical subsystem and the right one is the electrical model of the whole system. In the mechanical model, the rotor is simplified as a point particle with four forces acting upon it, with the effective distance r from the rotating center. Besides the inertia force on the tangential direction, there are three forces, namely, the torsion spring force F_k, the electrical

damping force F_e, and the mechanical damping force F_m. There are also the gravity F_g and tension T acting on the rotor. Besides the relative angular displacement θ used in Eq.(5-7), other two angular displacement α and β are introduced for convenience. α is the angular displacement of the harvesting device from human motion. β expresses the absolute angular displacement, relative to the world coordinates. From the above definition, the three angular displacements have the following relation:

$$\beta = \alpha + \theta \tag{5-10}$$

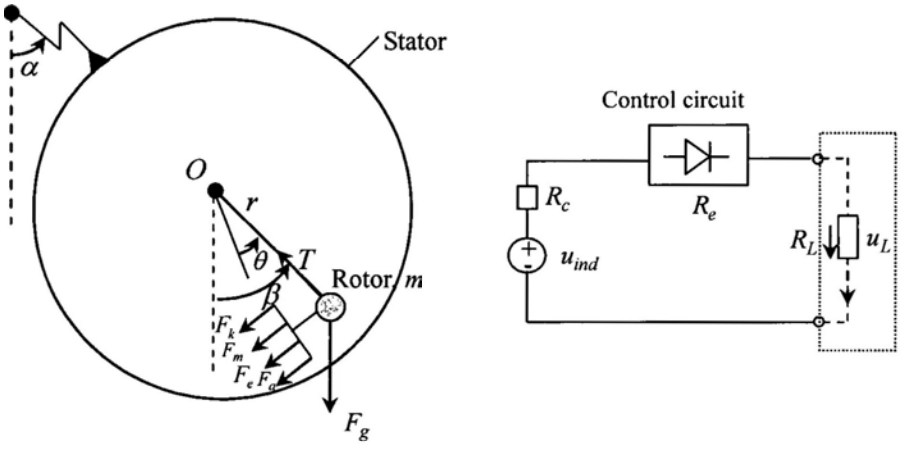

Fig.5-12: Lumped parameter model of the harvester

According to the Hook's Law, the torsion spring force F_k is:

$$F_k = -k \cdot \theta \tag{5-11}$$

Assumed that the angle between the rotating axis of the rotor and the plumb line is γ, the tangential component of the gravity on the tangential direction of the rotor trajectory is:

$$F_g = -mg \sin\gamma \sin\beta \tag{5-12}$$

The inertia force is:

$$F_a = -m \cdot r\ddot{\beta} \tag{5-13}$$

The electrical damping force converts the kinetic energy in mechanical system to electricity in electrical system, so the power done by the electrical damping force should be equal to the one done by electricity, that is:

$$F_e \cdot r\dot{\theta} = -\frac{u_{ind}^2}{R_c + R_e + R_L} \tag{5-14}$$

Inserting the Eq.(5-9) into Eq.(5-14), then the electrical damping force is:

$$F_e = -\frac{16(n_e N\Phi)^2}{9\phi_m^2 (R_c + R_e + R_L) r} \cdot \dot{\theta} \tag{5-15}$$

Here, R_c, R_e, and R_L are the resistance of the coils, the resistance in the control circuit, and the load resistance respectively. Defined the electrical damping coefficient C_e as:

$$C_e = \frac{16(n_e N\Phi)^2}{9\phi_m^2 (R_c + R_e + R_L) r} \tag{5-16}$$

And the mechanical damping force is expressed as the following equation, where C_m is the mechanical damping coefficient.

$$F_m = -C_m \dot{\theta} \tag{5-17}$$

According to Newton's Law, the following governing equation on the tangential direction of the rotor trajectory can be obtained:

$$k \cdot \theta + mg \sin\gamma \sin\beta + C_e\dot{\theta} + C_m\dot{\theta} + m \cdot r\ddot{\beta} = 0 \tag{5-18}$$

Inserting Eq.(5-10) into the above equation, one gets:

$$k \cdot \theta + mg \sin\gamma \sin(\alpha + \theta) + C_e\dot{\theta} + C_m\dot{\theta} + m \cdot r(\ddot{\alpha} + \ddot{\theta}) = 0 \tag{5-19}$$

In the above equation, the angular displacement of the device, α, is the input variable, and the relative angular displacement of the rotor, θ, is the output of the mechanical subsystem and its derivative is the input of the electrical subsystem which can be used to calculate the power output by Eq.(5-9). If the external excitation, i.e. the human motion such as the human arm swing, is defined as $\alpha = f(t)$, then the kinematical performance θ and $\dot{\theta}$ can be obtained by solving Eq.(5-19). Noted that the term $(\alpha + \theta)$ is not a small value, Eq.(5-19) can't be solved by analytical but can be solved numerically using Matlab®.

5.4 Numerical Analysis

This section will study the harvesting device to extract the arm swing of human body. The initial value of system parameters for simulation study is listed in Tab.5-1:

Tab.5-1: System parameters

Lager radius of permanent magnet, r_m	20 mm
Angle of the magnet sector, ϕ_m	25 deg
Thickness of the electrical steel, W_s	5 mm
Distance of air gap, W_g	1 mm
Sector angle of the plastic separator, ϕ_s	10 deg
Sector angle of each stator pole, ϕ_p	20 deg
Height of the permanent magnet, D	20 mm
Width of the cross section of permanent magnet, W_m	4 mm
Residual flux density of permanent magnet, B_r	1 T
Air permeability, μ_0	4π*e-7
Permeability of permanent magnet, μ_m	1.1* μ_0
Density of permanent magnet, ρ_{pm}	8230 kg*m^{-3}
Density of electrical steel, ρ_{pm}	7800 kg*m^{-3}
Total mass of rotor, m	
Spring constant of torsion spring, k	$=m*g$

Resistance of the coils and control circuit, R_c,	5 Ω
Load resistance, R_L	5 Ω
Mechanical damping coefficient, C_m	0.05

The common motion pattern of upper limb of human body during normal walking is out-of-phase swing, which can be modeled as a single simple pendulum that the mass concentrated at its center of mass [15], as shown in Fig.5-13. Therefore, during normal walking the trajectory of arm swing can be expressed as $\alpha = \alpha_0 \sin(\omega \cdot t)[rad]$, i.e. the harvester is imposed the excitation defined by a sine displacement. For healthy adults, the swing frequency during normal walking is 0.8~1.1Hz (or 5~7 rad/s) for different stride speeds [16]. Figure 5-14 shows the simulation results with a sine wave, $\alpha = \frac{\pi}{6}\sin(5 \cdot t)[rad]$, as the external motion input. The relative angular displacement $\theta = \beta - \alpha$ between the upper pendulum (the arm) and lower pendulum (the rotor) is a proximate sine function with phase delay. Compared with the external input motion, the frequency of the relative angular displacement is decreased, and the amplitude is smaller too. With the relative angular velocity of the rotor and the system parameters, the transient power output can obtained by numerical method, which result is shown in Fig.5-15.

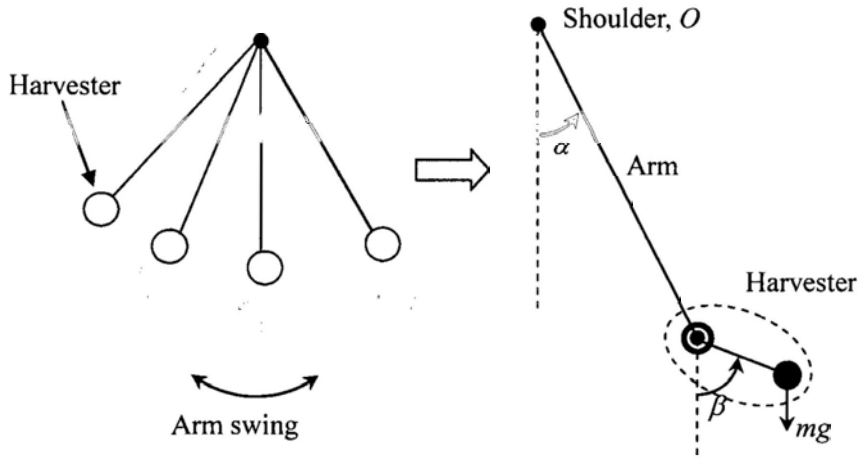

Fig.5-13: The working model of the harvesting device

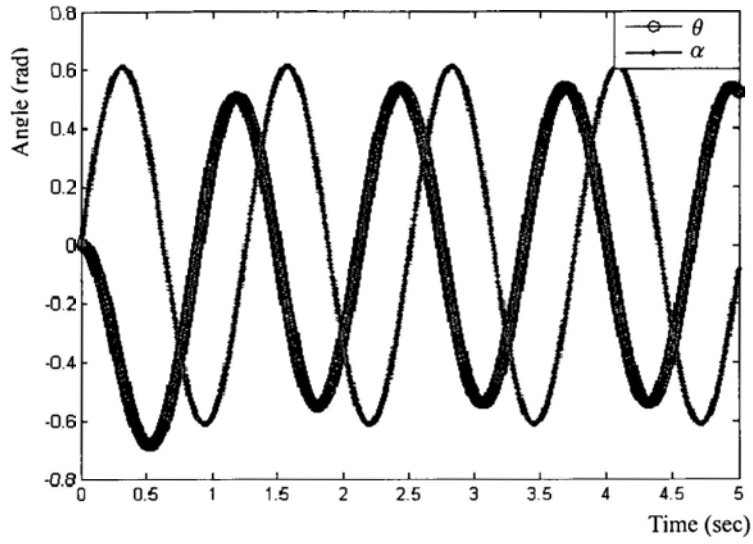

Fig.5-14: Kinematical performance for a sine wave as external excitation

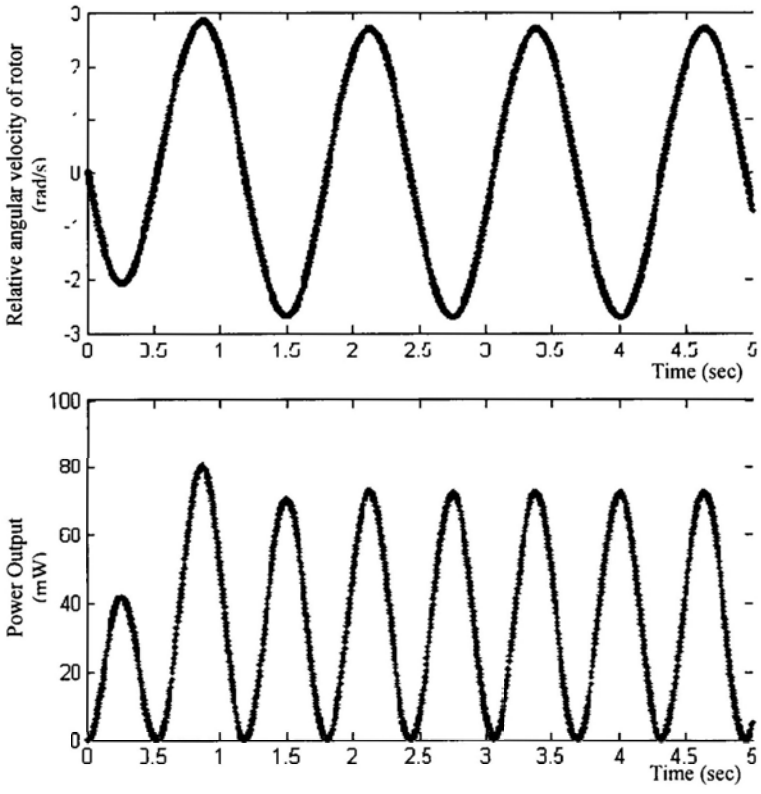

Fig.5-15: The relative angular velocity of rotor and transient power output

According to the conservation of energy, the kinetic energy of the rotor converts to electricity and other energy loss. Based on the definition of kinetic energy, $K = \frac{1}{2} J \cdot \dot{\theta}^2$, the rotor's topology should be taken into account to achieve maximum

moment of inertia, J, so as to harvest maximum energy. To get optimal moment of inertia, $J = mr^2$, the total mass of the rotor m and the effective radius r should be maximized.

With the relative angular velocity $\dot{\theta}$, the transient power output can be calculated by electrical damping force and the relative angular velocity of the rotor, as following:

$$P = -F_e \cdot r\dot{\theta} = C_e \cdot r \cdot \dot{\theta}^2 \tag{5-20}$$

Then the average conversion energy from mechanical motion to electricity can be calculated by the integral of the electrical damping force F_e with respect to time, as following:

$$\overline{P_{con}} = -\frac{1}{T}\int_0^T F_e \cdot r\dot{\theta} \cdot dt = \frac{1}{T}\int_0^T C_e \cdot r\dot{\theta}^2 \cdot dt \tag{5-21}$$

In the case that the harvester topology is unchanged, the structure arrangement of the rotor has effect on the power output. Given constant outer radius of the permanent magnet r_m and its initial thickness, the change of the sector angle of each magnet ϕ_m will affect the power output. Figure 5-16 shows the power output performance with respect to the magnet sector, where r_m changes in each curve from 15mm to 25mm with the step of 2mm. It is shown that the larger outer radius of the magnet is, the more power output, in other words, the bigger the rotor is, the more power output, and that the optimal sector angle increase a little with the outer radius of the magnet increasing.

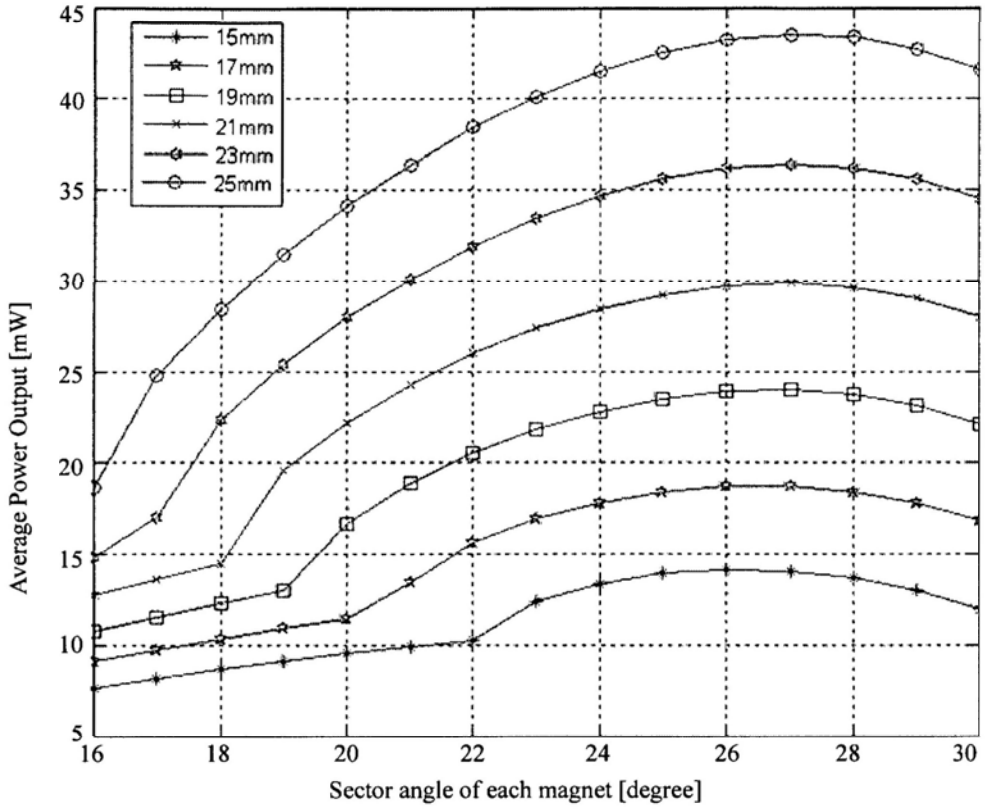

Fig.5-16 power output performance versus the sector angle of each magnet, in which curve there is the same outer radius of the permanent magnet r_m

Based on the Eq.(5-19), the natural resonance frequency in radians ω_n can be approximately defined as:

$$\omega_n \approx 2\pi f_n = \sqrt{\frac{k+mg}{mr}}\ [rad/s] \tag{5-22}$$

Since the gravitational acceleration is constant and the effective radius of the rotor is usually small (on centimeter scale), the natural resonance frequency is more than dozens of radians per second, which is far greater than that of human motion. Therefore the harvester can't achieve resonance during normal walking even if the stiffness of the torsion spring can be tuned. The function of the torsion spring is to make the harvester work even when it is placed on the horizontal plane where the gravity fails. In other word, the torsion spring is a replace of the gravity, so the value of the torsion spring stiffness can be calculated by $k = mg$. Actually simulation also shows that the torsion spring stiffness has tiny effect on the power output. Since the

power level of the harvester is low and in AC voltage, ranging from several to hundreds of miliwatts, and the loads usually requires steady DC bus for their operation, a direct AC/DC converter developed by Dwari [64] is used to rectify and boost the voltage.

External excitation, i.e. arm swing, affects power output. Figure 5-17 shows the power output performance with respect to different arm swing frequencies with the swing amplitude equal to 30deg, and Fig. 5-18 shows the power output performance with respect to different amplitudes with the frequency equal to 5rad/s. From the simulation, both the frequency and amplitude of arm swing have great impact on the power output, which is proximate to quadratic function. Therefore user can get higher power by improving the swing frequency and amplitude during the application of the harvester.

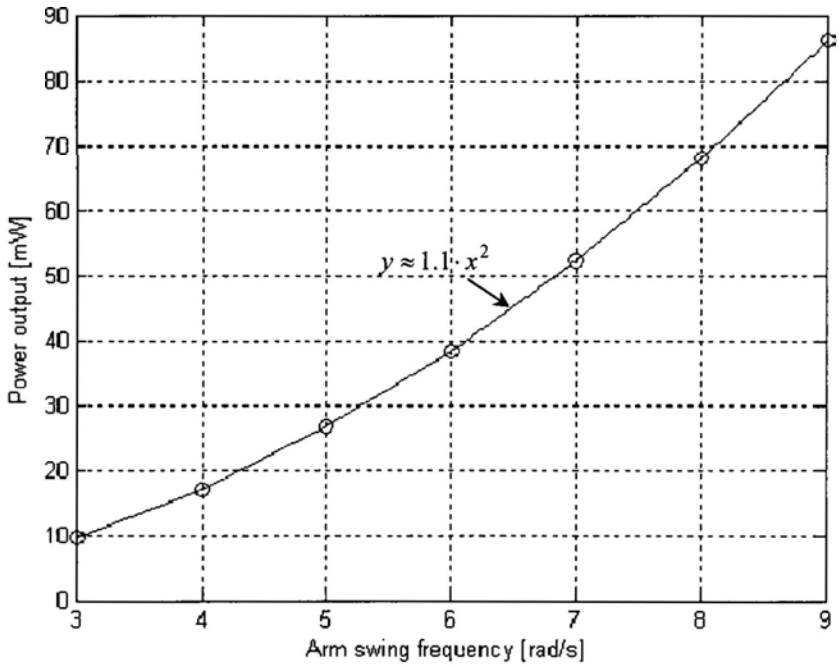

Fig.5-17: Power output versus different arm swing frequencies

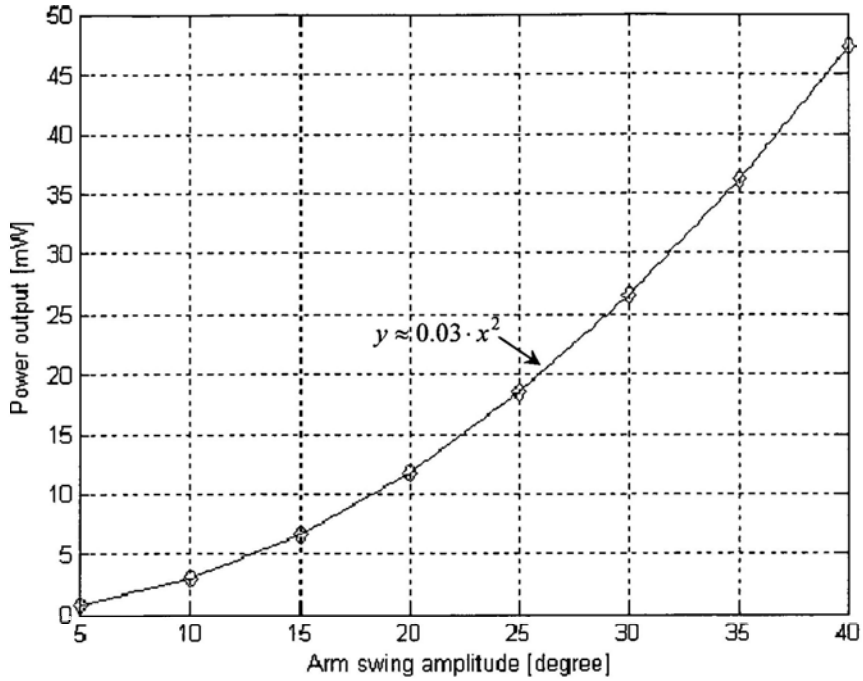

Fig.5-18: Power output versus different arm swing amplitudes

The energy input in a given period T can be calculated by the following equation:

$$E_{in} = \int_0^T J_r \dot{\theta} \ddot{\theta} dt \tag{5-23}$$

And energy efficiency for the harvester is computed by:

$$\eta = \frac{E_{out}}{E_{in}} = \int_0^T C_e r \dot{\theta}^2 dt \Big/ \int_0^T J_r \dot{\theta} \ddot{\theta} dt \tag{5-24}$$

From simulation based on the parameters on Tab.5-1, the energy input in 5 sec is about 365mJ, and the energy efficiency is 55%. Comparing to the kinetic energy of arm swing, the energy input to the energy harvester is very small, so the energy harvester will not increase too much burden for the arm motion. The energy loss in mainly caused from the electric conversion.

5.6 Discussion and Summary

Based on the discussion above, following conclusions can be drawn:

(1) A novel harvester for harvesting human kinetic energy is presented. The harvester is based on both the oscillating principle and the electromagnetic induction, by using eccentric rotor made of permanent magnet and coils as stator. With a torsion spring, the harvester works even when placed on horizontal plane.

(2) The electromagnetic performance is analyzed by professional analysis software and Magnetic Equivalent Circuit model, which can mathematically calculate the mechanical-electrical energy conversion. The kinematical model is also built to analyze the mechanical performance.

(3) Numerical analysis and system optimization is made. It shows that the watch-sized harvester can produce about 40 mW during normal walking. It also shows that total mass and effective radius of the rotor, the arm swing frequency and amplitude are critical to the power output, and the structure topology of the rotor also has obvious impact on the power output.

(4) The harvester can be served as the middleware to portable electronics, such as cell phone, photoelectric mouse. This energy harvesting principle can also be applied to extract kinetic energy from other kind of movement.

Chapter 6

The Crank-Slider Mechanism for Energy Harvesting from Foot Strike

Footwear is important for human, one of which functions are as shock-absorber to protect foot from intense foot strike against the ground. During walking, foot heel is subject to impact from the ground which can be up to 1.5 times human body weight. Usually shoe has a higher heel with buffering, and some has air cushion. There is not only large force but also displacement in the foot strike. Therefore it is ideal to harvest energy from human foot strike according to the foot strike characteristics, and to function as a buffering and shock absorber for foot. In this chapter, a new model for harvesting energy from human foot strike is developed. For the consideration on stability and efficiency, a spring-slider-crank mechanism is used in the harvester to covert the up-down foot strike motion into unidirectional rotation to drive the AC generator. The spring and slider compose an oscillating system to absorb the foot strike motion, and crank and slider make up of the motion conversion mechanism to transfer the bi-directional translation into unidirectional rotation. Gear sets are used to speed up the rotation. The performance of the harvester is analyzed and simulated.

6.1 Introduction

There is a large energy source in kinetic energy during human walking, where human foot strikes the ground periodically, that is, there is once foot strike for each foot step. During walking, the force on one foot can be up to 1.5 times the body weight, which can make the bare foot uncomfortable, especially in wild field or in sports. Therefore shoe used outdoors or for sports usually adopts a cushion for buffering the large impact from heel strike. As shown in Fig.6-1, it is a sneak having an air cushion which makes foot heel more comfortable when in sports. For more direct to buffer the heel strike, one shoe company directly adopts a helical spring attached to the shoe heel for absorbing the shock, as shown in Fig.6-2. Although it is uglier than usual shoe, this type of footwear can effectively reduce the shock from heel strike and can also relieve foot pain [65]. Both the air cushion and spring coil serve as damper or

shock absorber to protect the foot from the damping effect of shock. Since there is vibration in shoe heel during walking, it is ideal to scavenge such kinetic energy as byproduct.

Fig.6-1: Shoe with air cushion for buffering heel strike

Fig.6-2: The Z-Coil® footwear with a spring coil attached to the shoe heel, specifically to buffer foot strike and to relieve foot pain [65]

It has been calculated that up to 67 Watts of power are available from heel strike during normal walking for a 68 kg person with the walking frequency at 2 step per second and heel moving 5 cm [12]. There are mainly two methods to harvest the heel strike energy during human walking. One is to use piezoelectric effect to convert the pressure generated when the foot strikes the ground to electricity [38]. Unfortunately, the energy density is very low (only 8.3 mW at the heel and 1.3 mW at the toe). Another is to use electromagnetic induction to convert body motion to electricity. Chen [65] and Lakic [66] reported electromechanical generators to harvest the foot

step motion. However these designs are very complex with many parts, and can only harvest the press-down motion, which make these device is fragile, expensive and lower efficiency. This chapter is focused on how to harvest the mechanical energy from human foot strike motion during walking, and to provide the function to protect foot from shock. Compared to the existing designs, the proposed harvesting model is more concise and stronger, and can harvest not only press-down motion but also the release-up motion.

6.2 Description of the Harvester

Considering the walking pattern and the dimension constraint, the harvester is designed as a pad, 80mm in length, 60mm in width, and 50mm in height, as shown in Fig.6-3. The harvester mainly includes a fixed part and a moving part, where the moving part can glide relative to the fixed part guided by guiding pins and holes. The springs around the guiding pins provide the rebound force. The harvester adopts the crank slider mechanism to transmit the motion of the moving board from foot strike to the gear train and finally to the AC motor. Figure 6-4 shows the detail crank slider mechanism, where one end of the crank coupler is pinned to the moving board, and the other end is pinned to the crank. In this mechanism, the moving board serves as the slider which is the driven motion, and the crank transmit the rotation to gear train. Figure 6-5 is the close view of the crank slider mechanism.

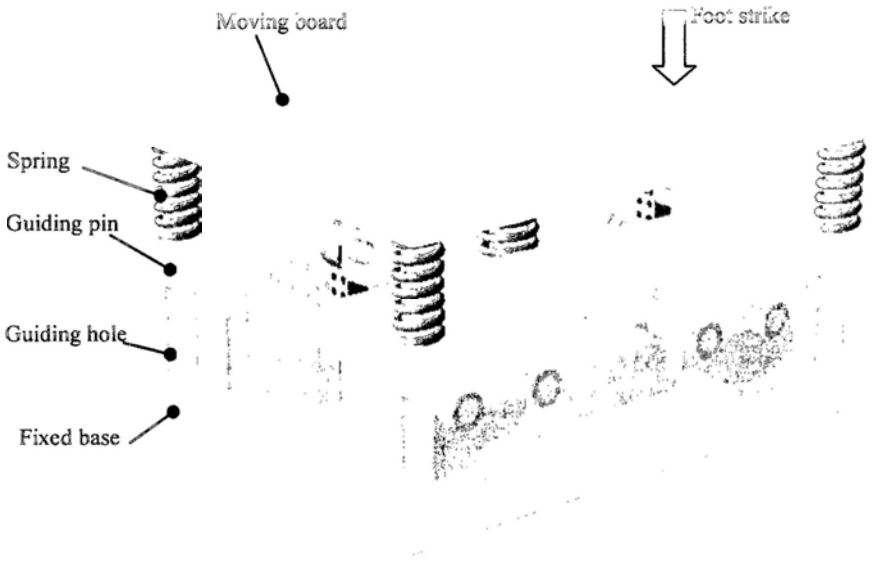

Fig.6-3: The general view of the harvester

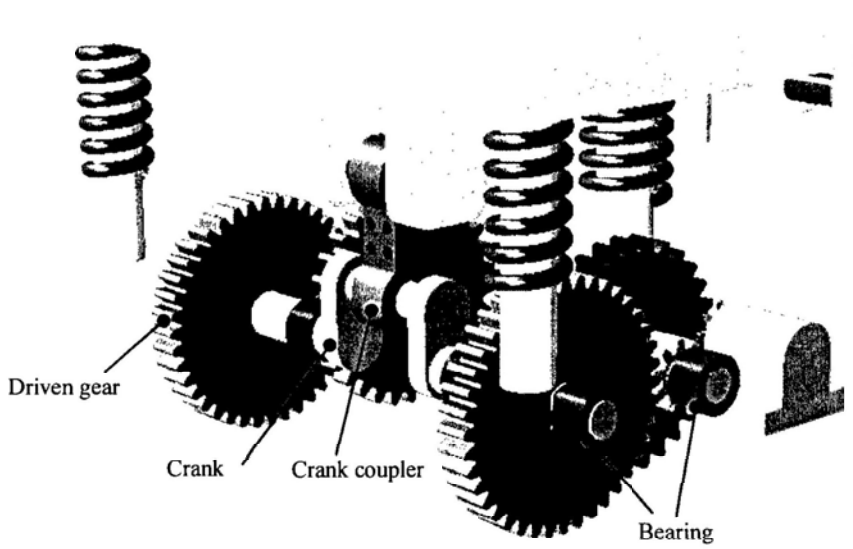

Fig.6-4: The crank slider mechanism

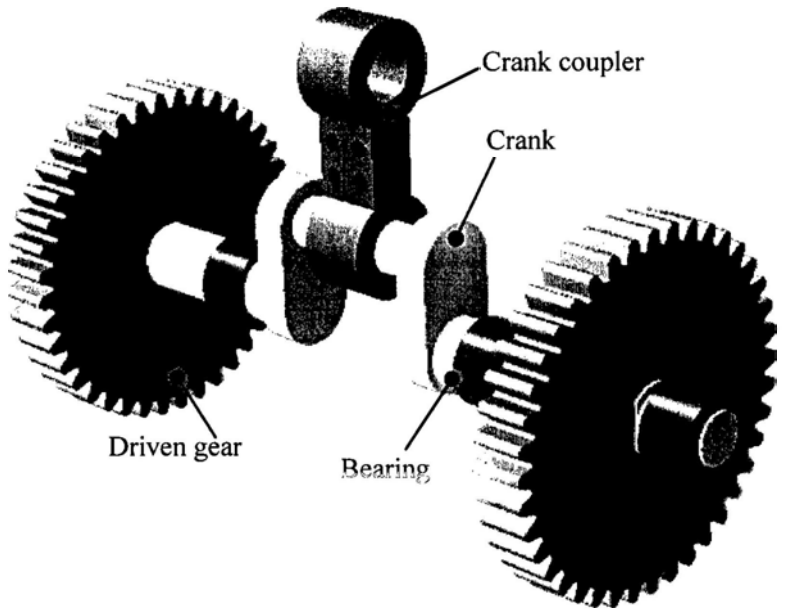

Fig.6-5: The close view of the crank slider mechanism

All the transmission parts are assembled in the fixed base, as shown in Fig.6-6. There are four identical transmission mechanisms, each of which consists of driven gear, intermediate gear and pinion, AC motor and its gear, as shown in Fig.6-7. All the gears are supported by shafts, which are fixed on the base through bearings. The fixed base and middle cover are screwed together to hold bearings.

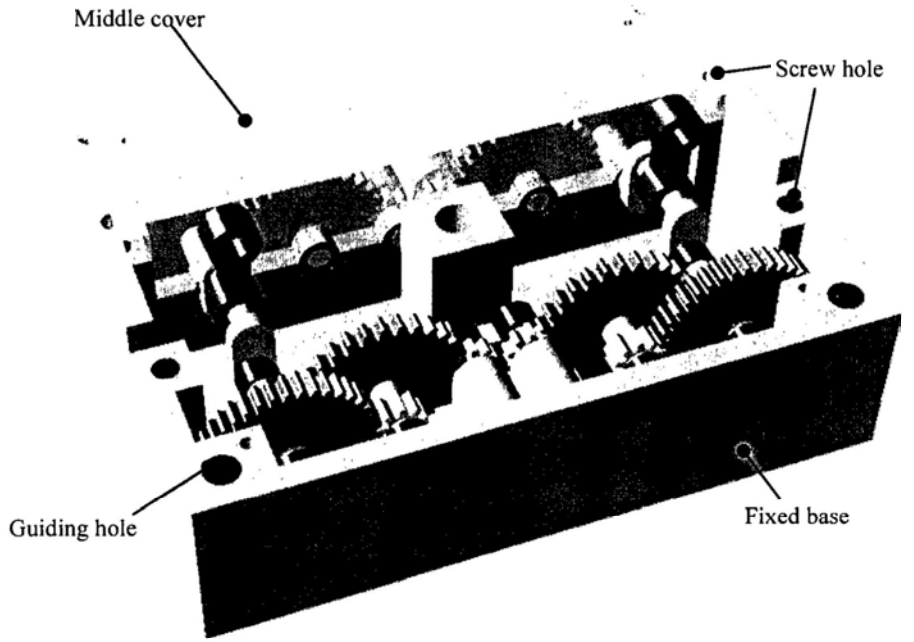

Fig.6-6: The fixed component of the harvester

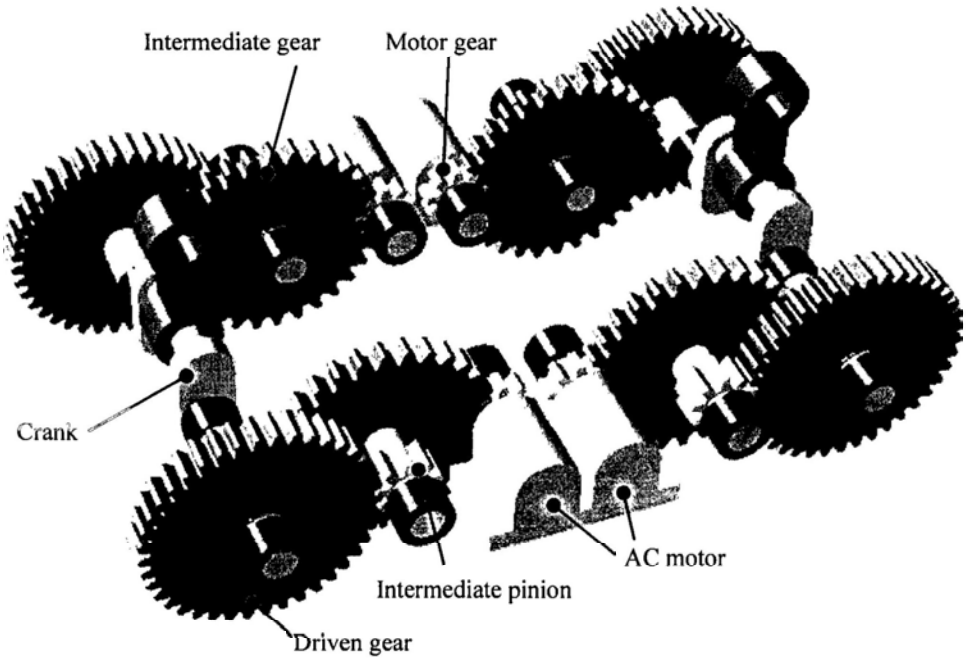

Fig.6-7: The gear train

Generally speaking, the harvester adopts spring-crank-slider mechanism, gear train and micro generator to harness heel strike motion. Figure 6-8 shows the schematic diagram of the harvester. First of all, the heel strike motion is up and down linear motion and the generator can only receive rotation, so the device uses a crank-slider

mechanism to convert the linear motion into rotational one, which includes a slider, gear as the crank and their pin-jointed crank coupler. Secondly, in order to continuously drive the harvesting device, a recovery mechanism for the slider is needed. In this design, a spring, constrained around a cylinder pole, is used to provide the recovery function for continuous motion. When heel touches the ground, the spring is pressed down; and the spring is released up when the heel pushes off the ground. Therefore during the heel touches and releases the ground, springs provide reciprocating motion for the harvester. Usually the step frequency is low but the driving force is large enough, so a gear train is used to speed up the rotation.

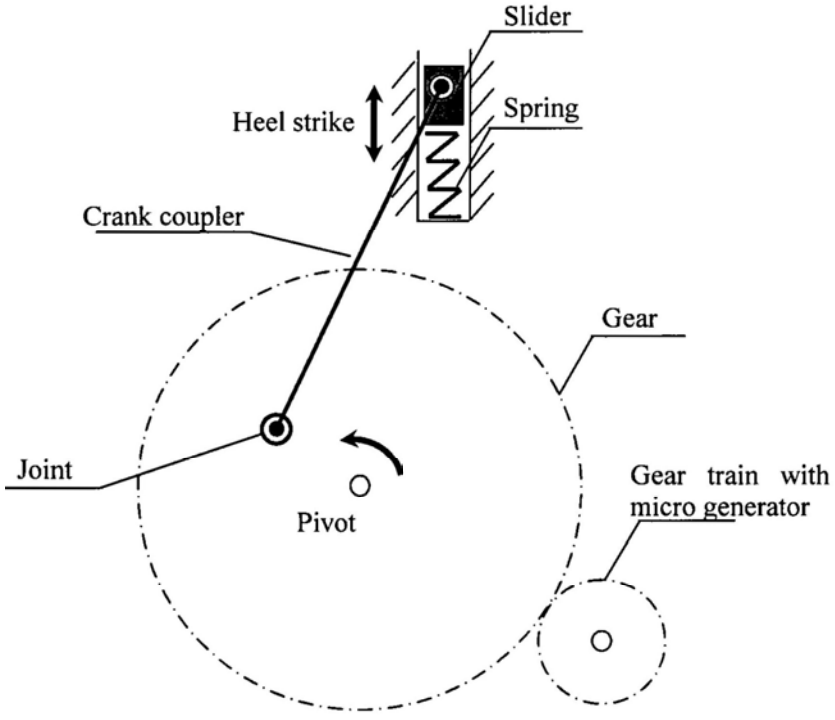

Fig.6-8: The schematic diagram of the harvester

From the physical model, there are four transmission sets and AC generators, which share the same slider-spring mechanism and control circuit. Figure 6-9 shows the flow chart of motion transmission and energy conversion. The heel strike drives the Moving Board, which serves as the slider, to produce the up and down translation movement. Such motion drives two identical crank-slider mechanisms to produce rotation, and each of such mechanism drives two identical gear trains and AC generators. Therefore there are four generators to generate electricity, all of which are connected to a control circuit to rectify into DC electricity and store in battery.

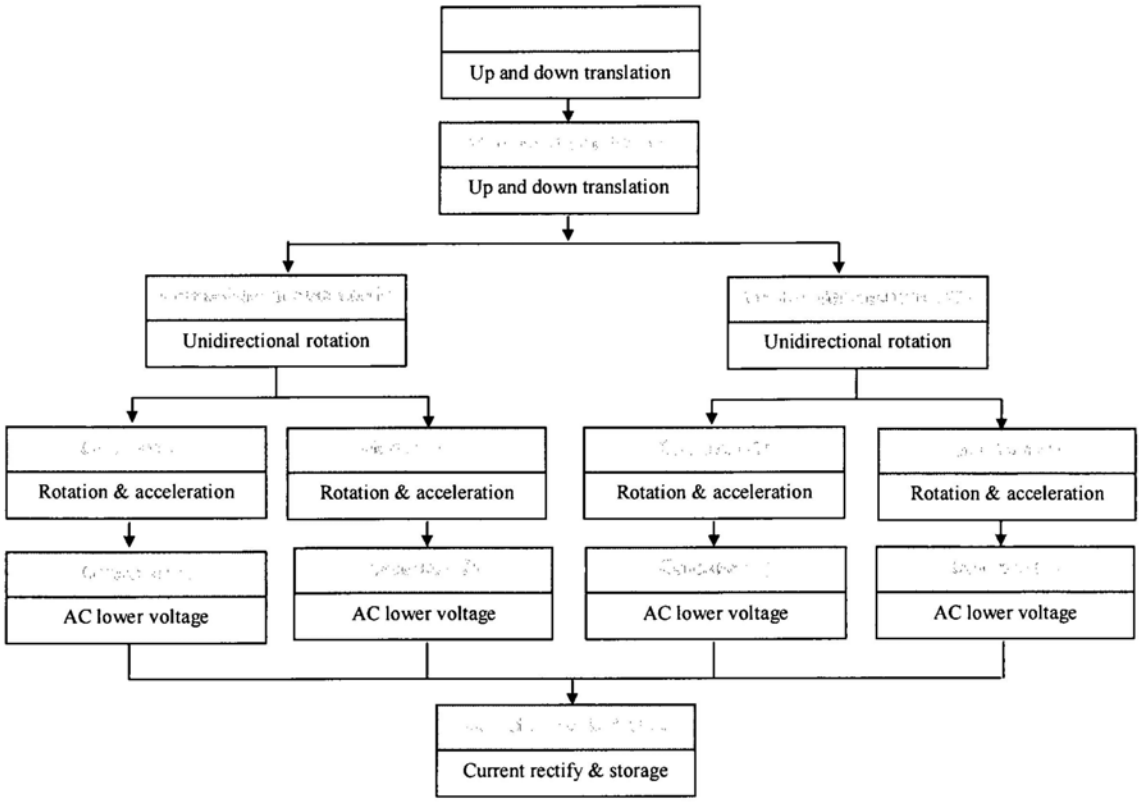

Fig.6-9: Flow chart of the harvester

This harvester is designed to insert into shoe heel. It can not only provide the function of shock absorber through the springs around the guiding poles, but also recycle part of the kinetic energy from foot step to generate electricity. When foot step up, i.e. leg leaves the ground and begins to swing, the pressed springs in harvester return energy to the foot for help the foot step. Compared with other similar designs, the presented design is more concisely. It employs the crank slider mechanism to transmit the motion from foot strike, which works not only when foot strike the ground but also when the foot leaves the ground. Because the crank slider mechanism can directly convert the up-down motion into unidirectional rotation, it needn't an extra mechanism to rectify the rotation direction. And what's more, because the impact force doesn't directly load onto the transmission components, the harvester is more reliable and stronger.

6.3 Analysis of the crank-slider mechanism

Crank-slider mechanism is the most critical mechanism in this harvesting device. Extracted from the physical model, Figure 6-10 shows the schematic diagram of the offset crank-slider linkage, where the grounded pivot O of the crank dose not lie on an extension of the line along which the pivot B is pin-jointed to slider. For a given set of linkage dimensions L_1, L_2, the offset distance L_0, and displacement of slider L_3, the following equations can be obtained by geometric and trigonometric relations. If the dimensions L_0, L_1 and L_2 are known, and the slider displacement L_3 is known too, then the angular displacement of the crank can be solved by these two equations.

$$L_1 \cos\theta_1 + L_2 \cos\theta_2 = L_3 \tag{6-1}$$

$$L_0 + L_1 \sin\theta_1 + L_2 \sin\theta_2 = 0 \tag{6-2}$$

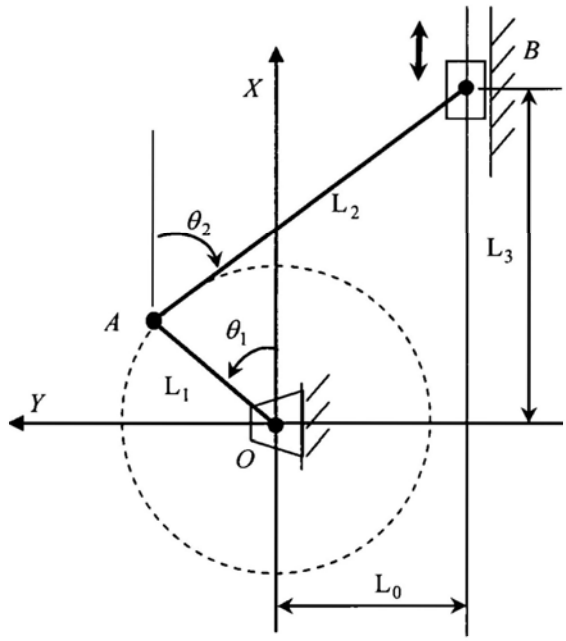

Fig.6-10: Offset crank-slider mechanism

For the offset crank slider mechanism, if the slider moves with constant velocity v_B from upper extreme point B^1 to lower extreme point B^2, then the crank rotates from position A^1 to position A^2 with the angle $\angle A^1OA^2 = \pi - \alpha$, however it will rotates with the angle $\angle A^2OA^1 = \pi + \alpha$ when the slider moves from B^2 to B^1. If both of time elapsed Δt are same, then the angular velocity of crank is different, which can be deduced from the following equation. Thus there is velocity fluctuation between the up stroke and the down stroke, which is not good to the generator. From the

Fig.6-11, the angle α is related to the offset distance L_0, that is, the bigger offset distance L_0, the greater angle α under the condition that other variables are constant. Therefore, it is best to set the offset distance zero, *i.e.* in-line crank-slider mechanism.

$$TR = \frac{\omega_1}{\omega_2} = \frac{\angle A^1OA^2 / \Delta t}{\angle A^2OA^1 / \Delta t} = \frac{\pi - \alpha}{\pi + \alpha} \tag{6-3}$$

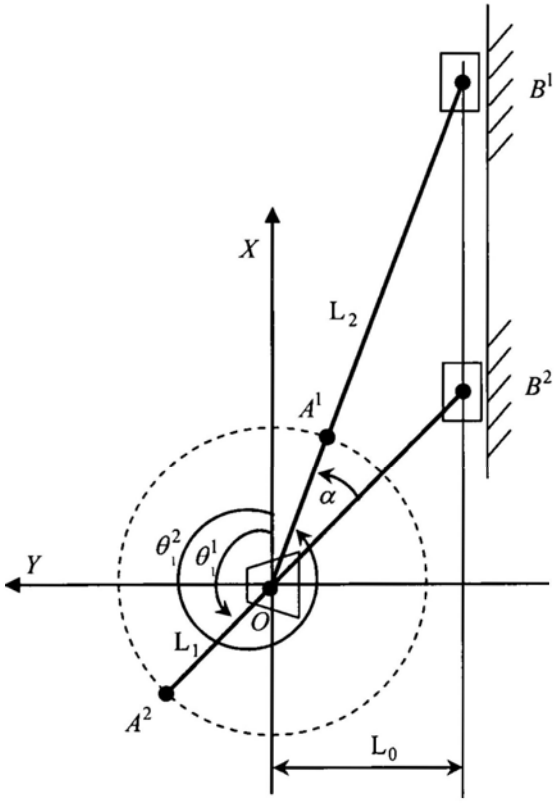

Fig.6-11: Extreme positions in offset crank slider linkage

For crank slider linkage, there is two deadlock points in the crank's cycle: one is at point A^1 where the angle between the crank and the crank coupler is 180°, and the other is at point A^2 where the angle is 0°. In order to avoid the deadlock problem, a "disturbed weight" is added to one end of the crank, as shown in Fig.6-12. For the initial condition when the slider is pressed due to the heel strike, *i.e.* the linkage lies as Fig.6-12, there is a disturbed force from the disturbed weight because there is acceleration from the heel strike. Therefore, the crank can be driven even if the linkage lies at deadlock point. When the pressed spring is released and slider moves upwards, the linkage lies at the second deadlock point A^2. Because the gear train is

rotating and the rotating inertia of moment from the disturbed weight, the linkage can easily pass this deadlock point.

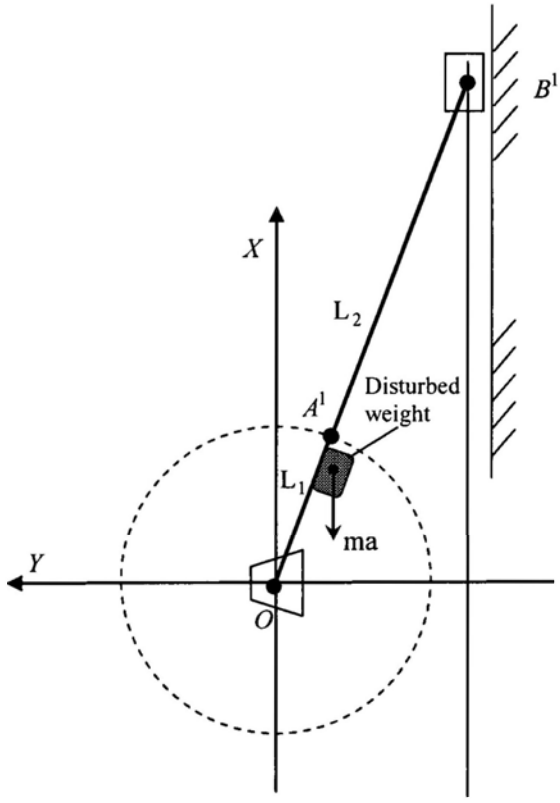

Fig.6-12: Solution for deadlock

The interference between the slider-crank mechanism and other component should be taken into consideration. The trajectories of crank and its coupler are drawn using Matlab®, as shown in Fig.6-13, from which other components should be arranged outside of the maximum profile of the trajectories to avoid interference.

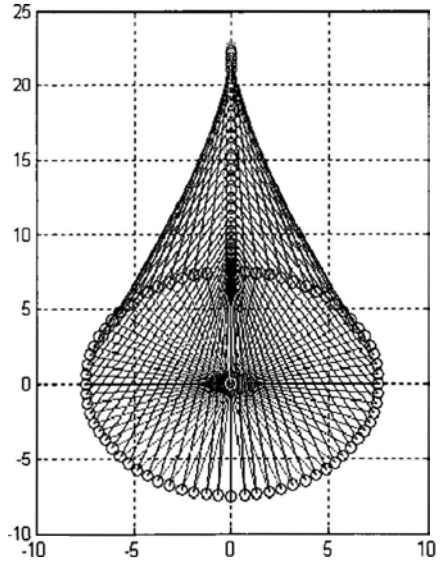

Fig.6-13: Trajectories of the slider crank mechanism

6.4 Analysis and Optimization of the Slider-Spring Mechanism

The springs in the harvester have three main functions: the first one is to serve as the shock absorber for the foot strike; the second one is to return force to the foot for helping foot step up; the third one is to restore the slider. In this section, the spring performance will be analyzed to fulfill these three functions, and optimization will be conducted to obtain a set of optimal parameters for the springs used in the harvester.

There are five springs in the harvester: four small identical springs at the four corners, and one large spring placed at the center. Assumed that the spring constant of the small four is k_1, and that of the large one is k_2. Because these five springs are connected to the harvester in parallel, the total spring constant is $K = 4k_1 + k_2$. If the spring has the deflection ΔS, then the spring force can be expressed as following according to the Hooke's Law.

$$f_s = K \cdot \Delta S \tag{6-4}$$

Usually the foot strike on the foot is about 1.5 times body weight. To relieve the strike on the foot, the harvester can be designed to absorb part of the body weight, *i.e.*:

$$f_s = K \cdot \Delta S = \beta \cdot mg \tag{6-5}$$

Where β is the absorption factor for the harvester, and m is the body weight. And the total spring deflection should be equal to the maximum displacement of the slider, *i.e.* $\Delta S = 2L_1$. Therefore, the total spring constant should be satisfactory with the following equation.

$$K = \frac{\beta \cdot mg}{2L_1} \tag{6-6}$$

If the slider position when all springs are in release is $x_B = 0$, and the position when springs are fully pressed down is $x_B = 2L_1$, then the deflection range of springs should be greater than $[0, 2L_1]$, *i.e.* when maximum deflection length of all springs

should be greater than $2L_1$ so that the slider can move up and down at full range. When the slider, *i.e.* the moving board, is fully pressed down, the whole body weight and the impact force are all loaded onto the transmission components of the harvester, which is harmful to the harvester, some action should be taken to avoid such damage. If the lowest position of the slider is the point when springs are extremely pressed down, i.e. when spring wires are attached together, the springs can support most of the body weight. And the slider should be able to restore to the highest position, when there is not any other restoring force but the spring force, so at the highest slider position the springs are also pressed slightly to provide thrust to restore the slider.

The most popular calculating formula of helical springs with circular cross-sectional wire is given as following.

$$k = \frac{G \cdot d^4}{8n \cdot D^3} \tag{6-7}$$

Where, G is the shear modulus; d is the wire diameter, n is the effective number of coils; D is the mean coil diameter. Therefore, with Eqs.(6-6) and (6-7), given an absorption factor, the dimensions of springs can be determined.

6.5 Transmission Analysis and Power Output Estimation

The harvester employs a set of gear train for each AC generator to speed up the rotation from the crank-slider mechanism, schematically shown in Fig.6-14. There are two gear pairs in the harvester, both of which are for acceleration. The total amplification ratio of the gear train can be expressed as following, where $Z_i, i = 1,2,3,4$ is the tooth number for each gear. In this harvester, two gear pairs have the same gear ratio, *i.e.* $Z_1/Z_2 = Z_3/Z_4 = 20$, then the total amplification ratio is 400, which can greatly boost the rotation speed.

$$GR = \frac{Z_1}{Z_2} \cdot \frac{Z_3}{Z_4} \tag{6-8}$$

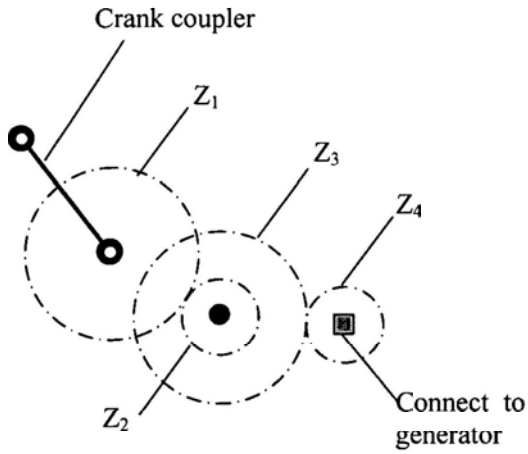

Fig.6-14: The gear train for each generator

The system parameters for obtaining the kinematical performance and simulation are shown in Tab.6-1.

Tab.6-1: System parameters

The harvester dimensions (released)	80*60*50mm^3
The total spring constant	15N/mm
Crank coupler length	20mm
Crank length	10mm
The absorption factor	0.5
Ratio of 1st gear set	20
Ratio of 2nd gear set	20
Mechanical energy efficiency	80%
Electric conversion efficiency	70%

Walking motion is generated by the ground reaction force of the stance foot. For straight forward walking, detailed analyses have been implemented as part of biomechanics. The relation between walking phase, step duration and reaction force is shown in Fig.6-15. The vertical reaction force of one foot has two peaks: one is at toe off of the other foot; the other is at heel strike of the other foot. The duration of one step, T, can be obtained from the step length w and the locomotion velocity v as $T = w/v$, or from the step frequency. The time duration of double foot support T^{ds}

can be approximated as $T^{ds} = 0.25 \cdot T$ [69]. For a single foot, the time duration when foot heel drives the moving board from free status to fully-expressed status is approximately equal to T^{ds}. During the period of foot swing T^{swing}, the pressed springs release up, when the moving board restores to its initial condition and drive the gear train again.

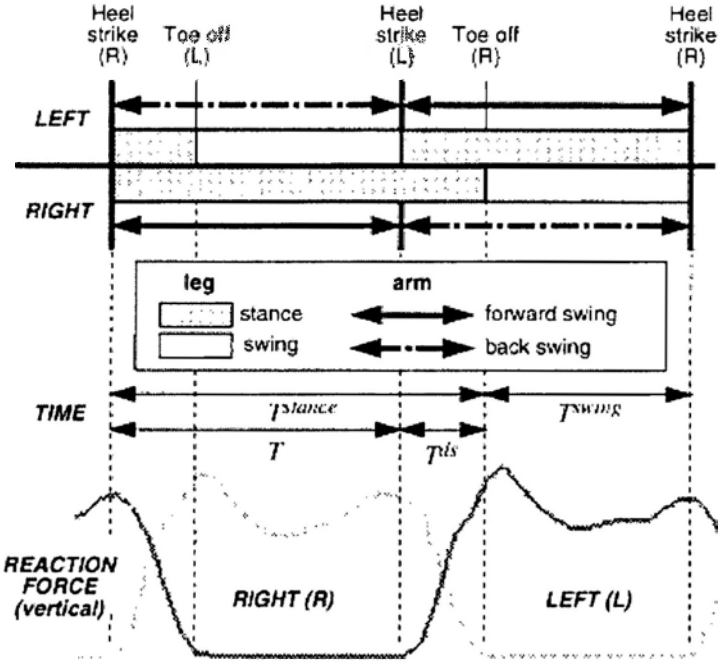

Fig.6-15: Step duration during normal walking [69]

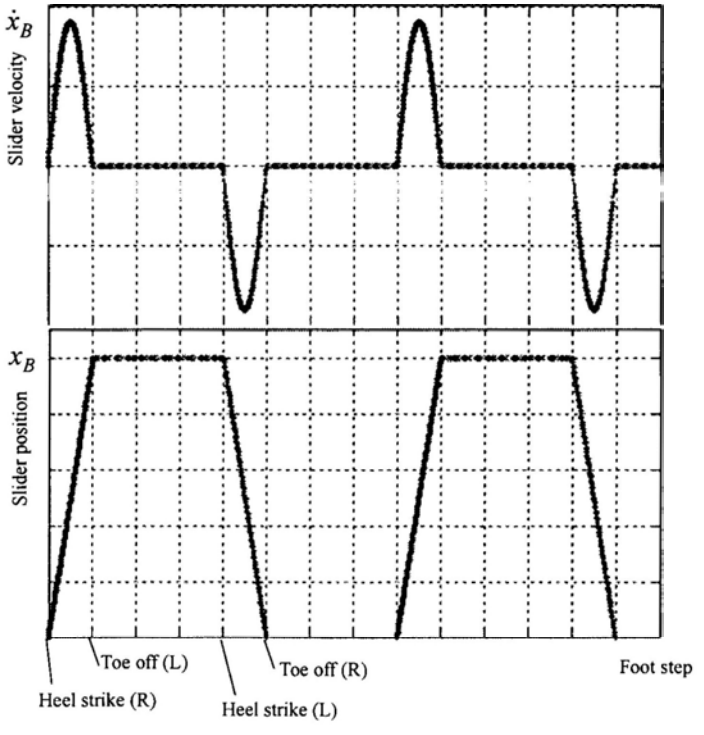

Fig.6-16: The velocity and position of the slider

For normal walking, the footstep frequency is about 2step/sec, so for a single harvester in a foot, there is once heel strike and then once toe off. Therefore, the harvester will work once per period, that is, the crank will rotate in a full circle. Figure 6-16 schematically shows the slider velocity and displacement in two footsteps during normal walking.

To estimate the power output, we can approximately use the work of springs to calculate the total input work W_{in} in a single period, as following, where K is the total spring constant, and $2L_1$ is the slider stroke distance.

$$W_{in} = 2 \cdot \frac{1}{2} K \cdot (2L_1)^2 = 4KL_1^2 \tag{6-9}$$

Considering the energy loss in transmission, including the crank-slider mechanism and gear train, and energy loss in mechanical-electrical conversion through the AC generator and electric circuit, which two efficiency factors are assumed as η_m and η_e, respectively, then the total output energy can be expressed as following.

$$E_{out} = 4\eta_m \eta_e KL_1^2 \tag{6-10}$$

Let the footstep frequency is f, then because every 2 steps has once heel strike, i.e. the working period of the harvester is two times that of footstep. So the average power output can be calculated by the following expression.

$$\bar{P}_{out} = \frac{E_{out}}{2T} = 2f \cdot \eta_m \eta_e \cdot KL_1^2 \tag{6-11}$$

The mechanical efficiency and electrical conversion efficiency of such kind of harvester are estimated to be 90% and 70%, respectively. Let the absorption factor for the harvester is $\beta = 0.5$, and a 60kg person has footstep frequency is 2 steps per second during normal walking, then the input energy for each step is 6J by Eq.(6-9). And the average power output can be calculated by Eqs.(6-5) and (6-11). The estimated average power output is about 2 watts for the harvester with the slider stroke length 10mm.

6.5 Discussions and Summary

The impact force of heel strike against the ground is very serious to the harvester, so the harvester presented in this chapter employs the crank-slider-spring mechanism to effectively avoid the direct impact to the transmission components which are most fragile. When the slider moves to the lowest position, the springs in the harvester are fully pressed, *i.e.* the wires attaches together, to support most of the body weight and its impact on the harvester. The dimensions of the crank, crank coupler and springs should be carefully calculated to ensure that the distance **H** from the upper point of the pressed spring to the ground-jointed center of the crank is equal to the difference between the crank coupler $\mathbf{L_2}$ and the crank $\mathbf{L_1}$, i.e. $H = L_2 - L_1$, so that the crank can pass its lowest position. However, manufacture may not achieve this requirement. Actually there is no problem when the requirement fails, that is, the crank can not pass the lowest point. If so, the crank-slider mechanism becomes crank-rocker mechanism, which can still convert the foot strike into rotation. In this case, when the slider returns to its upper position, the crank will not rotate from 180° to 360°, but from 180° to 0°, which will make the gear train rotates in reverse direction and then contribute to electricity in reverse direction. A rectification circuit can be used to change AC voltage into DC voltage, so the rocker-slider mechanism can work as well as the crank-slider mechanism.

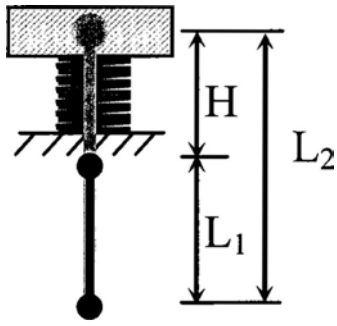

Fig.6-17: The status when springs are fully pressed

Four sets of gear train and generators share the same slider-spring mechanism and control circuit, which makes the system simpler and more concise. And multiple gear trains can decentralize the large foot strike, which can also improve the energy

conversion efficiency. The springs not only make the harvester harness more energy, but also provide thrust for the foot to step up.

Chapter 7

The Dual-Oscillating Mechanism for Energy Harvesting from Footstep Acceleration

There is rich kinetic energy in footstep motion during walking, so it is ideal to harvest the kinetic energy from human footstep motion as power source for portable electronic devices. In this chapter, a novel mechanism based on dual-oscillating mode is designed to harvest the kinetic energy from footstep motion. The harvester contains two oscillating sub-mechanisms: one is spring-mass oscillator to absorb the vibration from external excitation, i.e. the footstep motion, and the other is cantilever beam with tip mass for amplifying the vibration. Analysis shows that the dual-oscillating mechanism can be more effectively harness the foot step motion. The energy conversion sub-mechanism is based on the electromagnetic induction, where the wire coils fixed at the tip end of the cantilever beam serves as the slider and permanent magnets and yoke form the changing magnetic field. Analysis shows that the harvester, with total mass 70g, can produce about 100mW of electricity at the walking speed of 2 steps per second.

7.1 The Harvester Structure

The bottom rear part of a shoe, i.e. the heel, is designed to support the heel of the foot, which is usually higher than the shoe sole. Therefore it is ideal to employ the room of the shoe heel to set up a harvester to harness the footstep motion. Figure 7-1 shows the appearance of the harvester, which is a box container where the harvester is fixed. The container is made of non-magnetic mental to endure human body weight and the impulsive force from heel strike. There are two helical springs on the harvester: one is attached to the bottom base of the container, and the other is attached to the upper cover of the container. And the container cover is fixed via screws to the container body.

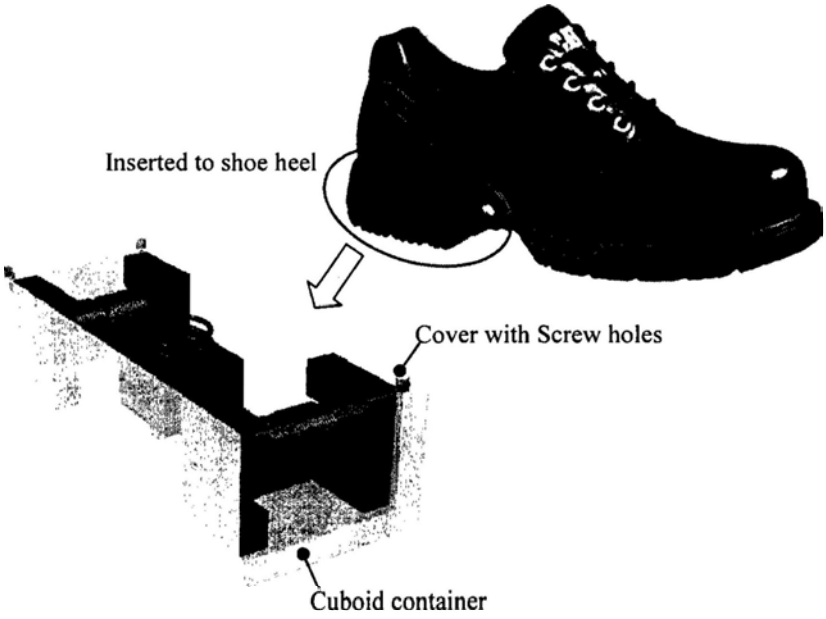

Fig.7-1: The overview of the dual-oscillating harvester

The harvester is symmetric, and there are independent magnetic fields in the harvester. As shown in Fig.7-2, there are two sets of components to produce magnetic field arranged at the two ends of container body. Each set is composed of two pairs of *NdFeB* permanent magnets arranged in opposite magnetization direction and yoke made of electric steel. Permanent magnets are attached to yoke, which forms a magnetic circuit with the counterpart.

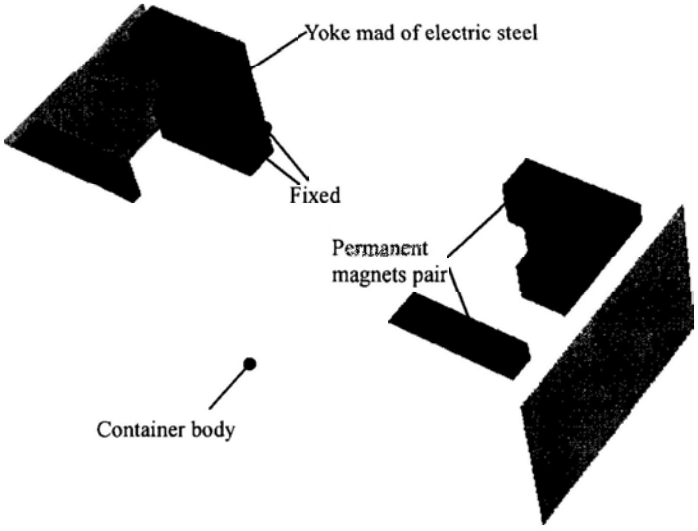

Fig.7-2: The structure for producing magnetic field

The oscillating mechanism is used to produce vibration from external excitation, as shown in Fig.7-3. There are a proof mass, called oscillating weight, and two helical springs attached to the oscillating weight, which forms the first tier of oscillating mechanism to absorb the external excitation. Two identical cantilever beams attached to the oscillating weight, and the weight at its tip end, make up of the second tier of oscillating mechanism to amplify the vibration from the oscillating weight. The wire coils are wound at the tip end of the cantilever beam as the proof mass for the second tier of the oscillating mechanism. With the magnetic field produced by permanent magnets, the vibration from the two tiers of oscillating mechanism makes the wire coils generate induction voltage.

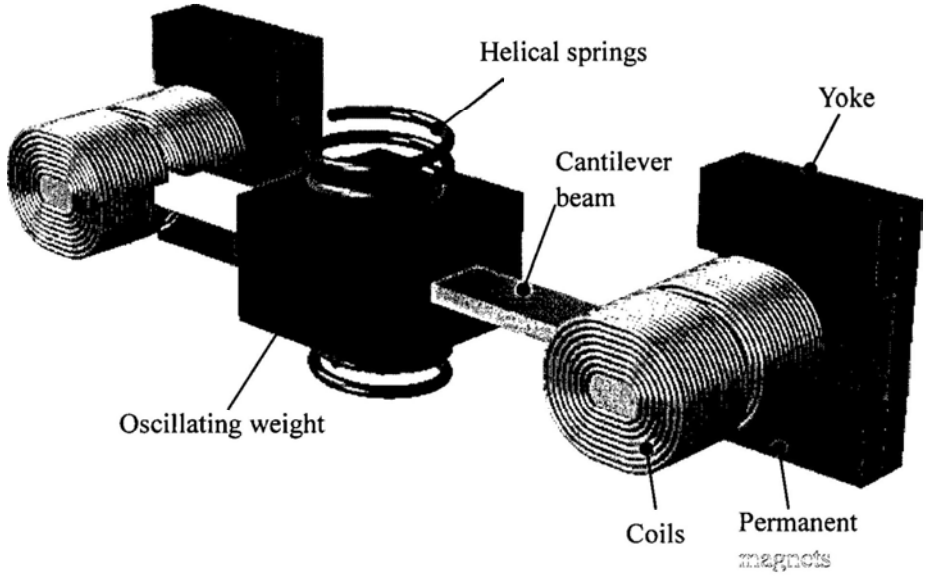

Fig.7-3: The structure of the oscillating mechanism

Abstracted from the physical model, Fig.7-4 shows the schematic diagram of the harvester, which can be divided into three functional parts: vibration absorber, vibration amplifier and harvesting mechanism. The vibration absorber, consisting of an oscillating weight and two helical springs attached to the oscillating weight and the container base, transmits vibration from external excitation to the oscillating weight. The vibration amplifier consists of a cantilever beam and a tip mass composed of the wire coils and their iron core, which is similar to spring-mass system, to amplify the vibration from the oscillating weight. The harvesting

mechanism mainly consists of permanent magnet pairs and coils. The magnets are arranged to produce changing magnetic field, from which the moving coils can produce induced voltage due to the electromagnetic induction effect.

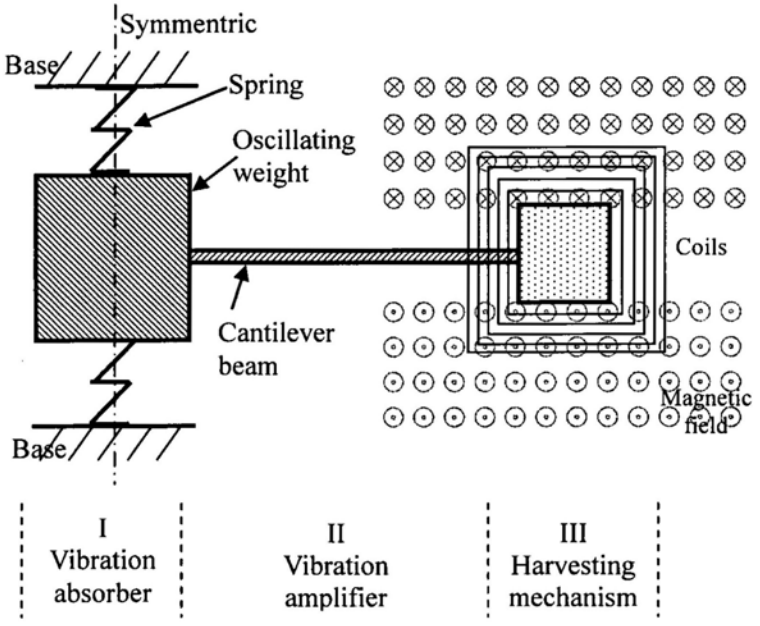

Fig.7-4: The schematic diagram of the dual-oscillating harvester

7.2 Electromagnetic Analysis

The energy conversion, from kinetic energy to electricity, is based on electromagnetic induction. The schematic diagram of magnetic structure and magnetic flux path are shown in Fig.7-5. There are two pairs of permanent magnets separated by plastic spacers, arranged with different magnetization direction to produce different flux directions. All permanent magnets are attached to yoke made of electric steel. Yoke and permanent magnets constitute the magnetic flux path, shown as dash lines in Fig.7-5. In this harvester, the magnets, yokes and spacers are all symmetric, so the coordinate is created at the symmetric center where Z direction is perpendicular to the ground and X direction is the magnetization direction of the permanents. When the harvester is excited by external motion, the coils will vibrate on the YOZ plane where the magnetic flux is at its maximum.

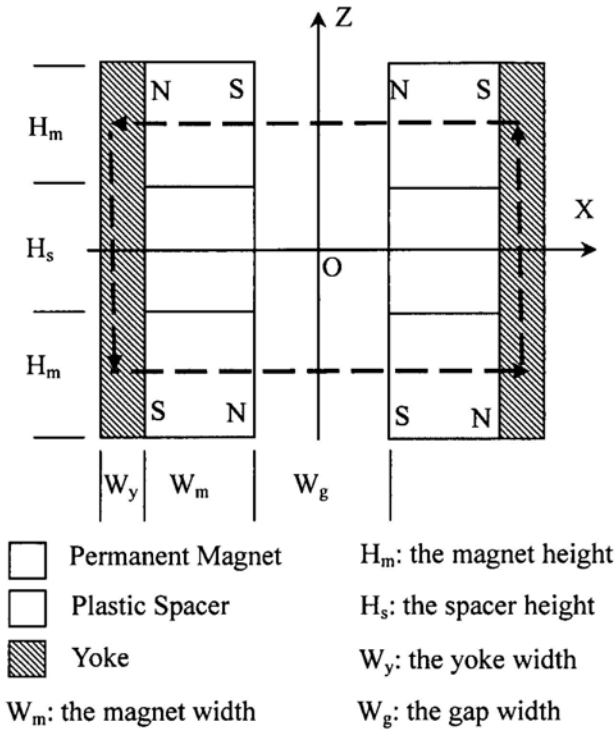

Fig.7-5: Schematic diagram of magnetic structure and the flux paths

FEA models were built in Ansys® to investigate the magnetic field. The structures related to magnetic field are simplified as the left figure of Fig.7-6, where the areas with different material properties are displayed in different color. There are four types of material areas: permanent magnets magnetized from left to right (in red), permanent magnets magnetized from right to left (in deep blue), the electric steels (in pink) and the air area (in light blue). The right figure of Fig.7-6 shows the meshing division, where the magnets and electric steel are refined to obtain high precision.

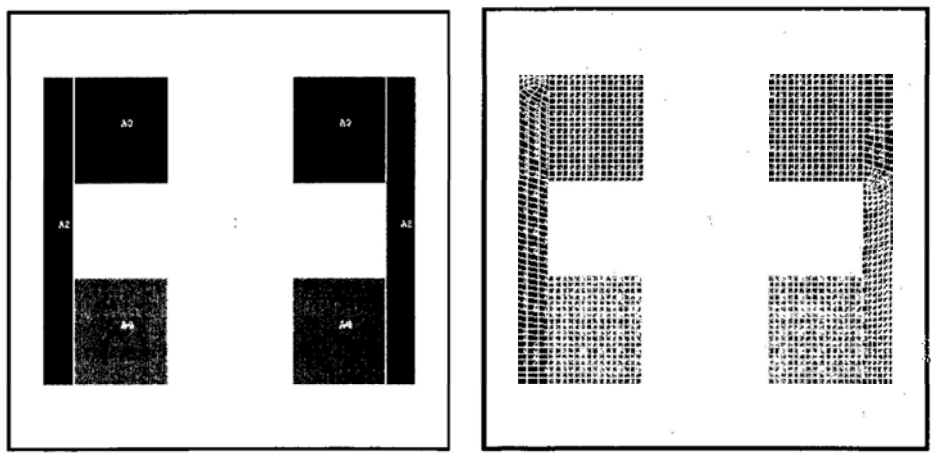

Fig.7-6: FEA model and its mesh in Ansys®

After resolving, the magnetic flux density is plotted in vector, shown in Fig.7-7, which shows that the two pairs of magnets and their yoke forms a magnetic circuit. The density of 2D flux lines, shown in Fig.7-8, also indicates that the flux density is concentrated around the magnetic circuit. It also shows the flux distribution of the magnetic field, from which the flux density at the center of pole pitch is higher than that at the fringes.

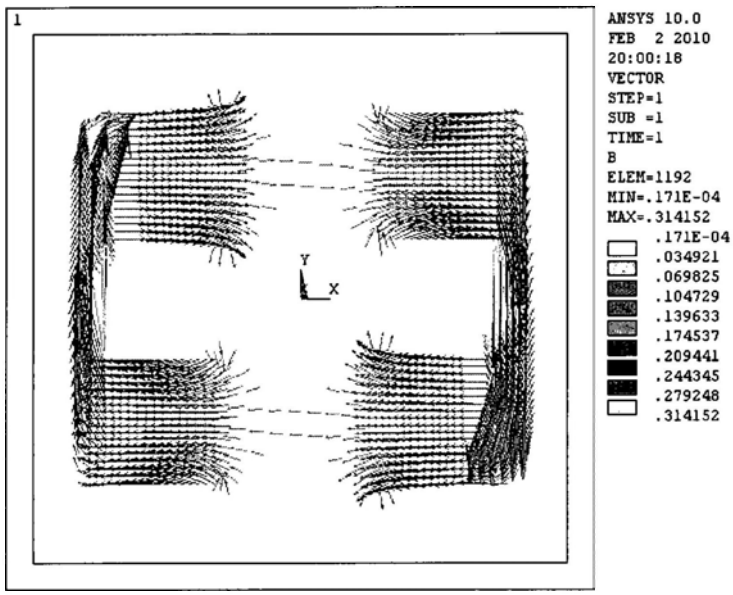

Fig.7-7: The magnetic flux density plotted in vector

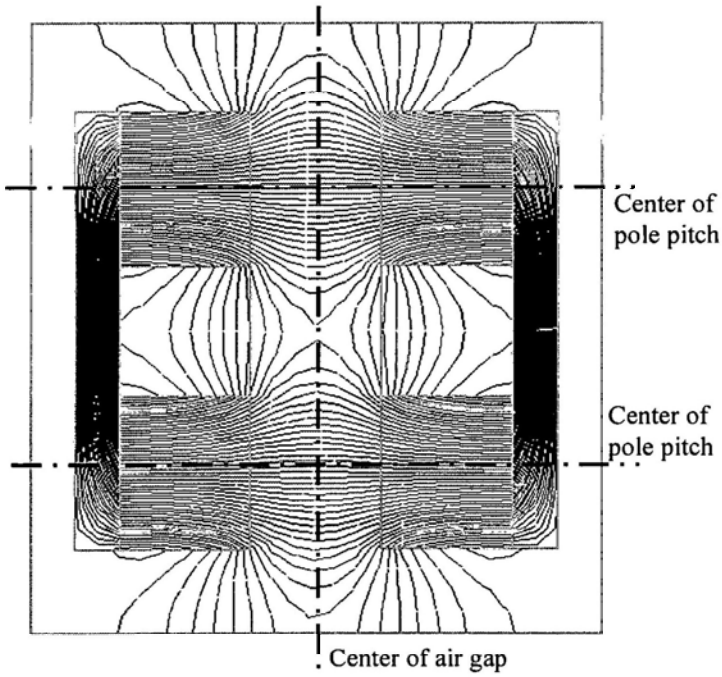

Fig.7-8: 2D Flux distribution of the magnetic field

In order to calculate the flux through coils, the component of flux density perpendicular to coils should be projected to x direction. Figure 7-9 shows the color map of the x-component of magnetic flux density, which indicates that the x-component is also concentrated around the magnetic circuit, especially around the pole pitches. The analysis shows that the flux density in the air gap is different for different air gap distance. Figure 7-10 shows the x-component distribution of flux density, where all curves share the same pattern, similar to sine waves. The smaller air gap distance, the larger flux density at the center of each magnet pitches; however, the flux density around the pitch fringes for different air gap distances is very close.

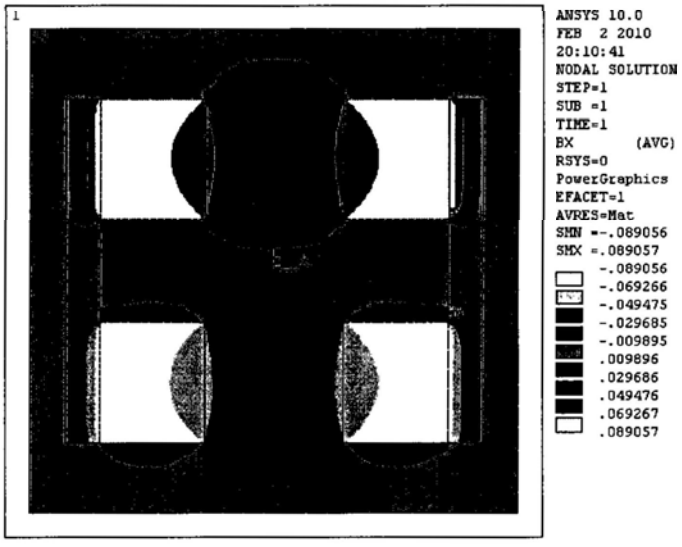

Fig.7-9: The x-component of magnetic flux density (perpendicular to coils)

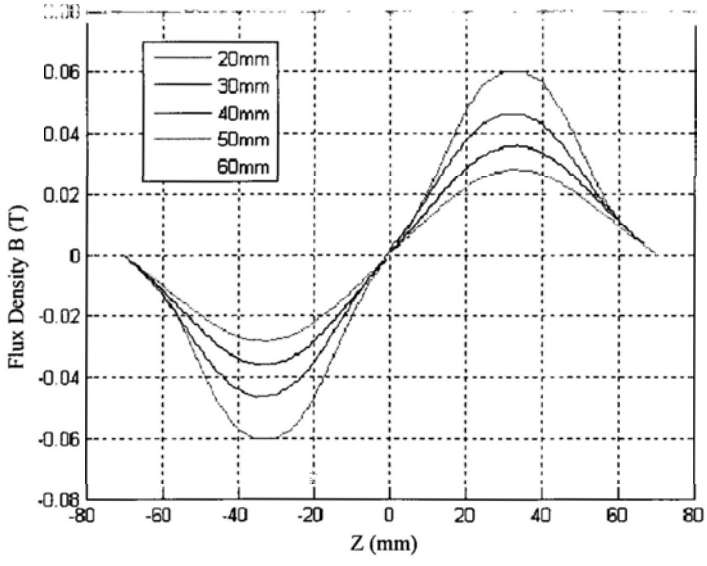

Fig.7-10: Distribution of flux density at the gap center for different air gap distances

The peak values of the flux density are obtained at the center of magnet pitch, which is distributed as a quadratic curve, shown in Fig.7-11. Actually the flux density from different X positions has the similar distribution pattern to those along Z direction (shown in Fig.7-11), as shown in Fig.7-12, where the closer position has the higher peak value.

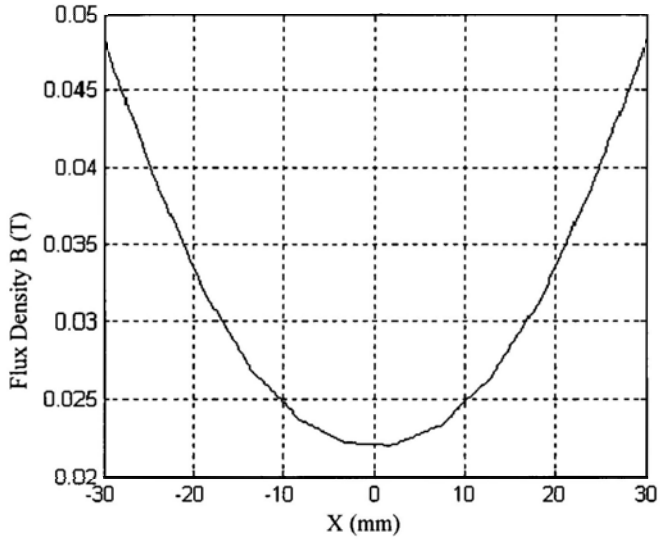

Fig.7-11: The peak value of flux density along the center line of pole pitch

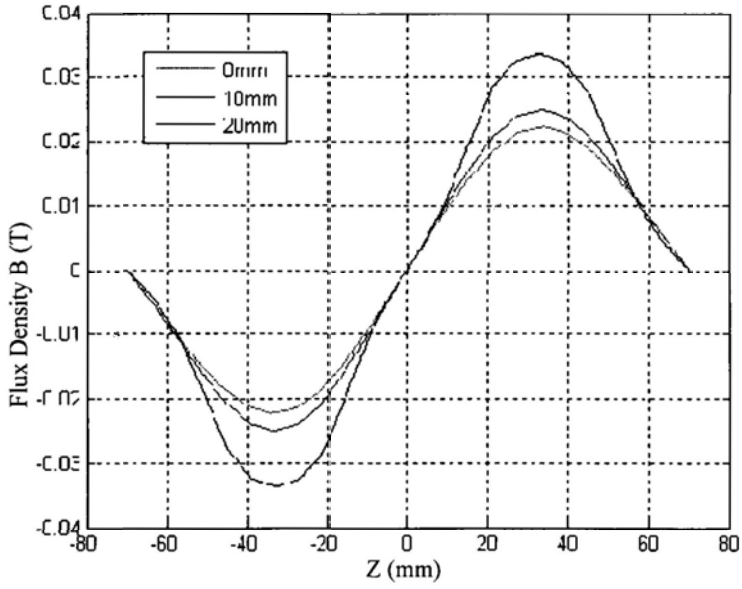

Fig.7-12: The distribution of flux density along Z direction for different X positions

For a single coil lying on the YOZ plane at the position $x = x_0$, the density of magnetic flux through the coil is changing along Z direction, so the total flux through the coil should be calculated by integral by the following equation, where $B(x_0, z)$ is the flux

density at point (x_0, z) and there is the assumption of equal distribution of flux density along Y direction.

$$\Phi_c = \int_{z-\frac{H_c}{2}}^{z+\frac{H_c}{2}} B(x_0, \hat{z}) \cdot D \cdot d\hat{z} \tag{7-1}$$

Where, D is the thickness of the permanent magnet, and H_c is the height of the coil. Based on the Faraday's Law, the induction voltage of a single coil is

$$\varepsilon = \frac{d\Phi_c}{dt} = \frac{d\Phi_c}{dz}\frac{dz}{dt} = \frac{d}{dz}\left(\int_{z-\frac{H_c}{2}}^{z+\frac{H_c}{2}} B(x_0, \hat{z}) \cdot D \cdot d\hat{z}\right) \cdot \dot{z} \tag{7-2}$$

For simplification, the height of winding coils can be equivalent to the height of the middle layer H_{cm}, and assumed that there are N coils, so the total induction voltage at one end of cantilever beam is:

$$V = N\frac{d\Phi_c}{dt} = N\frac{d\Phi_c}{dz}\frac{dz}{dt} = N\frac{d}{dz}\left(\int_{z-\frac{H_{cm}}{2}}^{z+\frac{H_{cm}}{2}} B(x_0, \hat{z}) \cdot D \cdot d\hat{z}\right) \cdot \dot{z} \tag{7-3}$$

The electrical damping force converts the kinetic energy to electricity, so the power done by the electrical damping force should be equal to the one done by electricity, that is:

$$F_e \cdot \dot{z} = -\frac{V^2}{R_c + R_e + R_L} \tag{7-4}$$

Here, R_c, R_e, and R_L are the resistance of the coils, the resistance in the control circuit, and the load resistance respectively. Inserting the Eq.(7-3) into Eq.(7-4), then the electrical damping force is:

$$F_e = -\frac{\left[N \cdot D \cdot \frac{d}{dz}\left(\int_{z-\frac{H_{cm}}{2}}^{z+\frac{H_{cm}}{2}} B(x_0, \hat{z}) d\hat{z}\right)\right]^2}{R_c + R_e + R_L} \cdot \dot{z} \tag{7-5}$$

Define the electrical damping coefficient C_e as:

$$C_e = \frac{\left[N \cdot D \cdot \frac{d}{dz} \left(\int_{z-\frac{H_{cm}}{2}}^{z+\frac{H_{cm}}{2}} B(x_0, \hat{z}) d\hat{z} \right) \right]^2}{R_c + R_e + R_L} \tag{7-6}$$

Since the flux density is changing in the magnetic field, the electrical damping coefficient will change along the Z direction. From the FEA analysis by Ansys®, it is easy to obtain the flux density distribution curve, and then the electrical damping coefficient can be calculated by Eq.(7-6). Figure 7-13 shows the distribution curve of electrical damping force along Z direction, which has two peaks where lines of the pole pitch are near the two centers.

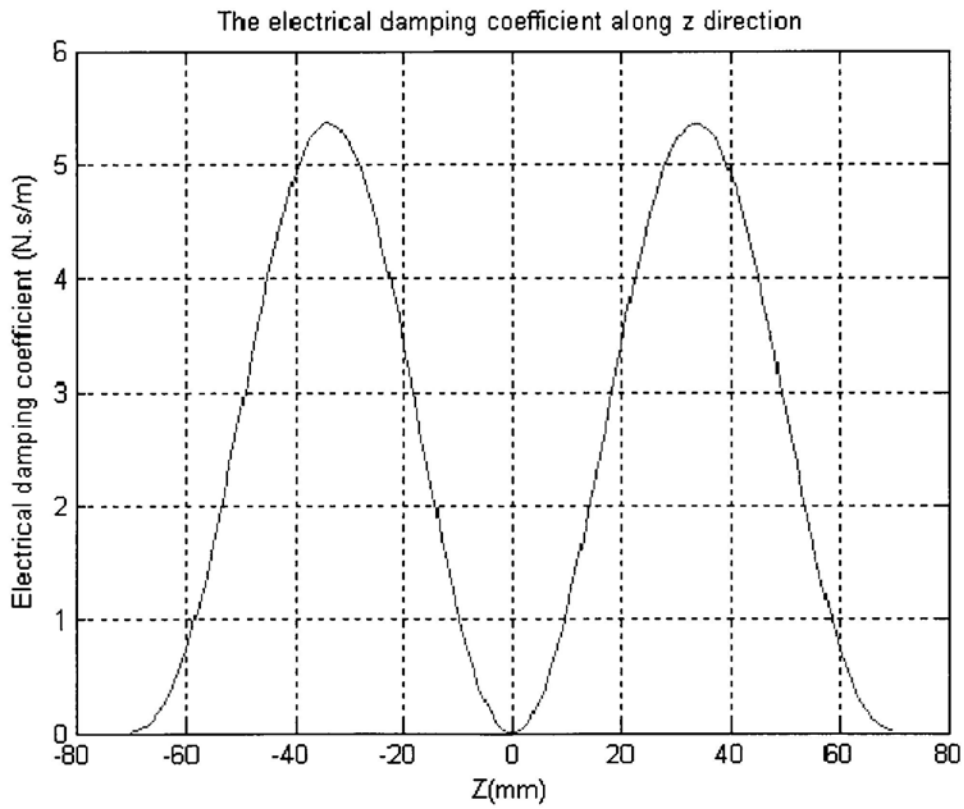

Fig.7-13: The distribution curve of electrical damping coefficient along Z direction

7.3 Kinematical Analysis

There are two coupled sub-oscillating mechanism in this harvesting system: the vibration absorber and the vibration amplifier. The vibration amplifier is a rectangular cantilever beam with a tip mass m_2 which made up of a non-magnetic material core and the wire coils wound around the core. For analysis convenient, the cantilever beam can be equivalent to a spring with the spring constant k_2, which can be calculated as following.

$$k_2 = \frac{Ebh^3}{4L^3} \tag{7-7}$$

Where b, h and L are the width, thickness and the length of the beam, respectively; and E is the Young's module of the beam. Since the mass of the beam is much less than the tip mass, its mass is neglected for analysis convenience. The vibration amplifier is subject to both the mechanical damping force C_{m2} and the electrical damping force C_e which represents the energy converted into electricity.

For the vibration absorber, there are two helical springs attached to the oscillating weight m_1, which can be combined together and has a combined spring constant k_1, calculated by $k_1 = [k_{11} + k_{12}]$, where k_{11} and k_{12} are the spring constant of the upper and lower spring respectively. The vibration absorber is also subject to mechanical damping force C_{m1}.

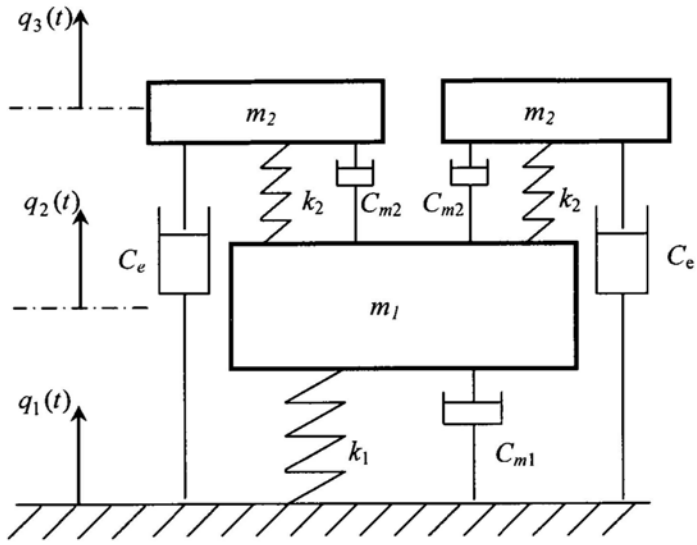

Fig.7-14: The schematic model of the oscillating mechanism

Figure 7-14 shows the coupled schematic model of the oscillating mechanism, where base excitation is $q_1(t)$, and the displacements of the oscillating weight of the vibration absorber and tip mass of the vibration amplifier are $q_2(t)$ and $q_3(t)$ respectively, then the kinetic energy, potential energy and Rayleigh potential can be obtained as following. Kinetic energy is:

$$T = \frac{1}{2} m_1 \cdot \dot{q}_2^{\,2} + 2\left(\frac{1}{2} m_2 \cdot \dot{q}_3^{\,2}\right) \tag{7-8}$$

Potential energy is:

$$V = \frac{1}{2} k_1 (q_2 - q_1)^2 + 2\left[\frac{1}{2} k_2 (q_3 - q_2)^2\right] + m_1 g q_2 + 2 m_2 g q_3 \tag{7-9}$$

Rayleigh potential is:

$$R = \frac{1}{2} C_{m1} (\dot{q}_2 - \dot{q}_1)^2 + 2\left[\frac{1}{2} C_{m2} (\dot{q}_3 - \dot{q}_2)^2 + \frac{1}{2} C_e (\dot{q}_3 - \dot{q}_1)^2\right] \tag{7-10}$$

Then the *Lagrangian* function becomes

$$\begin{aligned} L &= T - V \\ &= \frac{1}{2} m_1 \cdot \dot{q}_2^{\,2} + 2\left(\frac{1}{2} m_2 \cdot \dot{q}_3^{\,2}\right) - \frac{1}{2} k_1 (q_2 - q_1)^2 - 2\left[\frac{1}{2} k_2 (q_3 - q_2)^2\right] - m_1 g q_2 - 2 m_2 g q_3 \end{aligned} \tag{7-11}$$

For this two degree-of-freedom system, it has two variables. The base excitation q_1 is known, so q_2 and q_3 are set as variables. Hence, the Lagrangian equation in terms of q_2 is:

$$\frac{d}{dt}(\frac{\partial L}{\partial \dot{q}_2}) - \frac{\partial L}{\partial q_2} + \frac{\partial R}{\partial \dot{q}_2} = 0 \tag{7-12}$$

Gives

$$m_1\ddot{q}_2 + k_1(q_2 - q_1) - 2k_2(q_3 - q_2) + m_1 g + C_{m1}(\dot{q}_2 - \dot{q}_1) - 2C_{m2}(\dot{q}_3 - \dot{q}_2) = 0 \tag{7-13}$$

And the *Lagrangian* equation in terms of q_3 is:

$$\frac{d}{dt}(\frac{\partial L}{\partial \dot{q}_3}) - \frac{\partial L}{\partial q_3} + \frac{\partial R}{\partial \dot{q}_3} = 0 \tag{7-14}$$

Gives

$$m_2\ddot{q}_3 + k_2(q_3 - q_2) + m_2 g + C_{m2}(\dot{q}_3 - \dot{q}_2) + C_e(\dot{q}_3 - \dot{q}_1) = 0 \tag{7-15}$$

Upon simplification, let $z = q_3 - q_1$, $y = q_2 - q_1$ and $x = q_1$, then Eq.(7-13) and (7-15) can be rewritten as following.

$$\begin{bmatrix} m_1 & 0 \\ 0 & 2m_2 \end{bmatrix}\begin{bmatrix} \ddot{y} \\ \ddot{z} \end{bmatrix} + \begin{bmatrix} C_{m1} + 2C_{m2} & -2C_{m2} \\ -2C_{m2} & 2(C_{m2} + C_e) \end{bmatrix}\begin{bmatrix} \dot{y} \\ \dot{z} \end{bmatrix} + \begin{bmatrix} k_1 + 2k_2 & -2k_2 \\ -2k_2 & 2k_2 \end{bmatrix}\begin{bmatrix} y \\ z \end{bmatrix} = \begin{bmatrix} -m_1\ddot{x} - m_1 g \\ -2m_2\ddot{x} - 2m_2 g \end{bmatrix} \tag{7-16}$$

Define the mass matrix **M**, damping matrix **C** and stiffness matrix **K** as following, respectively,

$$\mathbf{M} = \begin{bmatrix} m_1 & 0 \\ 0 & 2m_2 \end{bmatrix} \tag{7-17}$$

$$\mathbf{C}=\begin{bmatrix} C_{m1}+2C_{m2} & -2C_{m2} \\ -2C_{m2} & 2(C_{m2}+C_e) \end{bmatrix} \tag{7-18}$$

$$K=\begin{bmatrix} k_1+2k_2 & -2k_2 \\ -2k_2 & 2k_2 \end{bmatrix} \tag{7-19}$$

All of these coefficient matrixes are symmetric. For this two degree-of-freedom system, the natural frequencies of the system can be solved by the following characteristic equation:

$$\det\left[-\omega^2\begin{bmatrix} m_1 & 0 \\ 0 & 2m_2 \end{bmatrix}+\begin{bmatrix} k_1+2k_2 & -2k_2 \\ -2k_2 & 2k_2 \end{bmatrix}\right]=0 \tag{7-20}$$

Or

$$m_1m_2\omega^4-[k_2m_1+(k_1+2k_2)m_2]\omega^2+k_1k_2=0 \tag{7-21}$$

Equation (7-21) has four roots, $\pm\omega_1$ and $\pm\omega_2$ ($\omega_1 \le \omega_2$), and since the natural frequencies are positive, the natural frequency matrix can be expressed as $\Omega=\begin{bmatrix} \omega_1 & 0 \\ 0 & \omega_2 \end{bmatrix}$. To determine the mode shapes, the ω in equation $\left[K-\omega^2M\right]\{X_1 \quad X_2\}^T=0$ is replaced with ω_1 and ω_2 to obtain the eigenvector, which can combine to a normalization modal matrix:

$$\Phi=\begin{bmatrix} 1 & 1 \\ X_{21}/X_{11} & X_{22}/X_{21} \end{bmatrix} \tag{7-22}$$

With a certain design of the harvester, there are determinate mass m_1 and m_2, spring constant k_1 attached on the oscillating weight m_1, and the dimensions of the cantilever beam which can be used to calculate the equivalent stiffness constant k_2 by Eq.(7-7). Assumed that the oscillating mass m_1 and m_2 are attached together, then the natural frequency of the system can be expressed as $\omega_{n1}=\sqrt{k_1/(m_1+2m_2)}$, therefore the mechanical damping coefficient of oscillating mass m_1 can be expressed as $C_{m1}=2\xi(m_1+2m_2)\omega_{n1}$, where ξ is the system damping ratio. Similarly, the natural

frequency of oscillating mass m_2 is $\omega_{n2} = \sqrt{k_2/m_2}$ and its mechanical damping coefficient is $C_{m2} = 2\xi m_2 \omega_{n2}$. Then the characteristics of the system, including the natural frequencies and modal shape can be obtained by Eq.(7-21). After having the acceleration of the foot motion $\ddot{x}$, the displacement performance of the system can be solved by Eq.(7-16) using Matlab®.

7.4 Coupled Analysis and Power Output

This dual-oscillating harvester is used to harvest the vertical acceleration of human footstep motion not only during the foot swinging process but also when the foot heel strike the ground. Therefore there are two major components of the footstep acceleration: one is from the foot stride along with the body trunk, which is equal to the vertical acceleration of the body center; the other is from heel strike against the ground during walking, which can be expressed as a step function. Since the body center can be modeled as an inverted pendulum, therefore the vertical acceleration of body center can be expressed as a sine wave function as $\ddot{x} = a_0 \sin(\omega t)$. Then the foot acceleration on the vertical direction can be expressed as by combining a sine function with a step function. Figure 7-15 shows the sine acceleration from foot swing, step acceleration from foot strike and their combination.

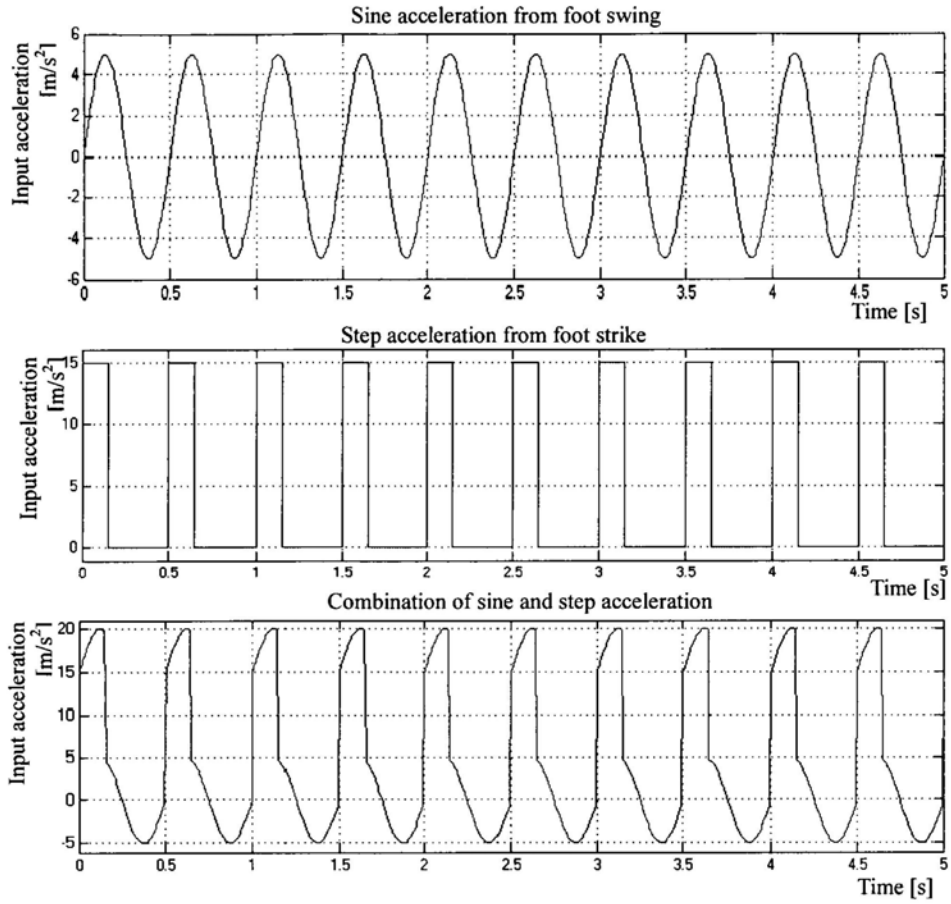

Fig.7-15: Acceleration performance during foot swinging

First of all, the system kinematical performance is studied at the condition of open circuit, that is, there is no power output. The system parameters for obtaining the kinematical performance and simulation are shown in Tab.7-1. Considering the external acceleration excitation of a step impulse function, expressed as $\ddot{x} = 10 \cdot \text{square}(0.5, 10)$ [m/s^2] in Matlab, where the time duration of the foot strike is 0.6 second and the acceleration amplitude is 10 m/s^2. Then the velocity performance of the oscillating weight and the coil is shown in Fig.7-16, where the damping ratio ξ is set to 0.1. From the figure, the cantilever beam really amplifies the vibration from the oscillating weight with the amplification factor of 1.5. With the same condition, the velocity response for periodical external excitation in acceleration is shown in Fig.7-17, 18, and 19. From these figures, the vibration in the cantilever beam has the same response period but has larger amplitude.

Tab. 7-1: the system parameters

Rigidity modulus of the helical spring, G	80GPa
Wire diameter of the helical spring, d	1mm
The Mean diameter of the spring, D	8mm
No. of active coils of the spring, n	5
The spring constant, k_1	$k_1 = \frac{G \cdot d^4}{8n \cdot D^3}$
Young's module of cantilever beam, E	71GPa
Width of the cantilever beam, b	1.5mm
Height of the cantilever beam, h	0.5mm
Length of the cantilever beam, L	15mm
Equivalent constant of the cantilever beam, k_2	$k_2 = \frac{Ebh^3}{4L^3}$
The mass of oscillating weight, m_1	10g
The mass of tip mass at cantilever beam, m_2	20g
Damping coef. of the oscillating weight, C_{m1}	$C_{m1} = 2\xi\sqrt{k_1(m_1 + 2m_2)}$
Damping coef. of the cantilever beam, C_{m2}	$C_{m2} = 2\xi\sqrt{k_1 \cdot m_2}$

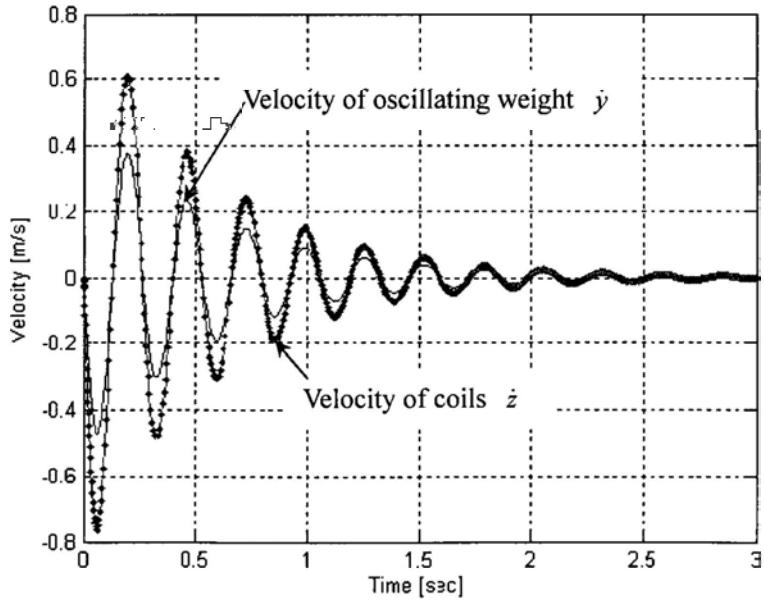

Fig.7-16: the velocity response from step impulse

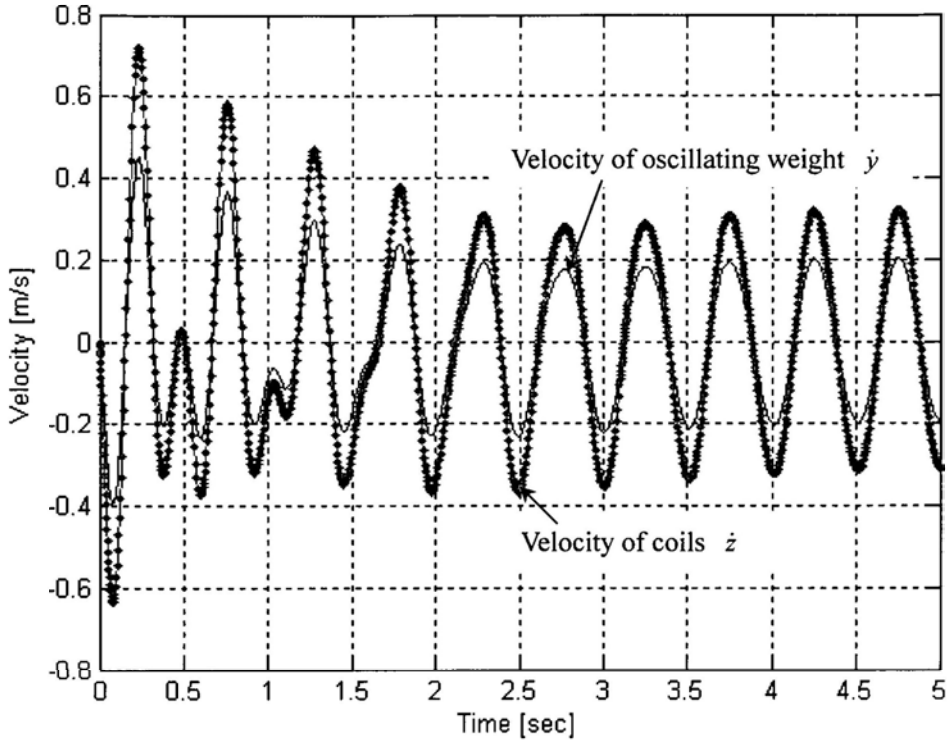

Fig.7-17: Velocity response from external acceleration in sine wave

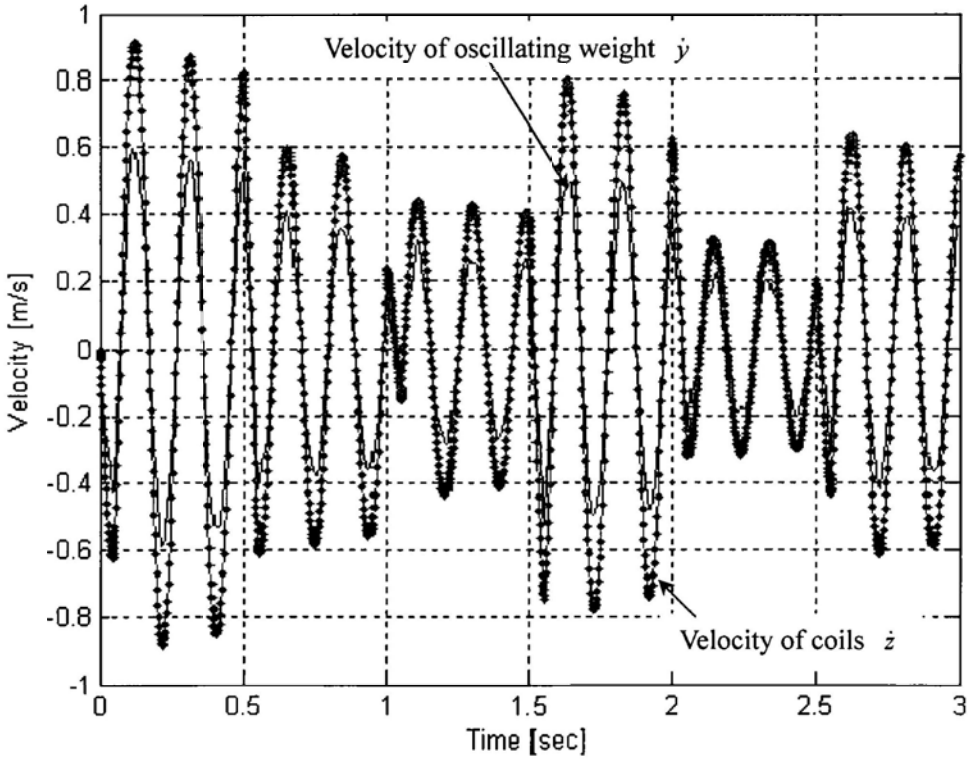

Fig.7-18: Velocity response from external acceleration in square function

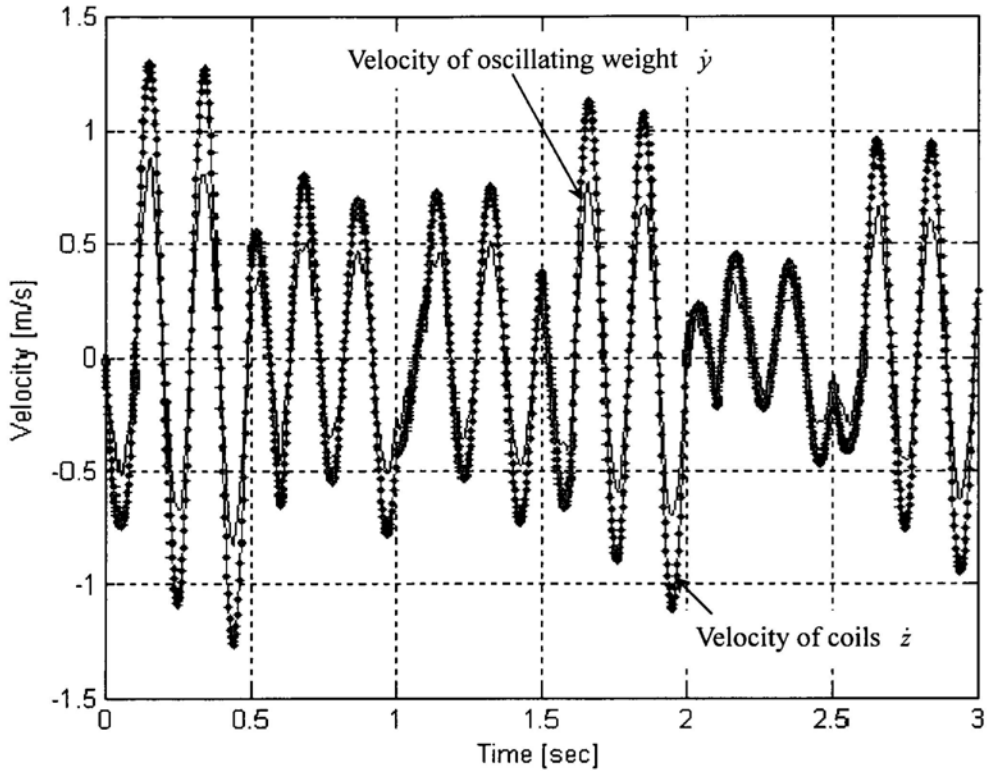

Fig.7-19: Velocity response from external acceleration combining square function and sine wave

For the condition of close circuit, there is electrical damping which the only factor different to the open condition. With the electrical damping coefficient curve (as Fig.7-13) and the external input acceleration, the kinematical performance of the oscillating weight (the vibration absorber) and the coils (the vibration amplifier) can be solved by Eq.(7-16) by numerical method with Matlab®. Figure 7-20 shows the displacement and velocity response in the case of close circuit. The electrical damping, which coefficient is greater than the mechanical damping coefficient, makes the oscillation decreasing more quickly. However, the vibration amplifier still can obviously speed up the vibration from oscillating weight.

With the relative velocity of the coils and the electrical damping coefficient, the transient power output can be calculated by Eq.(7-23). Figure 7-21 shows the transient power output of the harvester with the combination of sine function and step function as external input. Since the acceleration from heel strike is bigger than that from the foot swing, the power output performance also shows that there is higher power output at the time of heel strike.

$$p = C_e \cdot \dot{z}^2 \tag{7-23}$$

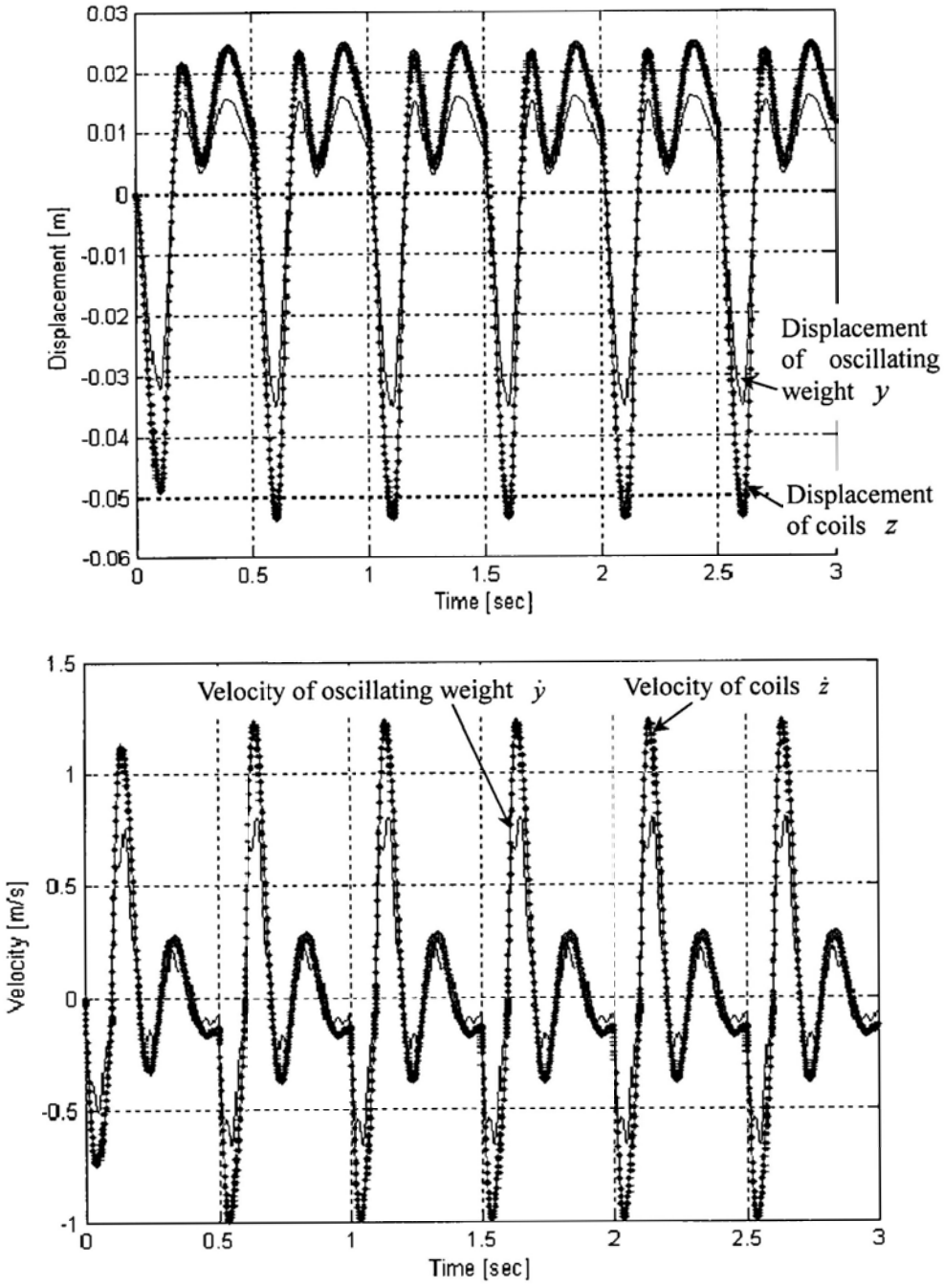

Fig.7-20: Displacement and velocity response from external excitation in close circuit

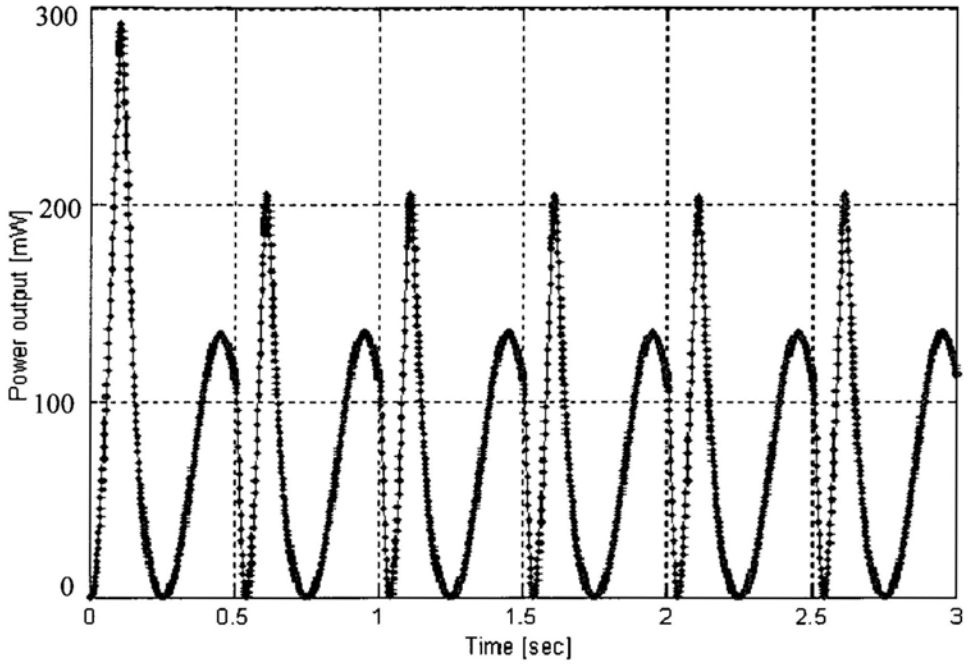

Fig.7-21: The transient power output in terms of time where the external input is the combination of sine function and step function

It is easy to obtain the average power output by making integral of the Eq.(7-23) in terms of time, as the Eq.(7-24). With numerical method, the average power output can be calculated by integral using the curve shown in Fig.7-21 and taking its average in terms of the integral time.

$$\overline{P} = \frac{1}{T}\int_0^T C_e \cdot \dot{z}^2 \, dt \tag{7-24}$$

The energy input to the harvester in a given period can be computed by the following expression.

$$E_{in} = \int_0^T (M + 2m)\ddot{y}\dot{y}dt \tag{7-25}$$

And the energy efficiency for the harvester is expressed as:

$$\eta = \frac{E_{out}}{E_{in}} = \frac{\int_0^T C_e \dot{z}^2 dt}{\int_0^t (M + 2m)\ddot{y}\dot{y}dt} \tag{7-26}$$

7.5 Optimization and Discussion

There are many factors influencing the power output, mainly including the spring constant k_1, the equivalent spring constant of the cantilever beam k_2, the oscillating weight m_1, the tip mass at the end of cantilever beam m_2, and the electrical damping C_e. In this section, the relations between the above-mentioned parameters and the average power output will be analyzed, and finally find a set of optimal parameters to design the harvester.

From the above section 7.3, the spring constants and the proof mass obviously influence the dynamic performance, and then affect the power output. First of all, two ratios are defined for convenience: one is the mass ratio r_m of oscillating weight m_1 to tip mass m_2, and the other is the spring ratio r_k of the helical spring k_1 to the cantilever beam k_2.

$$r_m = \frac{m_1}{m_2} \tag{7-25}$$

$$r_k = \frac{k_1}{k_2} \tag{7-26}$$

Figure 7-22 shows the relations between the average power output and the spring ratio and mass ratio, where the mass ratio is constant for each curve and the electrical damping coefficient is 0.2. From the figure, the curves share the same pattern even for different mass ratio. For a single curve, there is a single peak where the power output achieves its maximum. After the peak, all the curves decrease quickly and incline to small difference. For free oscillation and free vibration, the spring constant should be selected near the peak for maximum power output. And the mass ratio should be as higher as possible.

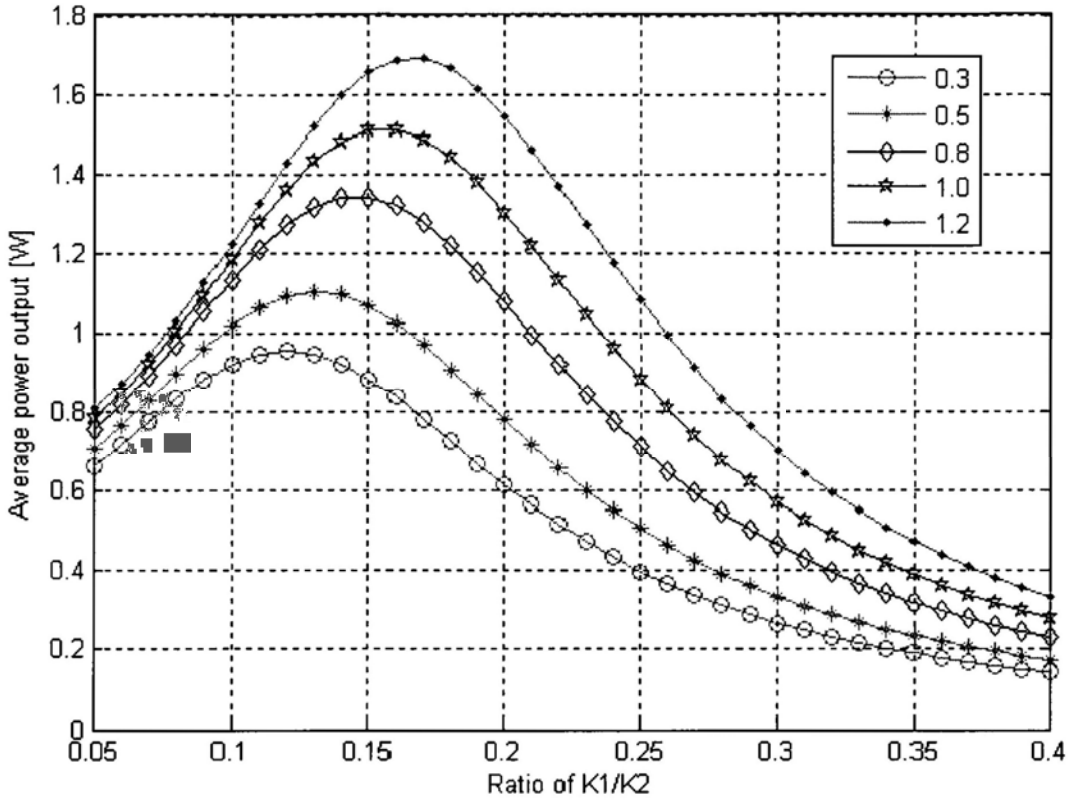

Fig.7-22: The average power output in terms of the spring ratio, where the mass ratio is constant for each curve

For this damping system, the electrical damping is a critical variable for the power output. Figure 7-23 shows the power output performance in terms of spring ratio, where the electrical damping coefficient is constant for each curve. From the figure, the electrical damping coefficient has large effect on the power output. For higher electrical damping, the spring ratio has small effect on the power output. Similar to Fig. 7-22, the performance curves incline to tiny difference when the spring constant increases. It obviously shows that the bigger electrical damping coefficient will not necessary to get higher power output.

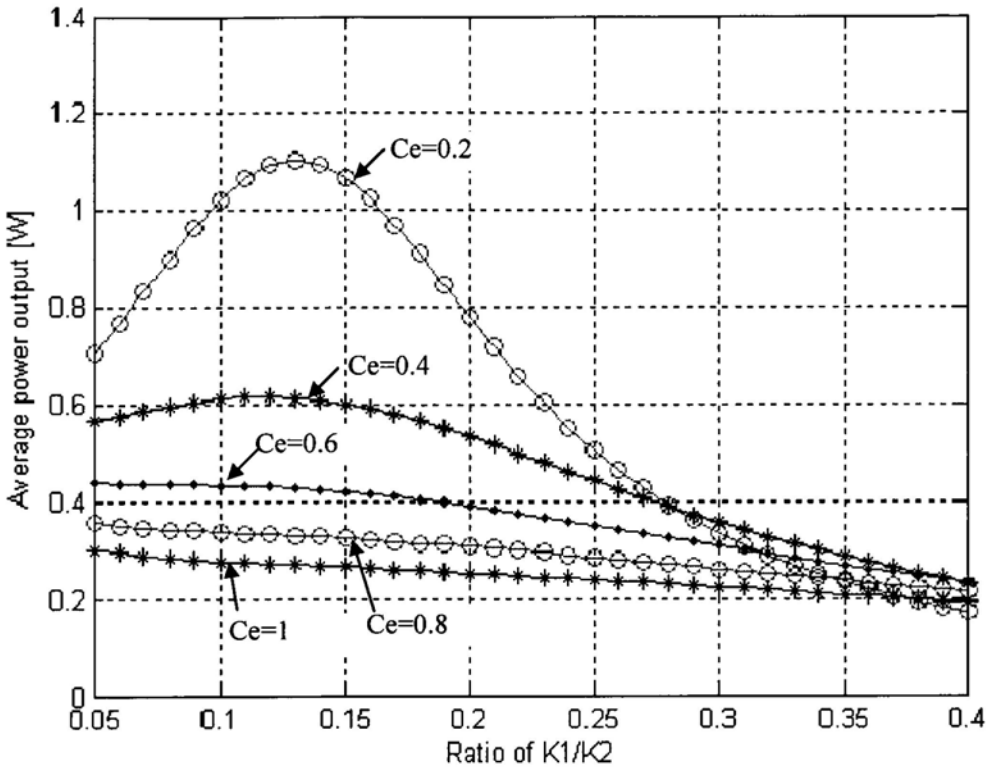

Fig.7-23: The average power output in terms of the spring ratio, where the electrical damping coefficient is constant for each curve

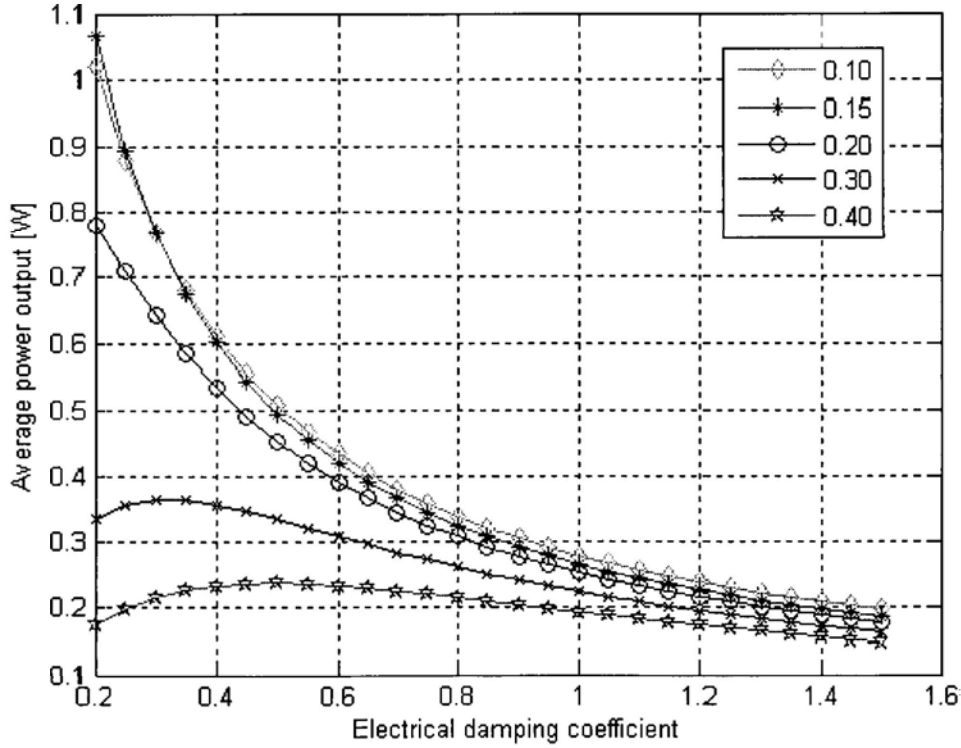

Fig.7-24: The average power output in terms of electrical damping coefficient, where the spring ratio is constant for each curve

Although there is peak value for some specific parameters, the design dimension of the harvester constrains the parameter selection. Due to the height constraint of the harvester container, the optimal electrical damping coefficient and spring constants for highest power output should not be able to be chosen. Figure 7-25 shows maximum displacement of the coils in Z direction in terms of the electrical damping coefficient, where each curve has the same spring constant and mass ratio $r_m = 0.5$. From the figure, the maximum displacement is quite different for different spring constants, and the curve is flatter trend for the lower spring constant. For the harvester to insert into shoe heel, the container height should not be greater than 35mm for each side, so the spring constant more than 0.4 should be used for design.

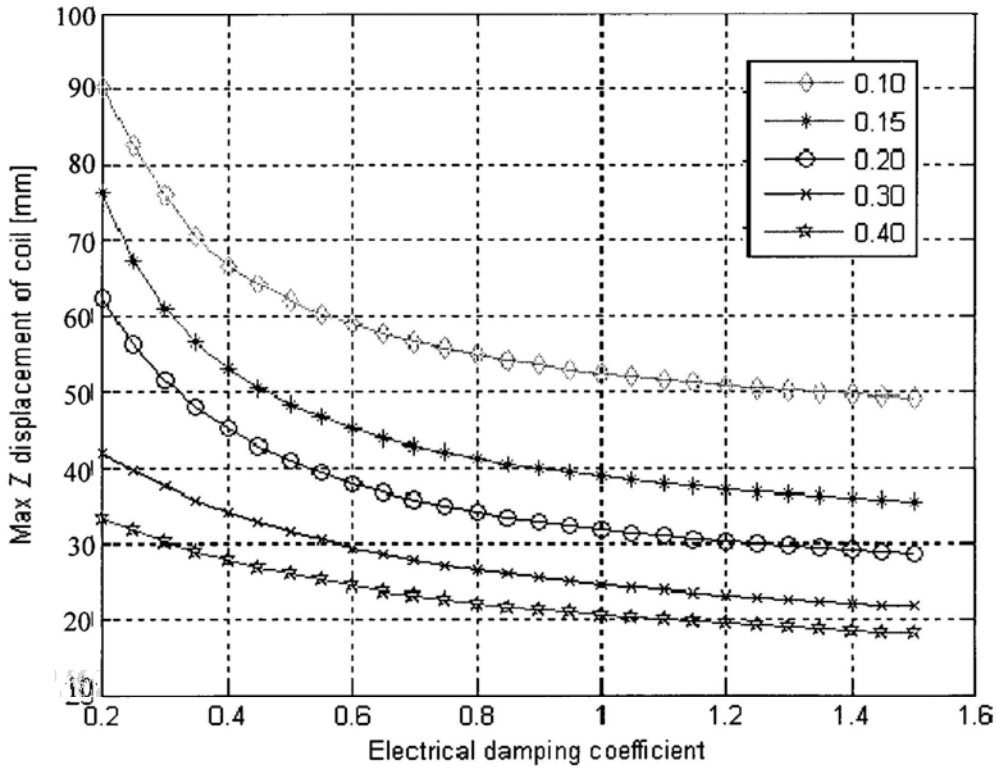

Fig.7-25: The maximum displacement of coil in Z direction in terms of electrical damping coefficient, where the spring ratio is constant for each curve

Higher mass ratio can improve the oscillating performance, but the maximum displacement increases too. Figure 7-26 shows the maximum displacement of coil in Z direction in terms of mass ratio, where the spring ratio is constant for each curve, and Fig. 7-27 is its corresponding power output. From the figures, the higher mass ratio and the lower spring ratio, the higher power output and the higher displacement. Considering the dimension constraint, the spring ratio can be 0.4 and the mass ratio

can be 0.5 to fit the dimension constraint.

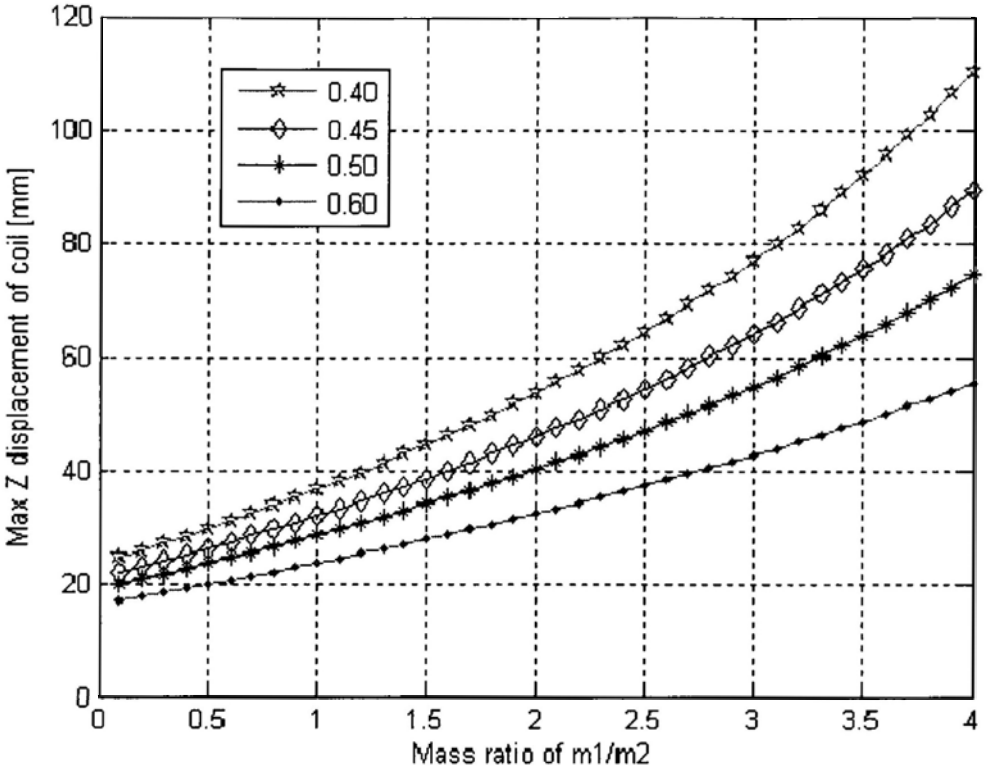

Fig.7-26: The maximum displacement of coil in Z direction in terms of mass ratio, where the spring ratio is constant for each curve

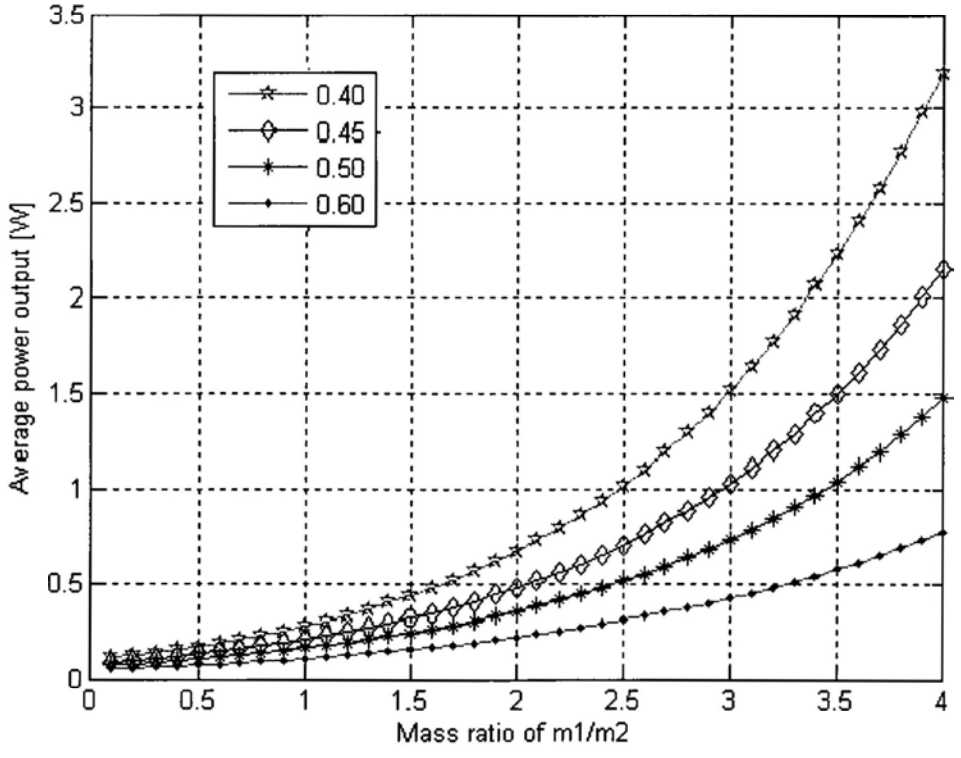

Fig.7-27: The average power output in terms of mass ratio, where the spring ratio is constant for each curve

The electrical damping affects the velocity performance of the coils, where higher electrical damping will lead to more quickly decreasing oscillation. Therefore, there should be an optimal value of electrical damping for maximum average power output. Figure 7-28 shows the average power output in terms of different electrical damping. From the figure, there is an optimal range of electrical damping coefficient to achieve higher power output. Therefore the structure for electromagnetic induction should be optimized to make the electrical damping coefficient fall into the optimal zone. From the Eq.(7-6), the thickness of the permanent magnets can be reduced to decrease the magnetic flux density. With the average power output curve in Fig.7-28 and the electrical damping coefficient in Fig.7-13, the average power output for the harvester is be calculated to be about 100 mW. The energy input to the harvester in 3 seconds is about 700mJ, and the energy efficiency is about 43%. Comparing to the kinetic energy of the footstep motion, such energy conversion will not increase too much burden for the human body.

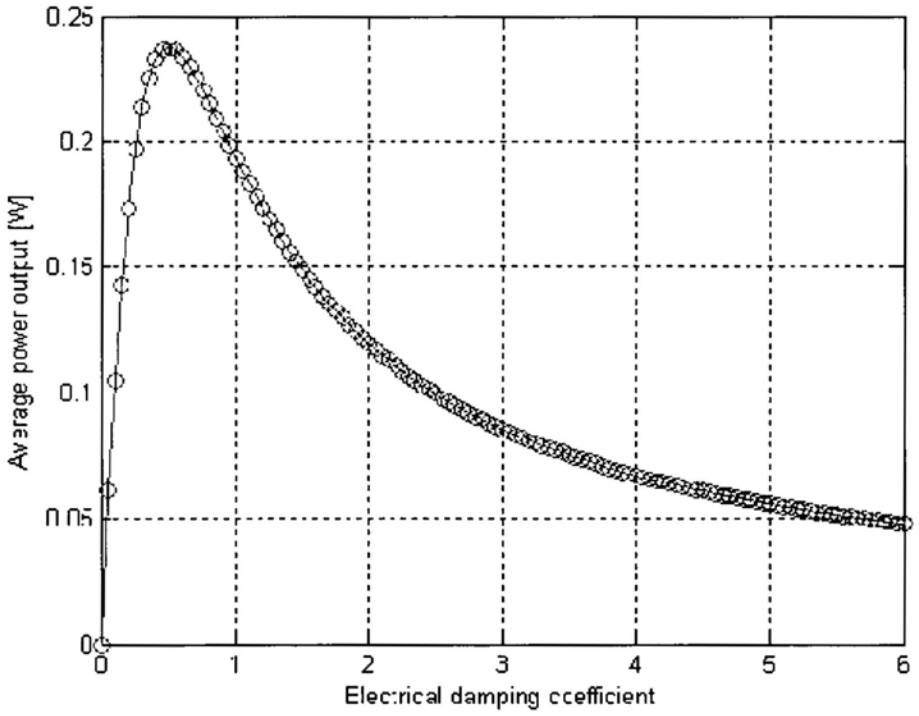

Fig.7-28: The average power output in terms of electrical damping coefficient, where the spring ratio is 0.4 and mass ratio is 0.5.

7.6 Summary

Based on the discussion above, following conclusions can be drawn:

(1) A novel mechanism for energy harvesting from human footstep motion is presented. It adopts the dual-oscillating mode to harness acceleration from footstep, including the mass-spring oscillating sub-mechanism absorb external excitation and the cantilever beam with tip mass to amplify the vibration, and the electromagnetic induction to convert kinetic energy to electricity.

(2) Electromagnetic and kinematical analyses are conducted to study the harvester's performance. Analysis shows that the dual-oscillating mechanism can more effectively amplify the vibration which contributes to higher power output.

(3) The dual-oscillating mechanism does not transmit motion and not directly contact with the input component, so it is stronger and more reliable than other designs of similar function.

(4) The harvester is designed to insert into shoe heel as power supplier for portable electronics, especially for the use in wild area. This energy harvesting principle can also be applied to extract kinetic energy from other kind of movement.

Chapter 8

Conclusions

8.1 Summary of the Achievements

The use of portable electronic devices is increasing every day and will continue to increase in the perceivable future. Its development is, however, hindered by the finite energy source, namely the battery. Moreover, huge amount of disposed batteries creates a big burden to our fragile environment. Thus, it has become necessary to find alternative power source, or at least supplementary power source.

Energy harvesting from environment is a sustainable mean to meet the need of energy of portable electronics. Available environment energy sources include solar light, wind, heat, vibrations and etc. Analysis shows that it is the human motion that is the most suitable energy source for portable electronics.

This thesis explores the feasibility of harvesting human kinetic energy to power portable electronics. The study is based mainly on the mechanical oscillating mechanism and electromagnetic transduction. Comparing to the existing work on harvesting human kinetic energy, this thesis focuses on the feasibility, effectiveness and convenience. The main contributions of the thesis are the design and analysis of four different types of energy harvesters. Specifically, following contributions are made:

(1) The general procedure to design energy harvester is proposed to facilitate the design and analysis process. On harvesting mechanical motion, the procedure is to analyze the pattern of the motion first, and then gives appropriate mechanisms, such as mass-spring system, cantilever beam system, and eccentric rotational mass system. Next, the electromagnetic transduction is added for energy transfer. Finally, the governing equations are derived, based on which the performance of the energy harvester can be predicted.

(2) The first design is the automatic winding mechanism used in mechanical watch movement. Such a mechanism has been used for many years. However, a detailed mathematical analysis has not been seen. The thesis presents a complete design of an automatic winding mechanism with mathematical analysis and experimentally validation. From the mathematical point of view, the automatic winding mechanism can be considered as a double pendulum system: the upper pendulum is the arm and the lower pendulum is the oscillating weight. It also includes a gear train that converts bidirectional motion to the unidirectional motion, as well as a reduction gear train that winds the mainspring. Computer simulation reveals that when the arm swinging as a sinusoidal function, the motion of the rotor is nearly a sinusoidal function with a different frequency. Additionally, the bigger the amplitude and/or the faster the arm swing, the faster the mainspring being wound. Experiments show that it needs 19 hours to fully wind the mainspring, which is close to the simulation result of 17.2 hours.

(3) The second design is a novel device for harvesting kinetic energy of human arm motion. Evolving from the first design, it is based on a combination of mechanical oscillation and electromagnetic induction. The oscillation of the eccentric rotor made of permanent magnet generates the electrical current from the coil stator. With a torsion spring, the harvester works even when placed on horizontal plane. Its electromagnetic and kinematical performance is analyzed in details. Based on the simulation results, design optimization is also carried out. It shows that the watch-sized harvester can produce about 40 mW during normal walking.

(4) The third design is a new device for harvesting energy from human foot strike. The harvester is designed to be inserted into shoe heel for both harvesting energy and serving as shock absorber. In the device, a spring and slider compose an oscillating system to absorb the foot strike impact force, and a crank and slider make up the motion conversion mechanism to transfer the bi-directional translation into unidirectional rotation. Gear sets are used to speed up the rotation. Based on the simulation, a harvester can be produce about 2

watts of power during normal walking.

(5) The fourth novel device for energy harvesting from human footstep motion is designed to insert into shoe heel as well. It adopts the dual-oscillating mode to harvest the acceleration force when the foot strikes the ground. It includes a mass-spring oscillating mechanism to absorb the external excitation, a cantilever beam to amplify the vibration, and an electromagnetic inductor to convert kinetic energy to electricity. Electromagnetic and kinematical analyses are conducted. Computer simulation shows that the dual-oscillating mechanism can more effectively amplify the vibration and hence, generate higher power output. A system with 50mmX40mmX20mm in dimensions and total mass 70g, can produce about 100mW of electricity at the walking speed of 2 steps per second. The dual-oscillating mechanism does not in direct contact to the input component. As a result, it is robust than that of the similar existing designs.

8.2 Future Work

The presented energy harvesters could be used as power supply for portable electronics. However, further research is still needed for industry prototypes and mass production. The involved future work includes:

(1) In the aforementioned analysis, the harvesters are assumed to connect to a resistive load. In practice, however, a DC voltage output is needed. Therefore, a power processing unit is needed to rectify the generated AC voltage. A power storage unit may also be needed.

(2) In order to build industrial prototypes and mass production products, engineering drawings and assembly drawings are needed. Moreover, much vigorous experiment testing is needed.

(3) Optimization should be conducted to fine-tune the designs to improve the power efficiency. Moreover, reliability analysis should be carried out as well.

Bibliography

[1]. Maynard, H.L., and Meyers, J.P., Miniature fuel cells for portable power: design considerations and challenges. *J. Vac. Sci. Technol. B* **20** (2002), pp. 1287–1297.

[2]. Turri, S., Miller, D., Ben Ahmed, H. and Multon, B., Design of an Electro-Mechanical Portable System Using Natural Human Body Movements for Electricity Generation, *Sensors and Actuators A: Physical*, 116(3), pp. 461-471, 2004.

[3]. Beeby, S., Tudor, M. and White, N., Energy Harvesting Vibration Sources for Microsystems Applications, *Measurement Science and Technology*, 2006(17), pp. 175-195, 2006.

[4]. Stephen, N., 2006, On Energy Harvesting from Ambient Vibration, *J. of Sound and Vibration*, 293(1-2), pp.409-425.

[5]. Roundy, S., Wright, P. and Rabaey, J., A Study of Low Level Vibrations as a Power Source for Wireless Sensor Nodes, *Computer Communications*, 2003(26), pp. 1131-1144, 2003.

[6]. Markart, T., Light Harvesting for Quantum Solar Energy Conversion, *Process in Quantum Electronics*, 24(3-4), pp. 107-186, 2000.

[7]. Landsberg, P., Badescu, V., Solar Energy Vonversion: List of Efficiencies and Some Theoretical Considerations, *Process in Quantum Electronics*, 1998(22), pp. 211-230, 1998.

[8]. Shenck, N., and Paradiso, J., Energy Scavenging with shoe-mounted pizoelectrics, *IEEE Micro*, 21(3), pp. 30-42, 2001.

[9]. Kornbluh, R., and et al., Electroelastomers: Applications of Dielectric Elastomer Transducers for Actuation, Generation, and Smart Structures, *Smart Structures and Materials 2002: Industrial and Commercial Applications of Smart Structures Technologies*, McGowan, R. ed., Vol. 4698, pp. 254-270, 2002.

[10]. Rome, L., Flynn, L., Goldman, E. M., and Yoo, T. D., Generating Electricity While Walking with Loads, *Science*, 309, pp. 1725-1728, 2005.

[11]. Donelan, J. M., and et al., Biomechanical Energy Harvesting: Generating Electricity During Walking with Minimal User Effort, *Science*, 319, pp. 807-810, 2008.

[12]. Starner, T. and Paradiso, J., *Low-Power Electronics Design*, Chapter 45, CRC Press, New York, 2004.

[13]. J.P. Fleurial, T. Olson, A. Borschevsky, T. Caillat, E. Kolawa, M. Ryan, and W. Philips., Electronic device featuring thermoelectric power generation. *United States Patent* 6,288,321, 2001.

[14]. T. Kanesaka, et al., Development of a thermal energy watch, *Micromechatronics*, vol. 43(3), pp. 29-36, 1999.

[15]. E. H¨ausler, L. Stein, and G. Harbauer, "Implantable physiological power supply with PVDF film", Ferroelectrics, Vol.60, pp. 277–282, 1984.

[16]. Crisan, A., Typing power, *United States Patent* 5,911,529, Jun 1999.

[20]. J. Donelan, et al.: Biomechanical energy harvesting: generating electricity during walking with minimal user effort, *Science*, Vol.319, pp.807-810, 2008.

[21]. Williams, C. B. and Yates, R. B., Analysis of a micro-electric generator for Microsystems, *Transducers 95/Eurosensors IX*, pp. 369-72, 1995.

[22]. Goto, H., Sugiura, T., Harada, Y., and Kazui, T.: Feasibility of using the automatic generating system for quartz watches as a leadless pacemaker power source, *Medical and Biological Engineering and Computing*, Vol.37, Iss.3, pp.377-380, 1999.

[23]. Gorge, G., Kirstein, M., and Erbel, R.: Microgenerators for Energy Autarkic Pacemakers and Defibrillators: Fact or Fiction? *Herz*, Vol.26, Iss.1, pp.64-68.

[24]. El-hami, M., Jones, P. G., James, E., Beeby, S. P., White, N. M., Brown, A. D. and Hill, M. (2001) Design and fabrication of a new vibration based electromechanical generator. *Sensors and Actuators A*, Vol.92 . pp. 335-342, 2001.

[25]. Duffy, M., and Carroll, D.: Electromagnetic generators for power harvesting, *PESC 04 (Aachen)*, vol.3 pp.2075–81,2004.

[26]. Carroll, D. and Duffy, M.: Demonstration of wearable power generator Power Electronics and Applications, *European Conf. (Dresden)*, 2005.

[27]. Sasaki, K., Osaki, Y., Okazaki, J., Hosaka, H., and Itao, K.: Vibration-based automatic power-generation system, *Microsystem Technologies*, Vol.11, pp.965–9, 2005.

[28]. Wang, J., Wang, W., Jewell, G.W., and Howe, D.: Design of a miniature permanent-magnet generator and energy storage system, *IEEE Trans. Ind. Electron.*, Vol.52, pp.1383–90,2005

[29].Niu, P., and Chapman, P.: Design and performance of linear biomechanical energy conversion devices, *PESC '06*, pp. 1–6, 2006.

[30].Beedy, S.P., Torah, R.N., Tudor, M.J., Glynne-Jones, G., O'Dnnell, T., Saha, C.R., and Roy, S.: A micro electromagnetic generator for vibration energy harvesting, *Journal of Micromechanics and Microengineering*, Vol.17, pp.1257-1265, 2007.

[31].Von Buren, T., and Troster, G.: Design and optimization of a linear vibration-driven electromagnetic micro-power generator, *Sensors Actuators A*, Vol.135, pp.765–75, 2007.

[32].Romero, E., Warrington, R. and Neuman, M.: Body motion for powering biomedical devices, *Proc. EMBC2009*, 2009.

[33].Joseph, A.D.: Energy Harvesting Projects, *IEEE Pervasive Computing*, Vol.4(1), pp.69-71, 2005.

[34].Beeby, S. P., Tudor, M.J. and White, N.M., Energy harvesting vibration sources for Microsystems applications, *Journal of Measurement Science and Technology*, Vol.17, pp.175-195, 2006.

[35].Sodano, H.A., Inman, D.J., and Park, G., A Review of Power Harvesting from Vibration Using Piezoelectric Materials, *The Shock and Vibration Digest*, Vol.36, pp. 197–205,2004.

[36].Antaki, J.F., Bertocci, G.E., Green, E.C., Nadeem, A., Rintoul, T., Kormos, R.L. and Griffith, B.P.: A gait-powered autologous battery charging system for artificial organs, *ASAIO J.* Vol.41, M588–95,1995.

[37].Kymissis, K., Kendall, C., Paradiso, J. and Gershenfeld, N.: Parasitic power harvesting in shoes, *Proc. 2nd IEEE Int. Conf. on Wearable Computing (Pittsburgh)*, pp.132–139,1998.

[38].Shenck, N.S., and Paradiso, J.A.: Energy scavenging with shoe-mounted piezoelectrics, *IEEE Micro*, Vol. 21, pp.30–42, 2001.

[39].Mateu, L., Fonellosa, F., and Moll, F.: Electrical characterization of a piezoelectric film-based power generator for autonomous wearable devices, *Proc. 18th Conf. on Design of Circuits and Integrated Systems (Ciudad Real)* pp.677–82, 2003.

[40].Mateu, L. and Moll, F.: Optimum piezoelectric bending beam structures for energy harvesting using shoe inserts, *J. Intell. Mater. Syst. Struct.*, Vol.16, pp.835–45, 2005.

[41].Renaud, M., Sterken, T., Fiorini, P., Puers, R., Baert, K. and van Hoof, C.,

Scavenging energy from human body: design of a piezoelectric transducer, *13th Int. Conf. on Solid-State Sensors Actuators and Microsystems (Seoul)*, pp.784–7, 2005.

[42]. Renaud, M., Fiorini, P., and van Hoof, C., Optimization of a piezoelectric unimorph for shock and impact energy harvesting, *Smart Materials and Structures*, Vol.16(4), pp.1125-1135, 2007.

[43]. Renaud, M., Fiorini, P., and van Hoof, C., Harvesting energy from the motion of human limbs: the design and analysis of an impact-based piezoelectric generator, *Smart Materials and Structures*, Vol.18, 035001

[44]. Cavallier, B., Berthelot, P., Nouira, H., Foltete, E., Hirsinger, L. and Ballandras, S.: Energy harvesting using vibrating structures excited by shock, *Ultrason. Symp.* Vol.2, pp.943–5, 2005.

[45]. Platt, S.R., Farritor, S. and Haider, H.: On low-frequency electric power generation with PZT ceramics, *IEEE/ASME Trans. Mechatronics*, Vol.10(2) pp.240–252, 2005.

[46]. Platt, S.R., Farritor, S., Garvin, K. and Haider, H.: The use of piezoelectric ceramics for electric power generation within orthopedic implants, *IEEE/ASME Trans. Mechatronics*, Vol.10(4), pp.455–61,2005.

[47]. Feenstra, J., Granstrom, J. and Sodano, H.: Energy harvesting through a backpack employing a mechanically amplified piezoelectric stack, *Mech. Syst. Signal Process*, Vol.22, pp.721–34, 2008.

[48]. Peano, F. and Tambosso, T., Design and optimization of a MEMS electret-based capacitive energy scavenger, *Journal of Microelectromechanical Systems*, Vol.14, pp.435–529, 2005.

[49]. Roundy, S., Wright, P. and Pister, K.: Micro-electrostatic vibration-to-electricity converters, *Proceedings IMECE*, pp.1–10, 2002.

[50]. Sterken, T., fiorini, P., Baert, K., Borghs, G. And Puers, R.: Novel design and fabrication of a MEMS electrostatic vibration scavenger, *PowerMEMS*, 2004.

[51]. Tashiro, R., Kabei, N., Katayama, K., Tsuboi, F. and Tsuchiya, K., Development of an electrostatic generator for a cardiac pacemaker that harnesses the ventricular wall motion, *Journal on Artifcial Organs*, Vol.2002, pp.239–245, 2002.

[52]. Mitcheson, P.D., Green,T.C., Yeatman, E.M. and Holmes, A.S.: Architectures for vibration-driven micropower generators, *J. Microelectromech. Syst.*, Vol.13,

pp.429–40, 2004.

[53]. Mitcheson, P.D., Miao, P., Stark, B. H., Yeatman, E.M., Holmes, A.S. and Green, T.C., MEMS electrostatic micropower generator for low frequency operation, *Sensors Actuators A* , Vol.115, pp.523–529, 2004.

[54]. Miao, P., Mitcheson, P.D., Holmes, A.S., Yeatman, E.M., Green, T.C. and Stark, B.H.: MEMS inertial power generators for biomedical applications, *Microsyst. Technol.*, Vol.12, pp.1079–1083, 2006.

[55]. Arakawa, Y., Suzuki, Y. and Kasagi, N.: Micro seismic power generator using electret polymer film, *Power MEMS 2004 (Kyoto)*, pp.187–190, 2004.

[56]. Tsutsumino, T., Suzuki, Y., Kasagi, N. and Sakane, Y.: Seismic power generator using high-performance polymer electret, *Proc. MEMS '06 (Istambul)* pp.98–101, 2006.

[57]. Roundy, S., Wright, P.K. and Rabaey, J.M.: Energy scavenging for wireless sensor networks with special focus on vibrations, Kluwer Academic Publishers, 2004.

[58]. Reymondin, C. A., Monnier, G., Jeanneret, D. and Pelaratti, U., 1999, *The Theory of Horology*, the Technical College of Vallee de Joux, Switzerland.

[59]. Seiko corporation, www.seikowatches.com

[60]. Rolex corporation, www.rolex.com

[61]. ETA Inc, www.eta.ch

[62]. http://en.wikipedia.org/wiki/Double_pendulum.

[63]. CSM Instrument, www.csm-instruments.com

[64]. Dwari, S., Dayal, R., and Parsa, L.: A Novel direct AC/DC converter for efficient low voltage energy harvesting, *34th Annual Conference of IEEE Industrial Electronics,* pp.484~488, 2008.

[65]. http://www.zcoil.com/technology.php

[66]. Chen, S.-H.: Dynamoelectric shoes, *US Patent* No.5495682, 1996.

[67]. Lakic, N.: Inflatable boot liner with electrical generator and heater, *US Patent* No.4845338, 1989.

[68]. Eckhardt,H.D.: *Kinematic design of machines and mechanisms*, MgGraw-Hill, 1998.

[69]. Tsutsuguchi, K.; Shimada, S.; Suenaga, Y.; Sonehara N.; Ohtsuka S: Human walking animation based on foot reaction force in the three-dimensional virtual world, *The Journal of Visualization and Computer Animation*, 11(1), 2000, 3-16.